Computational mechanistic photochemistry: The central role of conical intersections

Martial Boggio-Pasqua

UNIVERSITÉ TOULOUSE III PAUL SABATIER

Université de Toulouse

Manuscrit

en vue de la soutenance de

l'Habilitation à Diriger les Recherches

par

Martial BOGGIO-PASQUA

Computational mechanistic photochemistry: The central role of conical intersections

Soutenue le 22 Juillet 2015

JURY

Pr. Maurizio PERSICO	Professeur, Université de Pise	**Rapporteur**
Pr. Nicolas FERRÉ	Professeur, Université d'Aix-Marseille	**Rapporteur**
Dr. Daniel BORGIS	Directeur de recherche, ENS Paris	**Rapporteur**
Pr. Isabelle DEMACHY	Professeur, Université Paris Sud	**Examinateur**
Dr. Thomas GUSTAVSSON	Directeur de recherche, CEA-Saclay	**Examinateur**
Pr. Fabienne ALARY	Professeur, Université Toulouse III	**Présidente**

Ecole doctorale : Sciences de la Matière
Unité de Recherche : Laboratoire de Chimie et Physique Quantiques (UMR 5626)

Foreword

This manuscript is written as an introduction to the field of computational photochemistry. It is not intended to be a textbook, as more emphasis has been made on illustrations rather than on methodologies and technical guidelines. In this way, I hope that it will be accessible to a large audience, from undergraduate students to more experienced scientists who would be interested in learning about this fascinating and relatively young field of research.

This manuscript would have never appeared without many of the people I had the chance to study or work with along these last twenty years or so. First, I would like to thank Prof. Jean-Claude Rayez who taught me quantum chemistry and transmitted his passion to me. I am indebted to Prof. Mike Robb and Dr. Mike Bearpark for all the knowledge they have imparted to me on computational photochemistry and for their support during my scientific career as a post-doctoral researcher. A large part of this manuscript is devoted to the work we have done together. My collaborator, Dr. Gerrit Groenhof, also played a critical role in some of the most successful stories I am presenting in this report. I would also like to thank Prof. Fabienne Alary and Dr. Jean-Louis Heully for giving me the opportunity to work in their team, for sharing their passion of theoretical chemistry with me and for their support during the writing of this manuscript.

Finally, I would like to dedicate this manuscript to my wife, Marjorie. Her support is a great source of motivation for me, and our two children, Lina (4 years old) and Timéo (2 years old) are a source of joy.

1. Introduction

In the past three decades or so, computational photochemistry has gained considerable credit as a tool to investigate photochemical reaction mechanisms in organic, inorganic and even biological chromophores.[1] This reputation has been gained thanks to the concomitant growing of computational power and theoretical developments in the field of quantum chemistry. These advances allow peering beyond the traditional interpretations of photochemistry focused on vertical excitations at the Franck–Condon geometry. The exploration of other regions of the complex multidimensional potential energy surfaces is becoming routine, and the synergy between accurate and global static calculations and either quantum or semiclassical nonadiabatic molecular dynamics simulations has allowed major breakthroughs in the understanding of photochemical and photophysical processes. Nowadays, computational investigations of photochemical processes such as photoisomerization, photoinduced electron transfer, photosensitization and photodissociation have become a standard practice.

While standard state-of-the-art ab initio quantum chemical methods are already capable of providing a complete description of what happens at the molecular level during bond-breaking and bond-forming processes in thermal reactions, the task is much more challenging when contemplating photochemical reactions. The main reasons are as follows: i) the description of electronic excited states can become very difficult because of their usual multiconfigurational character, ii) the reaction path cannot be described by a single potential energy surface, but rather two branches at least are required: one located on an excited state (reactant side) and the other located on the ground-state potential energy surface (product side), and iii) the Born-Oppenheimer approximation breaks down in the 'funnel' region where the excited-state reactant or intermediate is delivered to the ground state. The main difficulty associated with computations of photochemical processes lies in the correct description and practical computation of this 'funnel' region. Computational tools have been developed and strategies discovered to explore electronically excited-state reaction paths involving so-called conical intersections, which act as funnels for efficient radiationless electronic transitions. The goal of such computational approaches in the study of photochemical mechanisms is the complete description of what happens at the molecular level from photonic energy absorption to product formation.

In this manuscript, I will review my own contributions in this fascinating field of research. I will start by giving a short introduction on what is called *computational mechanistic photochemistry* and the central role played by conical intersections. Then I will review the basic concepts and computational strategy, which permit such investigations. Next I will give some illustrations based on the most interesting systems I had the chance to study. These include the study of organic and inorganic photochromic systems, the photoisomerization of a protein, the photostability of polycyclic aromatic hydrocarbons, photoinduced intramolecular charge transfer in donor-acceptor systems, and photoinduced proton-coupled electron transfer in biological systems. Finally, I will present some perspectives of future work.

1.1. Computational mechanistic photochemistry

The terminology *computational mechanistic photochemistry* is used in the present manuscript to designate theoretical studies aimed at understanding excited-state mechanisms involved in photochemical processes. The term photochemistry (or photochemical processes) is used here in the

broadest sense, i.e. it also includes photophysical processes such as nonradiative decay back to the original ground state (photostability) and radiative emission (photoluminescence). To understand the fate of a molecular system after photoexcitation, it is not only necessary to understand the excited-state properties of the molecule but also to determine how the system will evolve chemically in terms of bond making and bond breaking in these excited states. Thus, it is crucial to understand the reaction pathway describing the passage from the ground-state reactants to the final photoproducts evolving along the potential energy surfaces (PESs) of the photochemically relevant electronic states. This reaction path is called *photochemical reaction path* or *photochemical pathway*. As explained in more details later (see section 3.1.2), the photochemical pathway is determined by following the detailed relaxation and reaction paths of the molecule along the relevant potential energy surfaces from the Franck-Condon (FC) point (i.e., vertically excited geometry) to the ground state. Static calculations are performed to investigate the topology of the PESs. It requires finding all the relevant critical structures (minima, saddle points, barriers, surface crossings) involved along the reaction path and understanding how all these critical points are interconnected on the PESs. This interconnection is often determined by minimum energy path (MEP) calculations. Once the potential energy landscape for all the relevant electronic states is understood, very detailed mechanistic information can be derived on the photochemistry of the system. To give an illustration, we show in Figure 1 the mechanistic picture first derived more than twenty years ago on benzene photochemistry.[2] With this information in hand, one can interpret the experimental data regarding the competition between fluorescence and benzene to benzvalene photoisomerization depending on the photoexcitation wavelength.

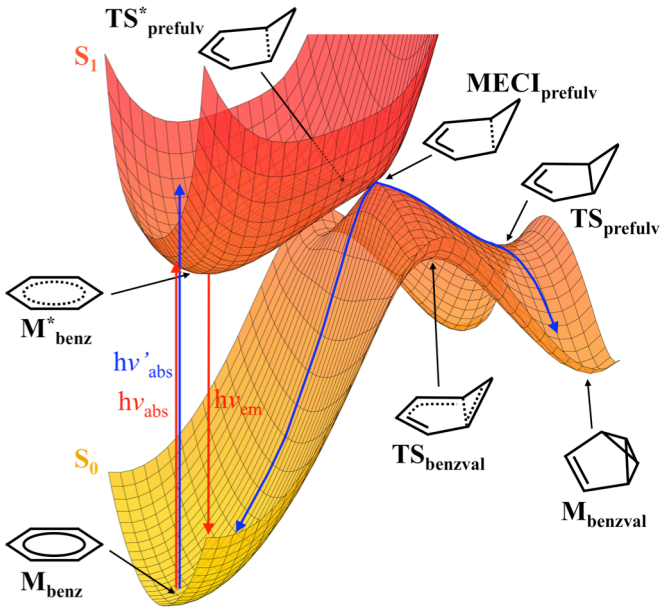

Figure 1. Schematic S_0 and S_1 potential energy landscapes along the benzene → benzvalene photochemical pathway. Red arrows show photon absorption followed by fluorescence. Blue arrows show photon absorption of higher energy followed by photoproduct formation.

The information obtained from this static approach is mainly structural, i.e. the calculated path describes the motion of a vibrationally cold molecule moving with infinitesimal momenta. While this path does not represent any *real* trajectory, it allows for a qualitative understanding of different

experimental data such as excited-state lifetimes, nature of the photoproducts formed, quantum yields and transient absorption and emission spectra. Beyond the static approach, detailed information about the time-evolution of a molecule after photoexcitation can be obtained from ab initio excited-state molecular dynamics (MD). Dynamics studies become all the more important when the system does not follow MEPs. In such cases, regions of the PES far from the computed photochemical pathway may become important and mechanistic pictures deduced solely from the topological investigation of the PESs may be erroneous. Moreover, dynamics simulations can bring semi-quantitative information on important experimental data such as excited-state lifetimes and quantum yields provided that a sufficient sampling of the system can be achieved (more details in section 3.2). Thus, static calculations of PESs and characterization of the photochemical pathway are often complemented by dynamics simulations to gain a more complete understanding of the molecular photochemistry.

1.2. Role of conical intersections

Back in the late 60s, the consensual view of a photochemical reaction was that the decay of an excited species was taking place at an excited-state energy minimum coinciding with an *avoided crossing* region between the excited- and ground-state PESs (Scheme 1a).[3] However, a conceptual shift was about to take place when Zimmerman,[4] Teller[5] and Michl[6] introduced independently the concept of *photochemical funnels*. These authors were the first to suggest that some photoproducts may be produced from the nonradiative decay of the excited-state species through a degeneracy (i.e., a *real crossing point*) between the excited- and ground-state PESs, rather than an avoided crossing (Scheme 1b). These degenerate points were first coined *conical crossings*[7] and are more commonly known as *conical intersections*.[8]

While conical intersections were thought to be an exception rather than the rule, more than two decades of computational photochemical studies have established that they are ubiquitous in polyatomic systems, and their involvement in excited-state processes represents a general mechanistic feature,[9,10,11,12] in analogy with transition states for thermal reactions.[13] Thus, the likeliness that an excited-state species enters a region where the excited state crosses the ground state is high. Such crossings provide very efficient funnels for radiationless deactivation (i.e., internal conversion). In other words, the transition probability at the crossing is very high (close to unity) and the associated kinetics is ultrafast (within a single molecular vibration, that is, on a femtosecond timescale). Not surprisingly, then, the search of photochemical funnels has become the grail of all the computational investigations in mechanistic photochemistry. Therefore, conical intersections deserve to be understood and the following section is dedicated to these intriguing critical points.

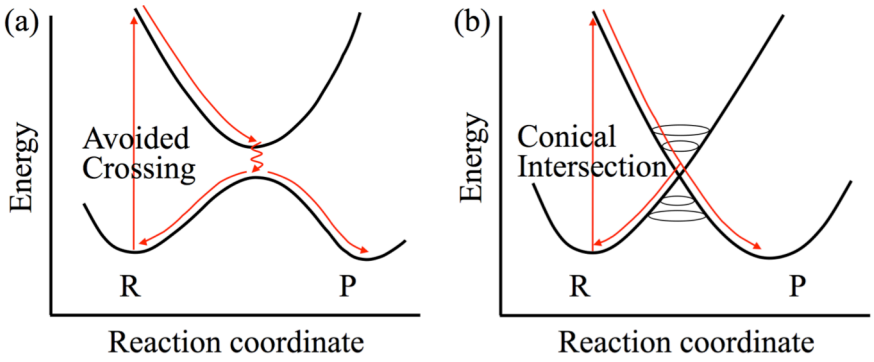

Scheme 1. Schematic potential energy profiles from reactants (R) to products (P) and deactivation pathways through (a) an avoided crossing, and (b) a conical intersection.

2. Conical intersections and associated crossing seams

2.1. Introduction to the theoretical concept of conical intersections

Condition of existence. The concept of conical intersection first appeared in the thirties of the 20th century.[7] But it is only about thirty to forty years later that the detailed study of this phenomenon began with the work of Herzberg,[8] Longuet-Higgins,[8] Zimmerman,[4] Teller,[5] Michl,[6] Mead,[14] Truhlar,[15] Robb,[9–12] Yarkony[16] and Baer[17] to cite just a few. This is when the idea that conical intersections act as funnels through which the excited state transfers nonradiatively to a lower state emerged. At first, conical intersections were regarded as a mathematical curiosity rather than a useful concept for explaining nonadiabatic events, and they were considered as extremely rare objects. Modern theoretical advances, however, have enabled the location of conical intersections routinely leading to the realization that they are much more common than previously thought. In fact, it is well established that they are ubiquitous in polyatomic systems[18] and in this new paradigm they play a central role in many photochemical transformations.[19] This has been confirmed experimentally thanks to the progress in ultrafast (femtosecond) techniques, which have enabled the determination of subpicosecond lifetimes for nonadiabatic events. These very fast processes cannot be explained with the traditional theories for avoided crossings and point to the involvement of conical intersections.

Given the importance of these conical intersections in photochemistry,[13,20] an obvious question involves the requirements for their existence. To address this question, we consider an electronic Hamiltonian, $\boldsymbol{H}^{el}$, through which two electronic states, ϕ_1 and ϕ_2, are interacting.[21]

$$\boldsymbol{H}^{el} = \begin{pmatrix} H_{11}(R) & H_{12}(R) \\ H_{12}(R) & H_{22}(R) \end{pmatrix}$$

where $H_{\mathrm{ij}} = \langle \phi_{\mathrm{i}} | \hat{H}^{el} | \phi_{\mathrm{j}} \rangle$, ϕ_{i} are called diabatic wave functions and R represents the nuclear coordinates. The eigenvalues of $\boldsymbol{H}^{el}$ are obtained by diagonalization of the two-by-two matrix, giving the following adiabatic energies:

$$E_{1,2} = \overline{H} \pm \sqrt{\Delta H^2 + H_{12}^2}$$

where $\overline{H} = (H_{11} + H_{22})/2$ and $\Delta H = (H_{11} - H_{22})/2$. For the adiabatic energies to be degenerate, two independent conditions must be satisfied:

$$H_{11}(R) = H_{22}(R)$$

$$H_{12}(R) = 0$$

Thus, at least two internal degrees of freedom are necessary to fulfill these two conditions. These conditions for degeneracy are well-known since 1929 when von Neumann and Wigner formulated what is known as the *non-crossing rule*.[22] For a diatomic molecule that has only one internal degree of freedom, it is not possible for two electronic states of the same symmetry to become degenerate. When two states have different (spatial or spin) symmetry, then the second condition ($H_{12} = 0$) is satisfied and the two states may cross (they will cross if $H_{11} = H_{22}$). This non-crossing rule is only valid for

diatomic molecules, as larger polyatomic molecules have many nuclear degrees of freedom, which may permit to satisfy the two necessary conditions for degeneracy. Thus, the correct view is that two electronic states of a polyatomic molecule can in principle intersect even if they belong to the same spatial and spin symmetry.

Branching space and intersection seam. If we denote the two independent coordinates fulfilling the degeneracy requirements by $\mathbf{x_1}$ and $\mathbf{x_2}$, and take the origin at the point where the two above conditions are satisfied, in the hypothesis of the first order (i.e., linear) approximation,[23] it can be demonstrated[24] that these two directions are given as the gradient difference vector

$$\mathbf{x_1} = \frac{\partial(E_1 - E_2)}{\partial R}$$

and the gradient of the *interstate coupling vector*

$$\mathbf{x_2} = \left\langle \psi_1 \middle| \frac{\partial \hat{H}^{el}}{\partial R} \middle| \psi_2 \right\rangle$$

where ψ_i are the adiabatic wave functions The first vector $\mathbf{x_1}$ is often denoted $\mathbf{g}$. The second vector is parallel to the *nonadiabatic coupling vector* (also called *derivative coupling vector*) often denoted $\mathbf{h}$.

$$\mathbf{h_{12}} = \left\langle \psi_1 \middle| \frac{\partial \psi_2}{\partial R} \right\rangle = \frac{\left\langle \psi_1 \middle| \frac{\partial \hat{H}^{el}}{\partial R} \middle| \psi_2 \right\rangle}{(E_2 - E_1)}$$

The vector $\mathbf{h_{12}}$ is the coupling term that gives the magnitude of the coupling between the adiabatic (Born-Oppenheimer) states ψ_1 and ψ_2 as a function of the nuclear motion along *R*. Note that this coupling becomes singular (infinite) at the conical intersection where $E_1 = E_2$.

The two first-order degeneracy-lifting coordinates $\mathbf{x_1}$ and $\mathbf{x_2}$ form the so-called *branching space* (also known as g-h space).[23] If one moves away from the conical intersection in the plane spanned by these two directions, the degeneracy is lifted at first order. As a consequence, the two crossing PESs intersect as a double cone (Figure 2a). Another consequence of the non-crossing rule concerns the dimensionality of the conical intersection. Because of the 2-dimensional branching space, conical intersections are not isolated points in space, but rather they are made of an infinite number of connected conical intersection points forming what is called the *intersection seam* or *crossing seam*. For a molecule with N^{int} internal degrees of freedom, it is possible to find $N^{int} - 2$ coordinates orthogonal to the branching space, which maintain the degeneracy at first order. This $(N^{int} - 2)$-dimensional space is a hyperline of degeneracy and is also called *intersection space* (Figure 2b). Consequently, conical intersections have a high dimensionality, which makes them all the more accessible during the course of the photochemical reaction. The search for the most relevant photochemical funnels aims therefore at finding minimum energy points along the crossing seams. These critical points are called *minimum energy conical intersections* (MECI) and can be efficiently optimized[24,25] using standard quantum chemistry codes.

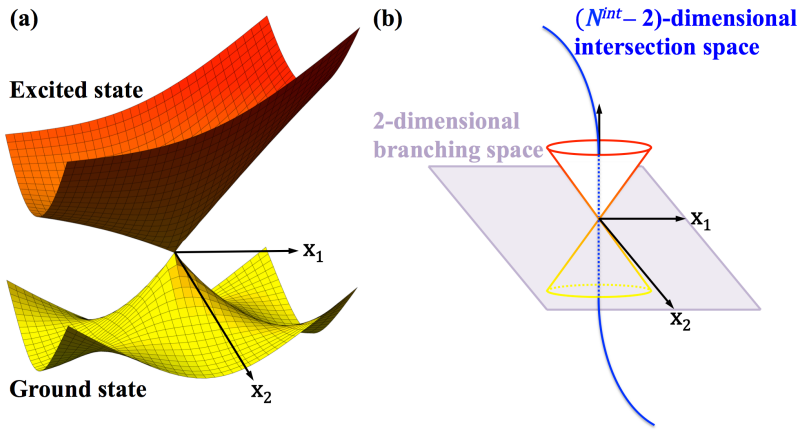

Figure 2. (a) Typical double cone topology for a conical intersection, and (b) relation between the branching space ($\mathbf{x_1}$, $\mathbf{x_2}$) and the intersection space (spanning the remainder of the (N^{int} – 2)-dimensional space of internal geometric variables).

Analogy with transition states. To understand the relationship between PES crossings and photochemical reactivity, it is useful to draw a parallel between the role of a transition state in thermal reactivity and that of a conical intersection in photochemical reactivity.[10] In a thermal reaction, the transition state (TS) forms a bottleneck through which the reaction must pass, on its way from reactants (R) to products (P) (Figure 3a). The motion through the TS is described by a single vector, called transition vector $\mathbf{x_{tv}}$ (i.e., the normal mode associated with the unique imaginary vibrational frequency). A transition state separates the reactant and product energy wells along the reaction path. An accessible conical intersection (Figure 3b) also forms a bottleneck but separates the excited-state branch of the reaction path from the ground-state branch. The crucial difference between conical intersections and transition states is that, while the transition state must connect the reactant energy well to a single product well via a single reaction path, an intersection is a 'spike' on the ground-state PES (see Figure 3b), and thus it may connect the excited-state reactant (R*) to two or more products (e.g., P_1, P_2, P_3) on the ground state via a branching of the excited-state reaction path (in the plane $\mathbf{x_1}$ and $\mathbf{x_2}$) into different ground-state relaxation pathways. The nature of the products generated following decay at a surface crossing will depend on the ground-state valleys (relaxation paths) that can be accessed from that particular structure.

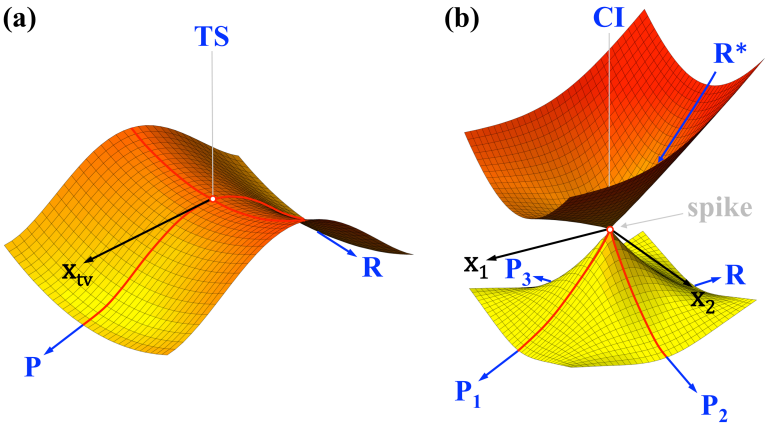

Figure 3. Comparison of the role of (a) a transition state (TS) in thermal reactivity and (b) of a conical intersection (CI) in photochemical reactivity.

2.2. Topological features

Different topological situations are possible for real crossings between PESs. One can have intersections between states of same spin multiplicity (e.g., between two singlets) giving rise to an (N^{int} – 2)-dimensional conical intersection hyperline (Figure 4a). Or intersections can be found between states of different spin multiplicity (e.g., singlet/triplet crossing) giving rise to an (N^{int} – 1)-dimensional intersection space, as the interstate coupling vector vanishes by symmetry (Figure 4b). (N^{int} – 1)-dimensional crossing seams can also be encountered between states of same spin multiplicity in two distinct cases: 1) when the vector $\mathbf{x_2}$ vanishes for other reasons than symmetry (this situation is encountered in photoinduced electron and energy transfer processes), or 2) when vectors $\mathbf{x_1}$ and $\mathbf{x_2}$ become parallel reducing the dimensionality of the branching space to one coordinate. Note that in these last two cases, the real crossing is not anymore a conical intersection strictly speaking, as there is only one degeneracy-lifting coordinate remaining. Thus, the crossing does not display anymore a double-cone topology and it is not possible anymore to get a change of sign of the wave function by making a loop around the locus of the crossing, which is a particular feature of conical intersections.[16a] Note also that in the case of singlet/triplet crossings, the interstate coupling is restored upon including the spin-orbit coupling (SOC).

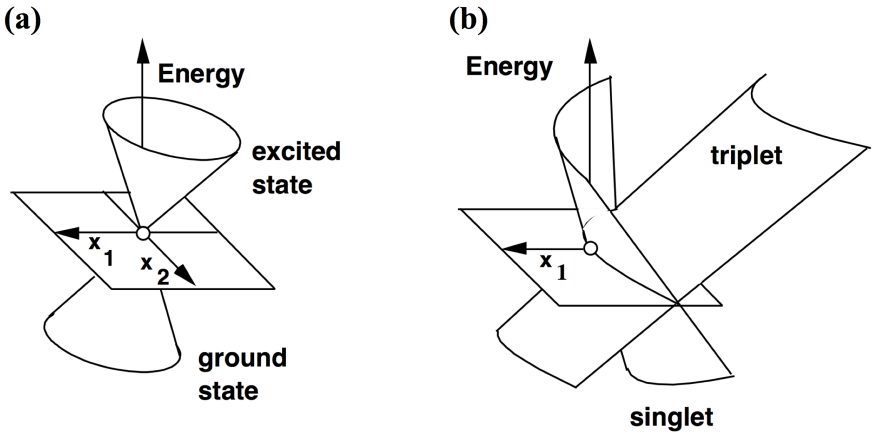

Figure 4. Possible topologies for real crossings between two states: (a) typical (N^{int} – 2)-dimensional conical intersection between states of same spin multiplicity (e.g., two singlets or two triplets), and (b) (N^{int} – 1)-dimensional intersection between states of different spin multiplicity (e.g., singlet and triplet) or between states of same spin multiplicity with a branching space reduced to one dimension ($\mathbf{x_1}$).

The topology of the PESs in the vicinity of a conical intersection can also be characterized by the relative orientation of the two potential surfaces, as discussed by Ruedenberg et al.[23] According to Ruedenberg's terminology, two limiting cases can be distinguished depending on the relative orientation of the slopes of the PESs. In the first case called *peaked* conical intersection (Figure 5a, top), the excited-state gradient points in opposite direction to the ground-state gradient, whereas in the second case called *sloped* (or *tipped*) conical intersection (Figure 5b, top), the two gradients are pointing toward the same direction. A direct consequence is that, in the peaked topology, there are at least two ground-state relaxation pathways, one leading to at least one photoproduct, the other one returning to the reactant (Figure 5a bottom). In the sloped topology, there may exist only one ground-state relaxation pathway pointing directly back to the original reactant (Figure 5b bottom). As a result,

peaked conical intersections are ideal candidate for photochemistry providing efficient funnels for products formation, while sloped conical intersections are more interesting for photophysics providing efficient funnels for ultrafast reactant recovery.

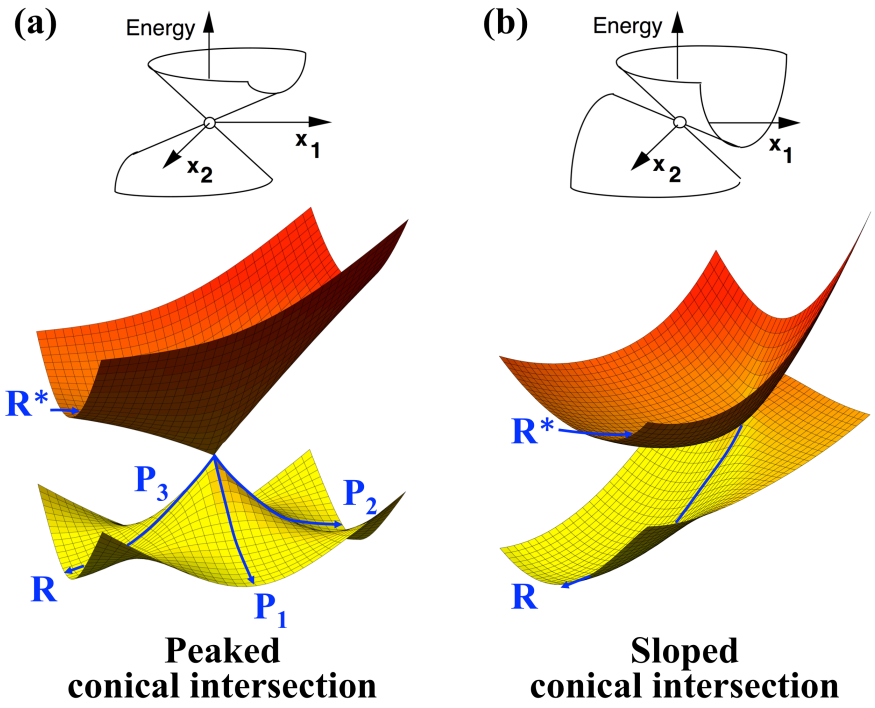

Figure 5. Possible topologies for conical intersections characterized according to Ruedenberg's terminology: (a) peaked conical intersection, and (b) sloped conical intersection.

2.3. The important coordinates in photochemistry

For a discussion of mechanistic photochemistry, one needs a minimum of three geometric variables to describe the nonadiabatic event: the reaction path, and the two vectors which span the branching space.[26] When the reaction path is contained in the branching space, one has a 'sand in the funnel' model (Figure 6a). However, as we shall show, there are many chemical problems where the reaction path lies almost *parallel* to the seam of the conical intersection. In this type of problem, dynamics is essential.

The 'sand in the funnel' model is characterized by a passage through the tip of the upper cone associated with the conical intersection. It can be described as sand flowing through a funnel or an hourglass. This situation is encountered when the reaction path is included in the branching space (i.e., the reaction path can be described as a linear combination of $\mathbf{x_1}$ and $\mathbf{x_2}$, Figure 6a). In this case, a minimum energy path will drive directly the system to the apex of the double cone corresponding to the MECI. Thus, the system will most likely decay in the region of the MECI. A different case is encountered when the reaction path is orthogonal to the branching space (i.e., the reaction path is included in the intersection space, Figure 6b). In such a case, a conical intersection seam can be found along the reaction path, as this coordinate preserves the degeneracy. Two possible scenarios can be found depending on how the seam is laid out. The seam may intersect the minimum energy path in which case the system will most likely decay along the crossing seam in a region necessarily higher than the MECI. This case will be illustrated in DHA/VHF photochromism (see section 4.1.2).

Alternatively, the seam remains located higher in energy than the minimum energy path, even at the MECI, and access to the seam requires some energy flow into the degeneracy-lifting coordinates $\mathbf{x_1}$ and/or $\mathbf{x_2}$. Depending on the amount of vibrational kinetic energy available in these modes, the system may decay at different regions of the seam. In Figure 6b, an illustration of an unreactive trajectory (blue arrow) and a reactive trajectory (white arrow) is shown depending on the vibrational kinetic energy available in the $\{\mathbf{x_1}, \mathbf{x_2}\}$ space. Thus, when the 'sand in the funnel' model is not appropriate because the reaction path does not lie in the branching space, a study of the reaction path and knowledge of the MECI is not enough to understand the photoreactivity. Only dynamics can provide reliable mechanistic information, as it will allow the exploration of the *chemically relevant* parts of the seam. In conclusion, the central idea in photochemistry should be the relationship between the reaction coordinate, the intersection seam and the path actually followed by the system.

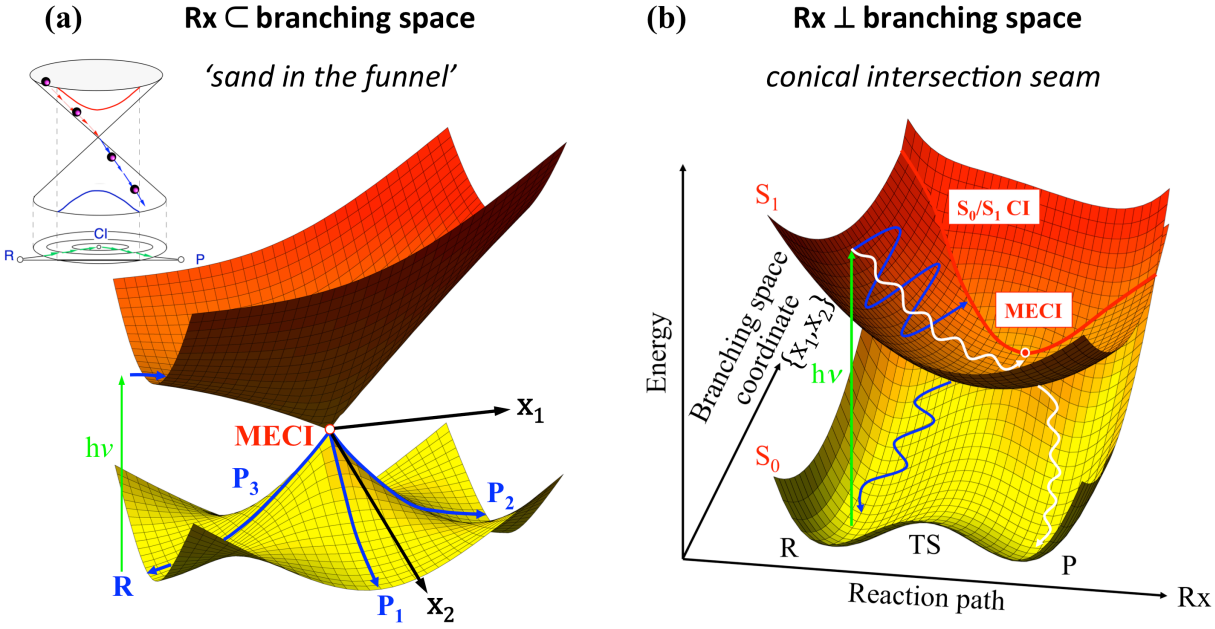

Figure 6. Representation of a conical intersection along the reaction path (Rx) (a) when Rx is included in the branching space ('sand in the funnel' model), and (b) when Rx is orthogonal to the branching space (conical intersection seam). In case (a), the MEP leads directly to the MECI. The inset shows the trajectory followed by a (classical) ball rolling through the intersection. In case (b), access to the conical intersection seam depends on vibrational motion within the branching space.

3. Mechanistic photochemistry: theoretical aspects

3.1. Determination of potential energy surfaces and reaction pathways

3.1.1. Electronic structure methods. To describe the electronic excited states, one needs a quantum mechanical method that provides a balanced description of all the states involved in the dynamics of the system. It needs to describe these states consistently along the entire photochemical pathway, meaning that the important electronic rearrangements taking place in all the states considered must be accounted for along the reaction path. In addition, a method with analytical energy gradients available is also required to explore any photochemical process, whether statically through geometry optimizations and MEP calculations, or dynamically through MD simulations. Because of the

important nonadiabatic effects often involved in the excited-state dynamics, particularly around conical intersections,[27] it is also desirable to use a multiconfigurational method that allows a proper description of the electronic state mixing in the corresponding regions of the PESs. For all these reasons, the complete active space self-consistent field (CASSCF) method has often been used to compute the PESs of excited states, or to investigate nonadiabatic dynamics *on-the-fly*.[28,29,30,31] Within the CASSCF framework, one chooses a set of active orbitals over which the active electrons can be distributed to generate all the electronic configurations, as in a configuration interaction (CI) calculation. Both CI coefficients and orbitals are optimized for a given (set of) state(s). The most critical feature of this kind of calculations is the choice of the active orbitals, known as the active space. A judicious choice of active space has to be selected in order to describe all the electronic rearrangements that will occur during the photochemical process under investigation.[32,33] It allows a reliable description of the static (or non-dynamical) electron correlation. However, to obtain accurate PESs, post-CASSCF treatments are usually necessary to recover the dynamic electron correlation missing at the CASSCF level.[34] This is the case in the popular complete active space second-order perturbation theory (CASPT2),[35] which has become one of the most popular post-CASSCF methods employed in photochemistry today.[36,37] To obtain useful mechanistic information in photochemical studies, the CASSCF approximation is often sufficient. However, if quantitative agreement with experiment is sought or if CASSCF does not provide a balanced description of the excited states because of the lack of dynamic electron correlation, then CASPT2 is necessary.

However, a computational bottleneck arises as the number of electronic configurations generated by the CI expansion in CASSCF quickly increases with the number of active orbitals along with the computational cost. Thus, it may be desirable to use a smaller set of electronic configurations in order to perform the CASSCF calculations. Furthermore, the computational demand in CASPT2 calculations will also depend on the size of the reference active space. One possible strategy is to use the restricted active space self-consistent field (RASSCF) approach. This method can be used either to reduce the number of electronic configurations that are considered in order to treat large polyatomic systems,[38] or to enlarge the active space to include dynamic electron correlation.[39] Another possible approach is to reduce the size of the active space in the CASSCF approach.[40] This is rather useful when one contemplates direct molecular dynamics simulations (see section 3.2) for which evaluation of CASSCF energy and gradient are required at every integration step along the trajectory. Therefore, simulations can rapidly become prohibitively expensive if the size of the active space gets too large.

Note that there exist other computational approaches to describe excited-state electronic structures, such as time-dependent density functional theory (TD-DFT) and equation-of-motion coupled cluster (EOM-CCSD), which have been used in excited-state molecular dynamics simulations.[41,42] Both approaches however suffer from deficiencies of the underlying mono-configurational description of the ground state in regions of bond breaking and bond formation. Moreover, TD-DFT is known to encounter severe problems in describing valence states of molecules exhibiting extended π systems, doubly excited states, charge-transfer excited states,[43] and conical intersections between ground and excited states.[44,45] Still, recent progress has been made to correct these problems in order to make TD-DFT a promising method for general photochemical studies.[46]

Other approaches based on semiempirical configuration interaction methods have been developed specifically for excited-state calculations.[47,48] These low-cost methods can be considered an alternative to the ab initio methods described above for studies of photochemical processes in large size

molecules or when a large number of trajectories is necessary to simulate the dynamics of the system. One particular semiempirical method, which has proved very useful in the context of the present manuscript, is the Molecular Mechanics Valence Bond (MMVB) hybrid method.[49] MMVB uses a parameterised Heisenberg Hamiltonian[50] to simulate CASSCF active orbitals in a valence bond space and the molecular mechanics MM2 force field[51] to describe an inert molecular σ framework. In short, the molecular system is divided into two parts: one to be treated by Valence Bond (VB) theory and the other to be treated by Molecular Mechanics (MM). VB wave functions can be written as eigenfunctions of what is known as the Heisenberg spin Hamiltonian. The parameters of this Hamiltonian have a simple physical interpretation in terms of Coulomb and exchange integrals and they are molecule- and state-independent. In the MMVB method they have been parameterised from CASSCF calculations on small model systems. The result is a parameterised VB Hamiltonian from ab initio data, which can reproduce CASSCF geometries and energies for covalent excited states,[52,53] and be used to study the nonadiabatic dynamics of the system.[54] The main advantage of the MMVB method is that it provides a description of excited states in large conjugated systems taking into account static correlation. Nevertheless, an important drawback is that it can be used for a limited number of problems at present since the VB part has only been parameterised for sp^2 and sp^3 carbon atoms and for covalent electronic states.[55] Besides MMVB, conventional quantum mechanical / molecular mechanics (QM/MM) methodology has been applied to study the photochemistry of chromophores embedded in a solvent bath or in a protein environment.[56,57]

3.1.2. Photochemical reaction path. Important mechanistic information on the photochemical behavior of the system can be derived by computing and analyzing the photochemical reaction path, i.e. the reaction coordinates and energies connecting the Franck-Condon point to the excited-state intermediate M* (if existing) to the ground-state products possibly via conical intersections. As illustrated in Scheme 2, the strategy used in computational photochemistry is based on the mapping of the photochemical reaction path computed by following the MEP from the starting (e.g., Franck-Condon structure FC) to the final points (e.g., ground-state product P) through a conical intersection. This strategy provides information on the structure and accessibility of the photochemical reaction path from a chosen starting point (e.g., the FC point). This technique has the advantage of limiting the investigation only to the region of the PES that is relevant for the description of the photochemical reaction. In other words, by following the MEP, we immediately focus on the driving forces responsible for the photoinduced nuclear motion. Critical structures directly accessible by the system such as intermediates, transition states and funnels will be located as *travelling points* along the MEP. Other stationary points and crossing regions may be very far from the MEP, both in terms of energy and geometry. They may or may not be important for the description of the process depending on the dynamical behavior of the system. For example, the decay point (i.e., the photochemical funnel) intercepted by the MEP may differ from the MECI such as in the case of DHA/VHF photochromism (see section 4.1.2). Thus, the information given by the MEP may be different (or complementary) from that provided by locating stationary points and minimum energy crossing points, yielding a more general and extended description of the potential energy landscape. Another example is the case of the conical intersection and the associated crossing seam lying close to the reaction coordinate but not intercepted by the MEP (see Figure 6b). In this instance, the crossing seam is obviously highly important to account for the nonradiative decay but only dynamics can account for this process.

From a practical point of view, standard methods for geometry optimizations are used to locate the various stationary points on the PESs. The MEP is determined by computing the intrinsic reaction coordinate (IRC).[58] Finding MECI requires special methods as two potential energy surfaces become degenerate and the gradient and Hessian cannot be unambiguously computed. Several algorithms are available (e.g., gradient projection method,[24,25] Lagrange multiplier method,[59] penalty function method[60]) to optimize MECIs and are implemented in various quantum chemistry codes (e.g., Gaussian[61] and Molpro[62] mostly used to perform the calculations reported in this manuscript employ the gradient projection method).

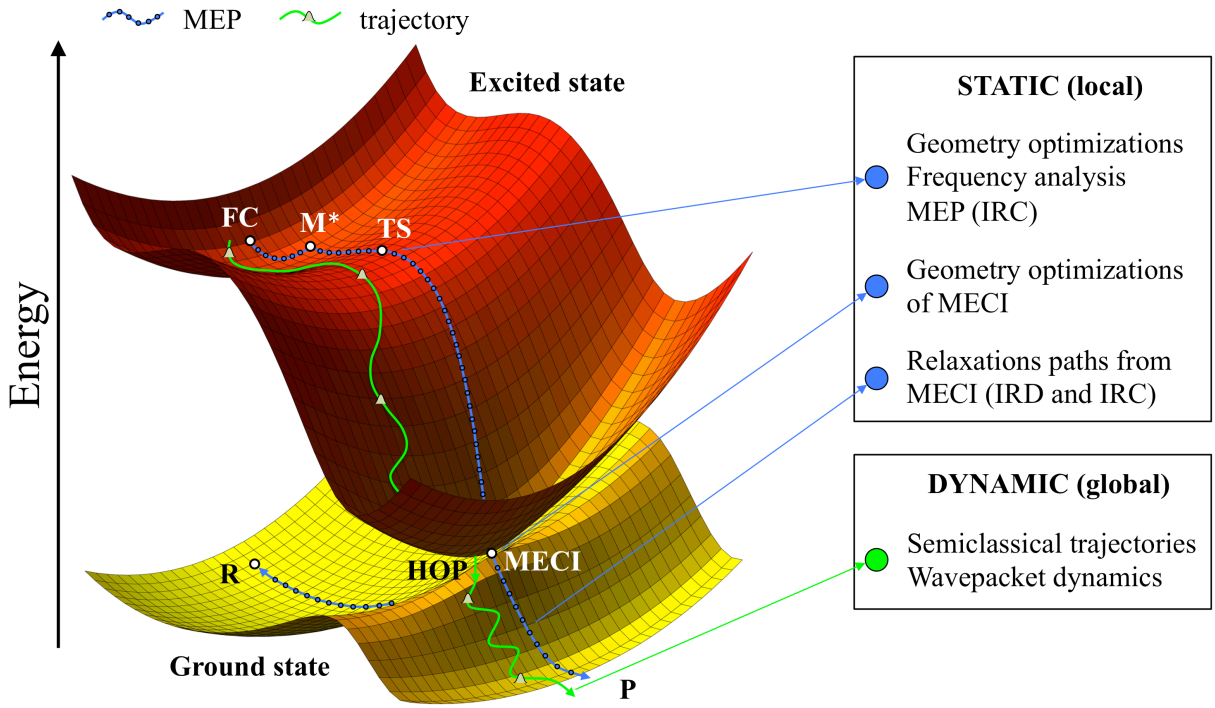

Scheme 2. Illustration of reaction path modeling.

Determining the various MEPs arising from a conical intersection where the branching of the photochemical reaction path occurs upon decay from a higher to a lower electronic state is not so standard. The interstate nature of such paths requires special methodologies to locate the energy valleys describing the relaxation process (e.g., the ground-state relaxation occurring after the decay at an MECI). Methods for computing relaxation paths starting from a crossing point are still not widely distributed. As explained earlier, an accessible conical intersection forms a structural bottleneck that separates the excited-state branch of a photochemical reaction path from one or more ground-state branches connecting the excited-state reactant to one or more ground-state products. The number and nature of the products generated following decay at a surface crossing will depend on the population of such branches, each one corresponding to a different relaxation path. To locate and characterize all the accessible branches developing on the lower cone of a conical intersection, the calculation of the *initial relaxation directions* (IRD)[63] departing from such a conical intersection can be performed.

The MEP connecting the reactant (R) to the product (P) of a thermal reaction is uniquely defined by the associated transition structure (TS). The direction of the transition vector $\mathbf{x}_{tv}$ (i.e., the normal mode corresponding to the imaginary frequency at the TS) is used to start an IRC calculation. One

takes a small step along this vector (shown in Figure 7a) towards P or R and then follows the IRC connecting this point to the product or reactant well. The small initial step vector defines the IRD towards the product or reactant. This procedure cannot be used to find the IRD for a photochemical reaction since, as discussed above, a conical intersection is a "singularity" and there is no such unique direction for this first step. However, note that if one computes the energy of the system along a circular cross section centered at the TS as illustrated in Figure 7a, then provided the radius of the circle is small enough, the energy minima M_1 and M_2 located on the circular cross section provide an alternative but equivalent definition of the IRD. Thus, this strategy can be transposed to the conical intersection for which several IRDs may develop. In this case, one can systematically search for minima on a hypersphere of a given radius and centered on the conical intersection. Figure 7b illustrates this approach in the case of a model elliptic conical intersection (i.e., in the first-order approximation). In this case, two steep sides exist on the ground-state surface in the immediate vicinity of the apex of the cone. It is thus obvious there are two preferential directions of downhill motion along these steep sides of the ground-state cone surface. As one moves away from the apex along these steep directions, real reaction valleys eventually develop (leading to the final photoproduct minima). A simple procedure for defining these directions involves the computation of the energy profile along a circular cross-section centered on the vertex of the cone. It can be seen that the profile contains two different energy minima. These minima (M_1 and M_2 in Figures 7b and 7c) uniquely define the two IRDs from the vertex of the cone. The two steepest descent lines starting at M_1 and M_2 define two MEPs that describe the relaxation processes in the same way the transition vector $\mathbf{x_{tv}}$ defines the MEP connecting reactants to products from a TS. Thus, while there is no analogue for the transition vector in conical intersections, the simple case of an elliptic cone shows that the IRDs are still uniquely defined in terms of M_1 and M_2. At this stage, one should notice that while the IRD from a TS connects the reactant to the product, there are two distinct IRDs from an elliptic conical intersection leading to two different photoproduct valleys (where one of these photoproducts may actually correspond to the original reactant).

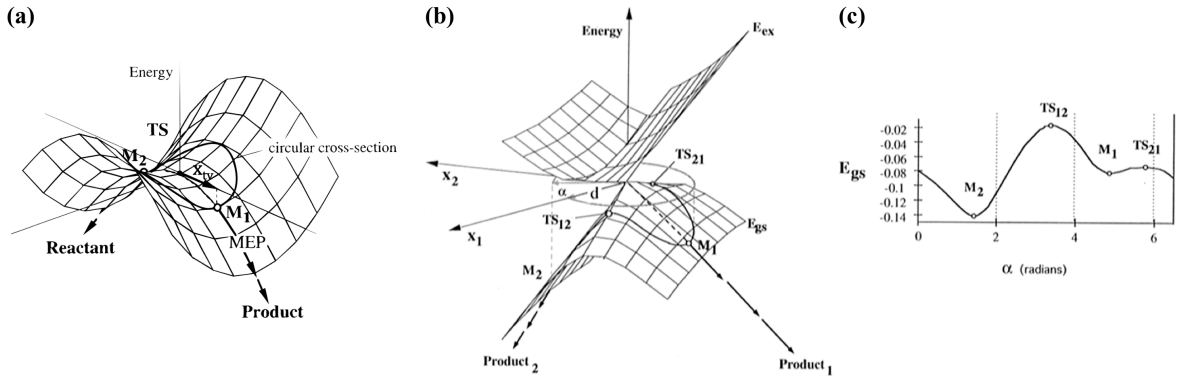

Figure 7. (a) Model PES showing a transition state (TS) and the corresponding energy profile along a circular cross section centered on the TS. (b) Model ground- (E_{gs}) and excited-state (E_{ex}) PESs for an elliptic conical intersection and the corresponding energy profile along a circular cross section centered on the crossing point. (c) E_{gs} energy profile along the circle defined in Figure 7b. The points M_1 and M_2 correspond to the two energy minima located along the circular cross section. The points TS_{12} and TS_{21} correspond to the two transition structures connecting M_1 and M_2. (Adapted from reference [63b])

In fact, for the elliptic cone model discussed above, there can be at most two minima (M_1 and M_2) defining two distinct IRDs (excluding the case where the cone becomes circular in which case there are an infinite number of equivalent directions of relaxation).[23] These minima are located within the branching space $\{\mathbf{x}_1, \mathbf{x}_2\}$. However, this model of the potential energy sheets at a conical intersection point is not general enough to give a correct description of all relaxation paths for a real system. Firstly, as illustrated in Figure 3b, there may be more than two possible IRDs originating from the same conical intersection. Secondly, some IRDs may lie "out" of the branching space since the real $\{\mathbf{x}_1, \mathbf{x}_2\}$ space is, in general, curved. However, the ideas introduced above can be easily extended to search for IRDs in the full n-dimensional space surrounding a conical intersection point by replacing the circular cross section with a hyperspherical cross section centered at the vertex of the cone. Thus the search for energy minima in a one-dimensional circular cross section (i.e., the circle in Figure 7b) is merely extended to an n–1 dimensional spherical cross section of the ground-state PES (i.e., a hypersphere), and the IRD will then be defined by the energy minima located on the hypersphere.

We must emphasize that the procedure outlined above is designed to locate the points where the relaxation paths begin (i.e., they define the IRDs). Once these points have been found for some small value of the hypersphere radius, then one must compute the associated MEP which defines the relaxation paths leading to a ground-state energy minimum. The standard IRC method[58] can be used for that purpose. As a consequence, the approach outlined above provides a systematic way to find the MEP connecting the vertex of the cone to the various ground-state photoproduct wells.

The whole procedure described above allows a reliable description of the photochemical reaction path. However, computations of MEP can become prohibitively expensive depending on the actual cost of the electronic structure method used to determine the PES. Alternative but more approximate methodologies exist such as *relaxed potential energy surface scans* along a given coordinate, and *linearly-interpolated transit path* (also called *linear least motion path*) calculations. Relaxed scans can lead to wrong pathways if the coordinate chosen for the scan is too approximate. Pathways based on intermediate geometries obtained from linearly-interpolated structures in internal coordinates are simple but very approximate. This method is useful for locating transition states and for providing an upper bound on the energy profile associated with a reaction path.

3.2. Excited-state molecular dynamics

The techniques outlined above provide information on the structure and accessibility of the photochemical reaction paths. As mentioned, this information is structural (i.e., non-dynamical) and provides insight into the mechanism of photoproduct formation from vibrationally "cold" excited-state reactants such as those encountered in many experiments where slow excited-state motion or/and thermal equilibration is possible (in cool jets, in cold matrices and in solution). In many cases, such structural or static information is not sufficient. Since reacting molecules have usually a finite amount of kinetic energy, a trajectory will not follow the MEP and may, in principle, deviate quite dramatically from it (e.g., in the case of "hot" systems where there is substantial vibrational energy). In this case, regions of the potential energy surface far from the computed photochemical reaction path may become important and a dynamical treatment of the reaction is unavoidable. In other words, in these cases, the photochemical reaction path may not provide a realistic nuclear motion followed by the system. We already discussed (see section 2.3) that to understand photochemical reactivity it may

be necessary to go beyond the idea of following a reaction path through a minimum energy conical intersection, and to look not only at how the reaction coordinate relates to the intersection seam, but also at the actual dynamical path of the system. In short, we need to know where the system meets the intersection seam in order to determine where it crosses to the ground state, and this depends not only on the topology of the potential energy surfaces but also on the dynamics of the system, i.e. the momenta of the particles. In addition, knowing the dynamics of a molecular system will provide detailed information about its time-evolution after photoexcitation giving access to timescales of the reaction and important experimental observables such as excited-state lifetimes, products quantum yield and branching ratios. Thus, understanding the underlying ultrafast dynamics of a molecule undergoing a photochemical process will help interpreting experimental data, be a powerful tool to predict the photochemical behavior of systems for which no experimental data are available, and even help designing new devices with a particular function.

If the PESs are known, the time-dependent Schrödinger equation can in principle be solved directly using what are termed wavepacket dynamics.[64] Here, a time-independent basis set expansion is used to represent the wavepacket and the Hamiltonian. The evolution is then carried by the expansion coefficients. While providing a complete description of the system dynamics, this approach represents however a formidable computational task and in practice, these methods are restricted to the study of typically 3 to 6 degrees of freedom. Even the highly efficient multi-configuration time-dependent Hartree (MCTDH) method,[65] which uses a time-dependent basis set expansion, can handle no more than 30 degrees of freedom. Recent developments[66] based on the variational multiconfiguration Gaussian (vMCG) wavepacket method[30] look very promising to treat larger molecules, but the description of such a method is out of the scope of this manuscript, as it has not been used here. Instead, we resorted to *semiclassical* simulations.

In the classical limit of the Schrödinger equation and in the case of an evolution on a single sheet of PES (adiabatic or Born-Oppenheimer approximation), the evolution of the wavepacket density can be simulated by a 'swarm' of classical trajectories driven by Newton's equations of motion

$$M\ddot{\boldsymbol{R}} = -\boldsymbol{\nabla} V$$

where V is the potential and $\ddot{\boldsymbol{R}}$ is the second-derivative of the position with respect to time, that is the acceleration. This approach is called *molecular dynamics* (MD). In ab initio MD, the potential V is obtained by solving the electronic Schrödinger equation. Then, the dynamics is designated as semiclassical because nuclei motion is treated classically, while the electrons are described quantum mechanically. In addition, we have to resort to *direct* or *on-the-fly* MD.[28–31,67] In contrast to standard dynamics simulations that require a predefined (analytical) PES over which the nuclei move, the PES (i.e., V) is provided here by explicit evaluation of the electronic wavefunction at every integration step along the trajectory. This makes the method very general and powerful, particularly for the study of polyatomic systems where the determination of an analytical multidimensional potential function is an impossible task. Because of the size of the systems reported in this manuscript, we have only carried out on-the-fly semiclassical dynamics simulations and we present in the following the two different approaches that we used to include nonadiabatic effects.

To add nonadiabatic effects to semiclassical methods, it is necessary to allow the trajectories to sample the different surfaces in a way that simulates the population transfer between electronic states. The simplest way to add a nonadiabatic correction is to use what is known as *trajectory surface*

hopping (TSH). First introduced on an intuitive basis by Bjerre and Nikitin,[68] and Tully and Preston,[69] a number of variations have been developed and reviews on the TSH methodology can be found in reference [70]. These methods all use standard semiclassical trajectories which use the hopping procedure to sample the different states, and so add nonadiabatic effects. The motivation comes from the early work of Landau[71] and Zener.[72] The Landau-Zener model is for a classical particle moving on two coupled one-dimensional potential energy curves. If the diabatic states cross so that the energy gap is linear with time, and the velocity of the particle is constant through the nonadiabatic region, then the probability of transition from adiabatic state 2 to adiabatic state 1 is given by

$$P_{2\to 1} = \exp\left(-\frac{1}{4}\pi\xi\right)$$

where ξ is the so-called Massey parameter[73]

$$\xi = \frac{\Delta E}{\hbar \frac{\partial R}{\partial t}\left\langle \psi_1 \middle| \frac{\partial \psi_2}{\partial R}\right\rangle} = \frac{\Delta E}{\hbar \dot{\boldsymbol{R}} \cdot \boldsymbol{h_{12}}}$$

where ΔE is the energy gap between the two adiabatic states and $\dot{\boldsymbol{R}} \cdot \boldsymbol{h_{12}}$ is the product of the velocity of the particle by the nonadiabatic coupling vector. This product can be rewritten as $\langle \psi_1 | \partial \psi_2 / \partial t \rangle$ and is often referred to as the *time-dependent nonadiabatic coupling* (also called *kinetic coupling* or *dynamic coupling*) responsible for the nonadiabatic transitions. Indeed, according to the Landau-Zener formula given above, for a vanishingly small energy gap, or a very large nonadiabatic coupling, such as encountered when the system approaches a conical intersection, the probability of changing adiabatic states approaches unity. We used two different surface hopping procedures to perform our on-the-fly TSH simulations. They are briefly presented below.

Tully's fewest switches surface hopping. The most popular implementation of the TSH method is based on Tully's fewest switches algorithm (FSA),[69,74] which gives a good compromise between accuracy and computational efficiency. In the FSA the quantum amplitudes are propagated coherently along the trajectory and the transition (i.e., hopping) probabilities are proportional to the variation of the quantum state populations with the constraint that the number of transitions (i.e., hops) is required to be as small as possible. In the adiabatic representation, the probability of hopping from the adiabatic surface 2 to the adiabatic surface 1 is given by

$$P_{2\to 1} = \max(0, q_{21})$$

with

$$q_{21} = \frac{2\int_t^{t+\Delta t} Re\left(c_2^*(\tau)c_1(\tau)\left[\dot{\boldsymbol{R}} \cdot \boldsymbol{h_{12}}\right]\right)\mathrm{d}\tau}{c_2(t)c_2^*(t)}$$

The complex-valued coefficients *c* are the quantum amplitudes of the expansion of the total electronic wavefunction in the basis of the adiabatic states and are obtained from the solution of the time-dependent Schrödinger equation.

To determine whether a switch from state 2 to state 1 will occur at each time step, a uniform random number ζ between 0 and 1 is generated and, in a two-state case, the hopping is performed if

$$\zeta < P_{2\to1}$$

In the case a surface hop is achieved, the velocity components are adjusted in the direction of the nonadiabatic coupling vector $\boldsymbol{h_{12}}$ in order to conserve the total energy of the system. If there is not enough velocity (kinetic energy) in the direction of the nonadiabatic coupling vector to maintain energy conservation during a hop, the hop is classically forbidden and is rejected.

Although the FSA is conceptually very simple, its implementation requires the computation of nonadiabatic coupling vectors and the integration of quantum amplitudes at every point of the trajectory. Moreover, the exact transition probability is given by a complex expression that involves, in addition to nonadiabatic couplings, also the relative phases of the real and imaginary components of the quantum amplitudes. For these reasons the use of the FSA may be impractical for the study of large systems or for QM/MM applications, where the explicit computation of nonadiabatic coupling vectors may no longer be feasible. In such cases it is desirable to use more approximate switching methods that involve a numerical evaluation of the nonadiabatic couplings in terms of wavefunction overlap at successive time steps, as proposed in the following approach.

Diabatic surface hopping. To decide when to undergo a transition to a different potential energy surface, one would in principle need to compute $\langle\psi_1|\partial\psi_2/\partial\mathrm{t}\rangle$ at every time step (Δt) of the simulation. In practice, however, it is possible to approximate $\langle\psi_1|\partial\psi_2/\partial\mathrm{t}\rangle$ as $\langle\psi_1(t)|\psi_2(t+\Delta t)\rangle/\Delta t$, i.e. the overlap between the excited-state wavefunction at the current time step and the ground-state wavefunction at the previous time step. In the case of simulations performed at the CASSCF level with state-averaged (SA) orbitals to model the wavefunctions, one can compute the overlap as the inner product of the corresponding SA-CASSCF eigenvectors $\boldsymbol{C}_1$ and $\boldsymbol{C}_2$:

$$\langle\psi_1(t)|\psi_2(t+\Delta t)\rangle = \boldsymbol{C}_1^t \cdot \boldsymbol{C}_2^{t+\Delta t}$$

Calculating the energy gap ΔE and $\boldsymbol{C}_1^t \cdot \boldsymbol{C}_2^{t+\Delta t}$ at every time step is straightforward, and we can use the Landau–Zener formula to calculate the probability of a transition between the two electronic states. In principle, the transition probability can be used to spawn a new trajectory on the other surface. However, since this procedure would lead to multiple trajectories that have to be computed simultaneously, spawning is too demanding in practice. In our diabatic surface hopping approach,[56] we only restrict hopping to situations where the transition probability approaches unity. This happens at the conical intersection seam, where $\Delta E \approx 0$ and $\boldsymbol{C}_1^t \cdot \boldsymbol{C}_2^{t+\Delta t} \approx 1$.

Because surface hopping is only allowed at the conical intersection seam, classical trajectories follow the same diabatic state at the crossing. Therefore, energy and momentum are obviously conserved. In principle, this strict diabatic hopping criterion could lead to an underestimation of the population transfer probability, because a surface hop in regions with strong nonadiabatic couplings far from the intersection is prohibited. In practice, however, the high dimensionality of the seam ensures that all trajectories encounter such regions of high transfer probability. A major advantage of restricting hopping to the seam is that we obtain information on the location of the seam in our trajectories. The latter is important for example to understand how the interactions between a chromophore and its environment alter the topology of the surfaces and the seam and thereby control the outcome of the photochemical process. The Landau–Zener model is clearly an approximation, but can help to keep a proper physical insight, which is crucial for understanding complex systems.

4. Applications: from organic photochemistry to photobiochemistry and inorganic photochemistry

After presenting some of the concepts and tools required to investigate photochemical processes from a theoretical point of view, we will now illustrate the power of computational photochemistry to rationalize and sometimes predict the excited-state behavior of various molecular systems, ranging from simple organic chromophores to biomolecules and transition metal complexes.

4.1. Organic photochemistry

4.1.1. *Photostability of polycyclic aromatic hydrocarbons*. The main aim of this series of studies is to present a consistent mechanistic picture for the photophysics of small cationic polycyclic aromatic hydrocarbons (PAHs). PAHs and their cations are of great interest in the field of astrophysics. PAH cations are extremely photostable following electronic photoexcitation and have been extensively studied as the leading candidates for the diffuse interstellar bands (DIBs).[75] Very little is known about their photophysics and reactivity, partly because of their inherent nonfluorescence and difficulties in isolating charged species. Gas-phase photofragmentation studies of a variety of PAH monocations have shown the high photostability of these species (dissociation onsets of 4-4.5 eV) and suggest fast relaxation times.[76] Their tendency to return efficiently on an ultrafast timescale to the ground-state reactant structure after electronic photoexcitation, without forming new photoproducts directly, was later confirmed and shown to be remarkable.[77] In the following, we present the main theoretical results obtained on naphthalene ($N^{\bullet+}$),[78] pyrene ($Py^{\bullet+}$)[79] and perylene ($Pe^{\bullet+}$)[80] radical cations, which allow a rationalization of their distinct photophysical behaviors.

Naphthalene cation. Relaxation dynamics study of cold (10–100 K) $N^{\bullet+}$ isolated in boric acid glass using transient grating spectroscopy revealed rapid and efficient relaxation of $N^{\bullet+}$ down to its ground state after photoexcitation at 680 nm to its D_2 state. A two-step relaxation kinetics was unveiled with a fast component (<200 fs) and a slow component (ca. 20 ps). The two steps were interpreted as an initial rapid D_2 to D_0 internal conversion, followed by slow vibrational relaxation of the hot D_0 state. The authors of this study further postulated that the observed fast step is due to the $D_1 \rightarrow D_0$ relaxation, concluding that the $D_2 \rightarrow D_1$ relaxation occurs on a timescale too short to be measured by their apparatus (<1 fs). Our computational study aimed at understanding this photophysical behavior from a simple static approach.[78]

The results of our CASSCF and CASPT2 calculations are summarized in Figures 8, 9 and 10. Figures 8 and 9 show the CASSCF potential energy profiles of the three electronic states involved in the photophysics of the naphthalene cation. These states are the ground, $D_0(A_u)$, and the first two excited states, $D_1(B_{1u})$ and $D_2(B_{2g})$ (where the label D_n refers to the order obtained for vertical transitions). The potential surface is displayed on two separate diagrams for clarity, because the reaction coordinate is not the same in both cases. All the optimized minima and crossings have D_{2h} point group symmetry and the structures are drawn up on these figures. The energy gradient vectors of the states at the Franck-Condon points and crossings are opposite to the forces acting on the molecule. These are shown to the right in Figures 8 and 9 to illustrate the driving force for the photophysics and the nature of the reaction coordinate, which is along the symmetry-preserving gradient difference vector ($\mathbf{x_1}$) in each case.

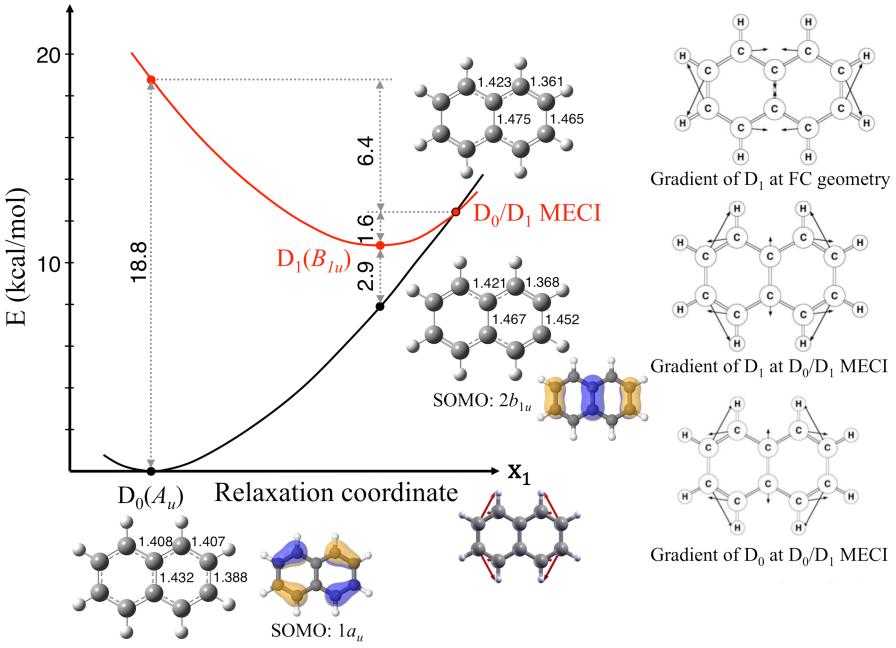

Figure 8. Optimized critical points of the naphthalene radical cation using CASSCF/6-31G* on the D_0 and D_1 states. Energies in kcal/mol. Vectors to the right display the energy gradients at the intersection and FC geometry.

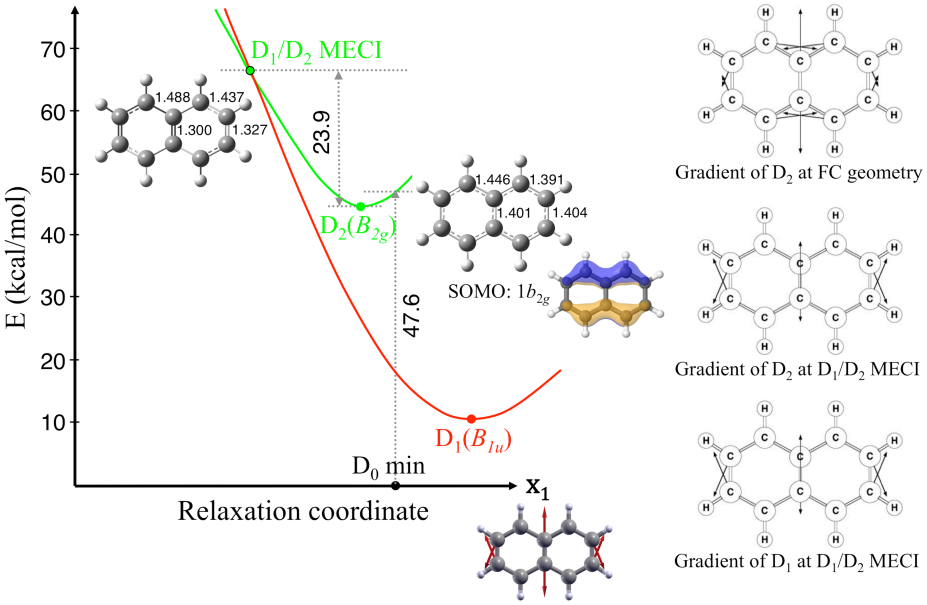

Figure 9. Optimized critical points of the naphthalene radical cation using CASSCF/6-31G* on the D_1 and D_2 states. Energies in kcal/mol. Vectors to the right display the energy gradients at the intersection and FC geometry.

Upon excitation to the D_2 state, the system will relax to the nearby D_2 minimum. The initial forces acting on the system correspond to the opposite of the gradient difference vector and points directly towards a D_1/D_2 MECI. This crossing is located over 20 kcal/mol above the D_2 minimum however. Upon nonradiative decay at the crossing region, the system further relaxes on the D_1 PES. The forces then drive the system directly towards the D_1 minimum. Along the same direction is located an easily accessible D_0/D_1 MECI less than 2 kcal/mol above this minimum. This funnel allows for a fast internal conversion back to the ground state. The photophysical mechanistic picture that emerges from these calculations is thus rather simple. It is illustrated in Figure 10. The efficient and ultrafast ground-state

recovery upon photoexcitation of $N^{\bullet+}$ results from easily accessible funnels between the populated electronic states. These funnels correspond to sloped conical intersections and the forces acting on the nuclei drive the system efficiently toward these funnels. Note however that, at the CASSCF level, the D_1/D_2 MECI is too high in energy to account for the ultrafast decay observed experimentally. Only at the CASPT2 level is the picture in better agreement with the experimental measurements. Indeed, at this level of calculation, the D_1/D_2 MECI is lowered in energy relative to the D_2 minimum energy. This is a direct consequence of larger correlation energy in the D_0 and D_2 states compared to the D_1 state.

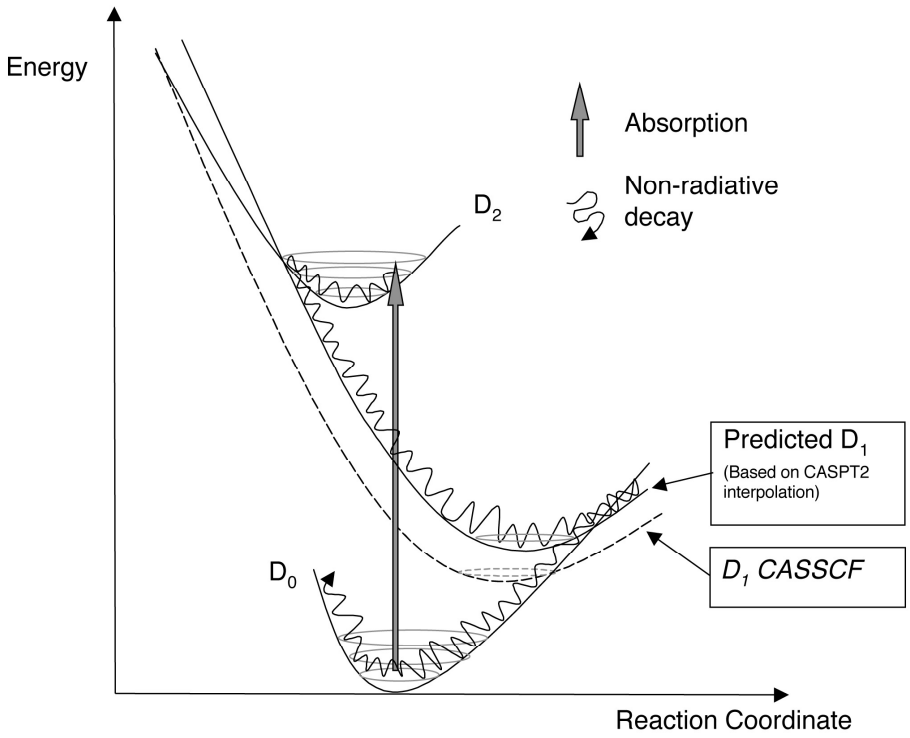

Figure 10. Schematic representation of the electronic relaxation mechanism of the naphthalene radical cation. Dashed curve: original CASSCF/6-31G* result for D_1 state. Solid curve: predicted relative increase in D_1 energies indicated by CASPT2 calculations, suggesting a lower energy D_1/D_2 MECI, allowing for nonradiative relaxation.

It is remarkable to note that the photophysics of $N^{\bullet+}$ is very different from that of its neutral counterpart. Neutral naphthalene (N) is known to exhibit mainly fluorescence in the near ultra-violet (UV) after photoexcitation to the S_1 excited state.[81] Like in benzene, it can probably undergo photoisomerization reactions to produce valence isomers such as naphthvalene and/or benzofulvene. This is in contrast with the ultrashort excited-state lifetime observed in $N^{\bullet+}$. Figure 11 compares the potential energy profiles of neutral and cationic naphthalene in the ground and first excited states. The $S_0 \rightarrow S_1$ vertical transition energy in N is much larger than the corresponding $D_0 \rightarrow D_1$ vertical transition energy in $N^{\bullet+}$. This is expected based on the nature of the excited states. The S_1 state of N results from transitions between occupied π orbitals to unoccupied (virtual) π^* orbitals ($\pi \rightarrow \pi^*$ transitions), while the D_1 state of $N^{\bullet+}$ results from a transition between occupied π orbitals ($\pi \rightarrow \pi$ transition). Therefore, it is not surprising that the energy gap is much lower in the cationic species. Upon geometry optimization of the excited state, the structure remains highly-symmetric (i.e., D_{2h} symmetry) both in

N and $N^{\bullet+}$. However, the energy gap with the ground state remains very large in N, while it is considerably reduced in $N^{\bullet+}$. As a consequence, crossing with the ground state can only occur in N upon pyramidalization of a benzene ring, which is an activated process with a barrier of about 30 kcal/mol. Thus, unless the system has enough vibrational kinetic energy to overcome this barrier, the system will remain trapped in the S_1 minimum until radiative decay (fluorescence) occurs. If the excitation energy is high enough to provide the system with sufficient energy to overcome the barrier, then the S_0/S_1 conical intersection can be reached and nonradiative decay to the ground state becomes efficient. The system can either return back to its original naphthalene structure, or, because of the peaked topology of the MECI, lead to new photoproducts corresponding to valence isomers. This behavior is very similar to the one observed in benzene (see Figure 1).

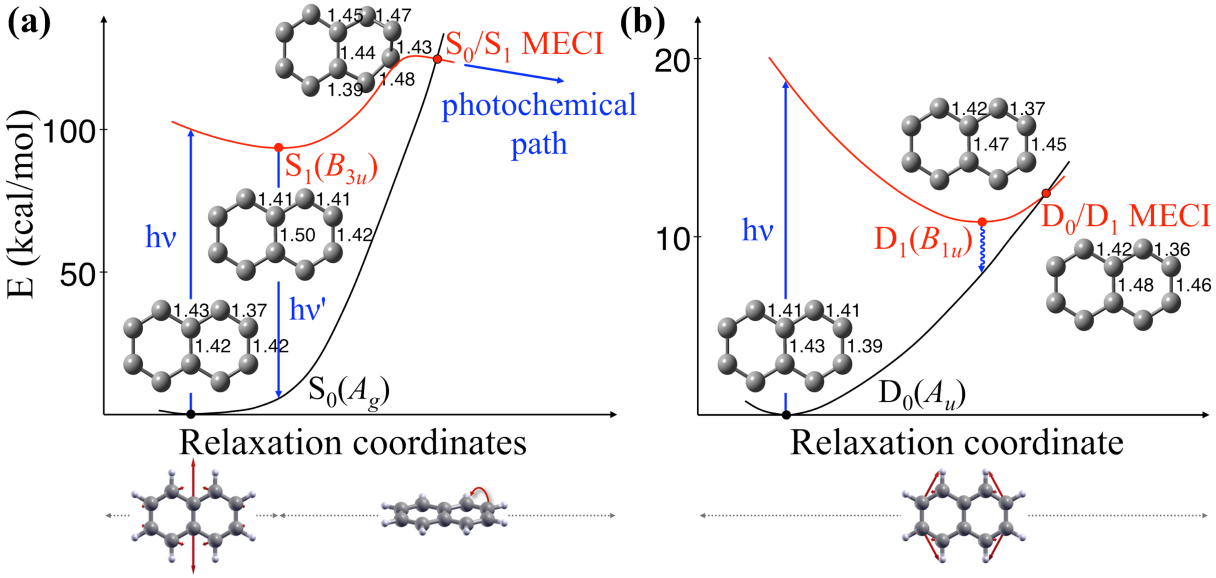

Figure 11. Comparison of the CASSCF potential energy profiles in the ground and first excited states of (a) neutral naphthalene and (b) naphthalene radical cation. The neutral PAH exhibits fluorescence or photoproducts formation depending on excitation energy, while the cationic PAH is highly photostable.

Pyrene cation. Regarding $Py^{\bullet+}$ no time-resolved photodynamics study has been reported so far. Because this cation is often considered to be a strong candidate for one of the DIB carriers,[82] we have investigated the topological features of the relevant PESs for this system.[79] The results are summarized in Figure 12. The presence of two easily accessible sloped D_1/D_2 and D_0/D_1 conical intersections suggests that $Py^{\bullet+}$ is highly photostable, with ultrafast nonradiative decay back to the initial ground-state geometry predicted via a mechanism similar to the one found in $N^{\bullet+}$. However, the two funnels involved are even more accessible in $Py^{\bullet+}$ compared to $N^{\bullet+}$, suggesting a shorter excited-state lifetime in this case. Thus, like for $N^{\bullet+}$, our model also predicts $Py^{\bullet+}$ to be nonfluorescent.

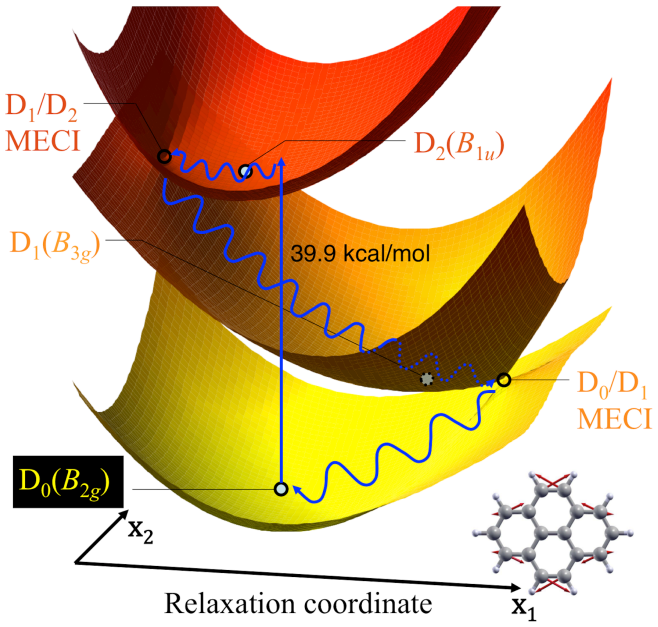

Figure 12. Schematic representation of the potential energy landscape and nonradiative electronic relaxation mechanism of the pyrene radical cation.

Perylene cation. By contrast with other PAH radical cations, $Pe^{\bullet+}$ seems to present a different photophysical behavior. While most small PAH cations display ultrafast ground-state recovery (<200 fs) in boric acid glass,[77] much longer times from 19 ps[77] up to 35 ps[83] were needed in the case of $Pe^{\bullet+}$. Even longer ground-state recovery times of up to 100 ps were obtained in a Freon glass at 77 K.[84] An exceptionally large D_0–D_1 energy gap inhibiting the internal conversion was put forward as a possible explanation for this behavior.[77] Photoinduced fluorescence of $Pe^{\bullet+}$ has been observed in neon and argon matrices at ~10 K.[85] This was the first report of the fluorescence spectrum of a PAH cation in any phase. However, a gas-phase experiment failed to reproduce these matrix results, for reasons that remain unclear.[86] Because of the distinct photophysical behavior of $Pe^{\bullet+}$ and apparently controversial experimental observations on the luminescence property of this radical cation, we were interested in investigating the ground and lowest excited-state PESs of this cation in order to rationalize the experimental results.[80] Figure 13 synthesizes the results. Photoexcitation to the D_2 state in the vicinity of a peaked D_1/D_2 MECI leads to ultrafast nonradiative decay to the D_1 state. Vibrational relaxation can then lead to populate two distinct excited-state minima on the D_1 PES. The most important result concerns the absence of accessible in-plane surface crossings between the D_0 and D_1 states; crossings which we have previously found for $N^{\bullet+}$ and $Py^{\bullet+}$, as discussed above. This accounts for the longer excited-state lifetime in $Pe^{\bullet+}$ and the most likely decay mechanism from the first excited state is a radiative deexcitation, in agreement with reference [85]. Note that we cannot completely rule out a competition with a nonradiative decay route via out-of-plane distortions, which may explain the absence of emission observed in reference [86], although fragmentation may also be connected with this.

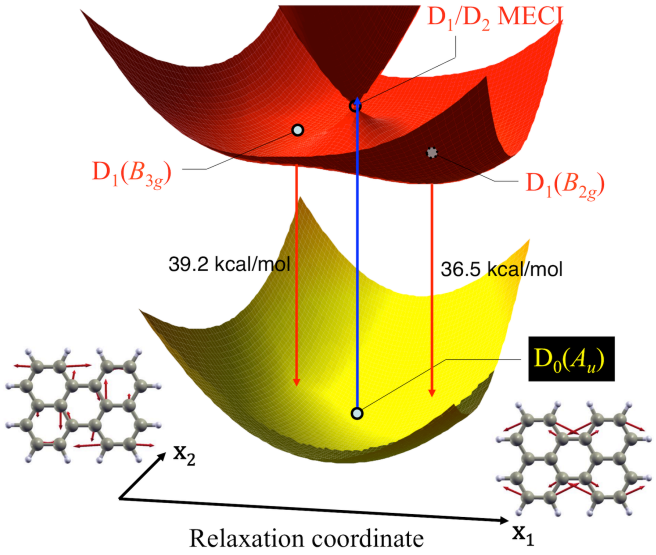

Figure 13. Schematic representation of the potential energy landscape and radiative electronic relaxation mechanism of the perylene radical cation.

4.1.2. *Photochromic systems*. Photochromism represents an increasing area of research in photochemistry because of its actual and potential applications. It is defined as a reversible phototransformation of a molecule between two forms having different spectral properties. This process, however, may not only induce spectral changes, but also change of refractive index, dielectric constant, dipole moment, oxidation/reduction potential or geometry of a molecule. The reverse (backward) transformation may proceed photochemically using light irradiation of different wavelength, thermally, or in redox processes. Photochromic molecular systems have entered the new generation of innovative functional materials with high added value. Applications are already widespread in nanosciences, biology, and photonic or optoelectronic devices as light-activated switches.[87,88,89] Whether in molecular information storage, holography, or as photomechanical actuators, photochromic compounds convert photonic energy into chemical energy (e.g., selective bond-breaking and bond-making reactions) within an ultrafast (picosecond or sub-picosecond) timescale. The change in electronic and molecular structures following electronic excitation results in a change of physical properties, which forms the basis of the applications listed above.

While the ultimate interest for these compounds is device applications, we are compelled to understand the mechanism of action of these and other photoactive molecules. Thus, knowledge and understanding of the precise reaction mechanisms underlying their photochromic activity at the molecular level are of particular interest because they are necessary for a rational design of new molecular systems with improved photochromic properties, potentially leading to innovative devices.

Various classes of photochromic compounds are currently under study as photochromic materials. The vast majority of them rely on organic compounds. One of the largest groups of photochromic switches is based on ring-opening/ring-closure reactions in photoinduced electrocyclic reactions. The systems presented below belong to this main class of molecular switches.

Dihydroazulene / vinylheptafulvene photochromism. The photochemical ring-opening reaction of dihydroazulene (DHA) to give vinylheptafulvene (VHF) (Scheme 3) is rapid and efficient, but VHF is photostable and does not react photochemically from the S_1 state to give DHA; the backward reaction only takes place thermally or via two-photon excitation.[90] We will show in the following that most of

these experimental observations can be explained by a conical intersection between the S_1 and S_0 states.[91]

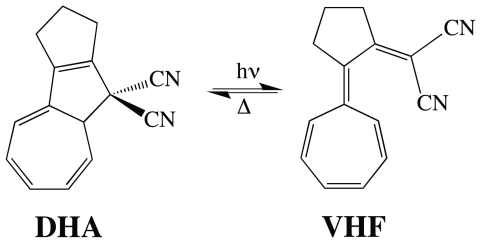

Scheme 3. The dihydroazulene (DHA) / vinylheptafulvene (VHF) photochromic system.

The S_0 and S_1 potential energy profiles along the reaction coordinate are shown in Figure 14 along with the main relaxation pathways. Upon photoexcitation to the S_1 state of DHA, the system relaxes to a local S_1 DHA diradicaloid minimum (M* on Fig. 14) following a complete inversion of single and double bonds within the π-system. Then, upon stretching the σ-bond that breaks to produce VHF, the system reaches a transition state TS* (11 kcal/mol above M* but 24 kcal/mol below the S_1 Franck-Condon energy) characterized by a transition vector dominated by adiabatic σ-bond breaking. Beyond the transition structure, the system proceeds downhill and barrierless to a conical intersection, S_0/S_1 MECI, which corresponds to the lowest energy point on the S_1 PES (over 50 kcal/mol below M*). This crossing presents a VHF-like structure, i.e. the 5-membered ring is opened, and at this funnel, efficient radiationless decay to S_0 will take place producing the VHF isomer (M_{VHF}). This picture is consistent with the observation of fluorescence following photoexcitation of DHA, as there is a local DHA S_1 minimum. The DHA→VHF isomerization quantum yield increases, at the expense of the emission efficiency, when the temperature is increased. This is consistent with the activated process to reach the funnel for photoisomerization.

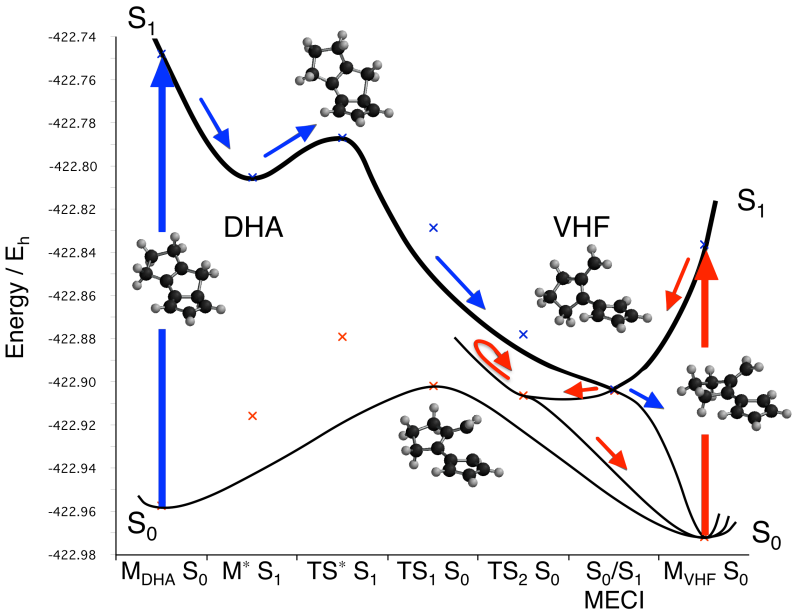

Figure 14. S_0 and S_1 potential energy profiles along the reaction paths of a relevant DHA/VHF model system. DHA→VHF photochemical path indicated by blue arrows. VHF→VHF photophysical path indicated by red arrows. Red and blue crosses indicate the S_0 and S_1 energies at various critical points.

In fact, the MEP calculated from TS* in the VHF direction does not actually reach S_0/S_1 MECI itself, the lowest-energy point optimized on the intersection. Instead, the MEP terminates at a higher energy point on the crossing seam, denoted S_0/S_1 X, which is over 30 kcal/mol above the MECI. This is made possible because the ring-opening reaction coordinate involves mainly a C-C σ-bond breaking, while the degeneracy-lifting coordinates at the S_0/S_1 MECI are dominated by rearrangements of the fulvene ring alone in the DHA/VHF model system (or of the seven-membered ring in the real system shown in Scheme 3). Thus, a crossing hyperline persists along the DHA→VHF reaction path (Figure 15). In addition to its higher energy, S_0/S_1 X is characterized by a shorter C-C bond distance for the broken σ-bond of 2.45 Å compared to the 3.45 Å C-C bond distance at S_0/S_1 MECI. This confirms that the MEP is intercepted by the crossing seam well before reaching the MECI. Analysis of the decay routes at S_0/S_1 X shows that the system may return to M_{DHA} or form M_{VHF} but, for inertial reasons, product formation will be highly favored over reactant regeneration.

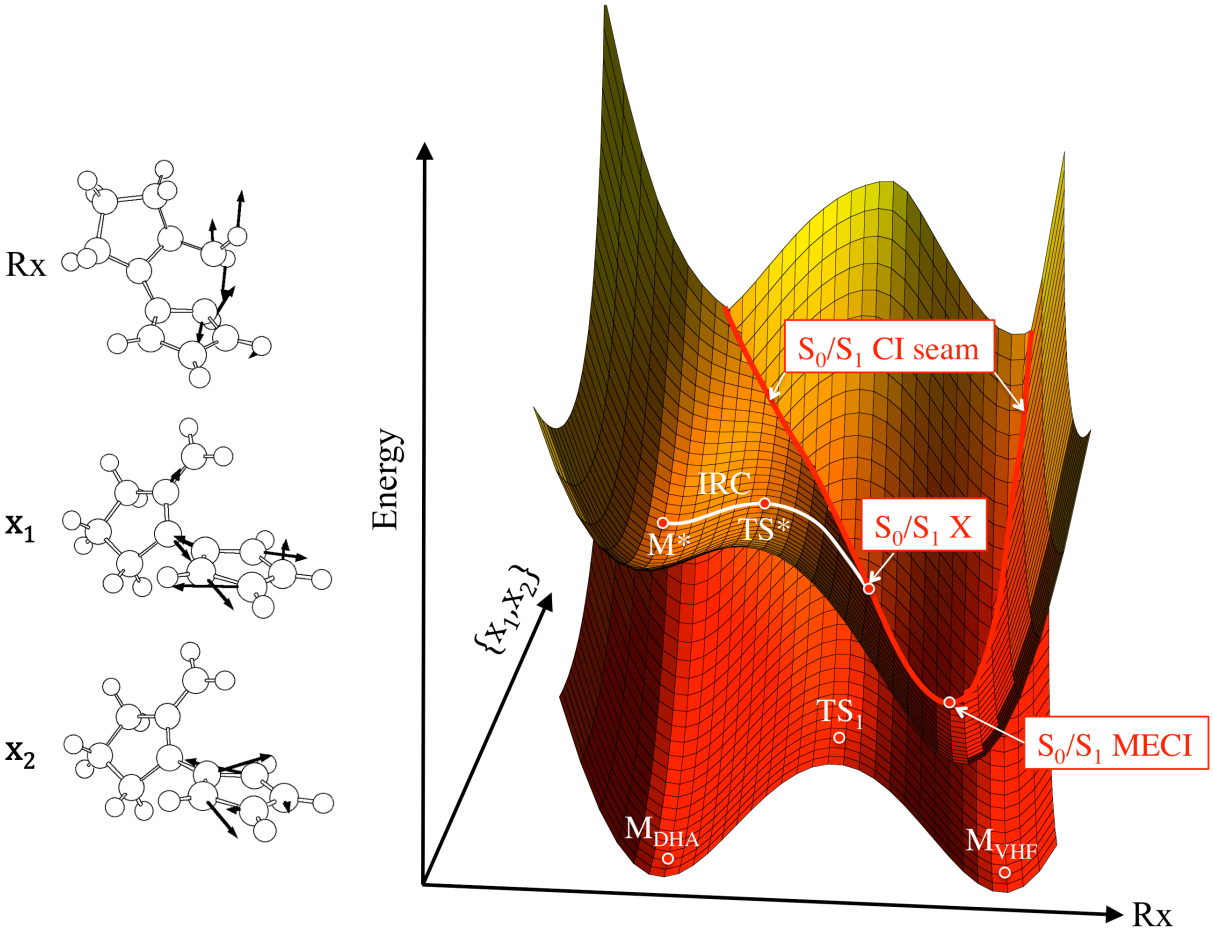

Figure 15. S_0 and S_1 potential energy landscape along the reaction path corresponding to the DHA→VHF photoisomerization. The IRC computed at TS* is indicated by the white line and shows how it is intercepted by the conical intersection seam at the structure S_0/S_1 X, lying much higher in energy than the minimum energy conical intersection, S_0/S_1 MECI. The relevant coordinates for mechanistic photochemistry are shown on the left for a DHA/VHF model system: the reaction coordinate Rx is orthogonal to the branching space.

Upon photoexcitation to the S_1 state of VHF, the system relaxes directly towards the S_0/S_1 MECI. The relaxation coordinate corresponds to the gradient difference vector characterizing the S_0/S_1 MECI. Consequently, the MEP on S_1 is naturally driven to the MECI like in the 'sand in the funnel' model (Figure 16). The topological feature on S_0 around this conical intersection only allows the system to reform VHF. After nonradiative decay to S_0 at the MECI, the system relaxes towards a transition state (TS_2). TS_2 has a very similar geometry to the S_0/S_1 MECI and is the lowest point along the $\mathbf{x_1}$ reaction path leading from M_{VHF} through the MECI onto S_0. Continuing on the same path through TS_2 leads to a steep rise in energy (Figures 14 and 16), and molecules approaching the S_0/S_1 MECI from the VHF side will therefore be reflected on this barrier back toward M_{VHF}. These particular topological features around the conical intersection account for the high photostability of VHF. Moreover, the presence of the S_0/S_1 MECI as the lowest critical point on the S_1 PES in the VHF region also explains the lack of fluorescence upon excitation of VHF.

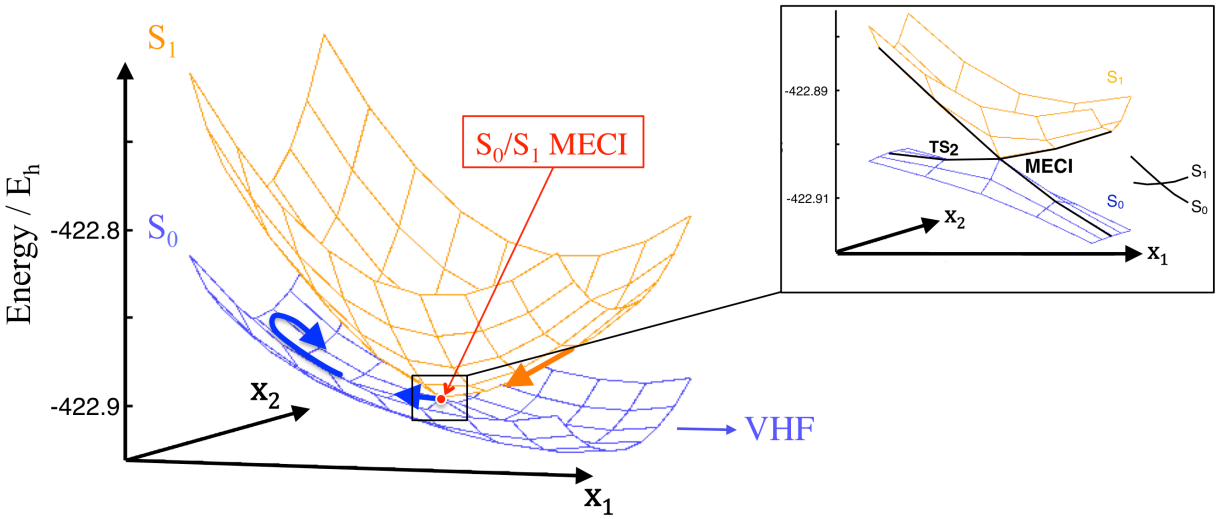

Figure 16. Topology of S_0 and S_1 PES in the vicinity of the S_0/S_1 MECI. Grid obtained by CASSCF single-point energy calculations at scanned structures along $\mathbf{x_1}$ and $\mathbf{x_2}$. The relaxation coordinate following VHF excitation to S_1 corresponds to $\mathbf{x_1}$. Thus, the MEP leads directly to S_0/S_1 MECI, as indicated by the orange arrow. After decay to S_0, a steep rise in energy is encountered along $\mathbf{x_1}$ and the system reverts back toward VHF.

Both the highly efficient DHA→VHF photoisomerization and high VHF photostability were confirmed by on-the-fly CASSCF[91] and MMVB[54] molecular dynamics. All the trajectories performed from TS* ended up producing VHF, while none of the trajectories started from VHF produced DHA. In addition, these dynamics simulations also illustrated the access of the higher energy part of the crossing seam in the region of S_0/S_1 X during the DHA→VHF photoisomerization.

Dithienylethenes photochromism. Dithienylethenes (DTEs) belong to the diarylethene family and are remarkable photochromic systems where the chemical transformation involves a ring-opening reaction via single bond breaking (Scheme 4). These systems exhibit remarkable switching sensitivity and rapid response: both ring-opening (cycloreversion) and ring-closure (cyclization) reactions occur with high quantum yields and in the picosecond time domain.[88a]

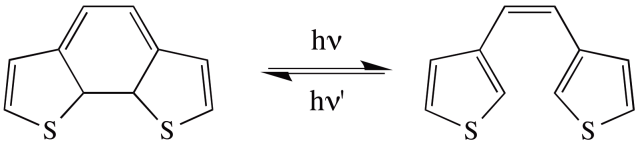

Scheme 4. Dithienylethene (DTE) photochromic system.

Because the distribution of π-bonds is different in both isomers, they have distinct absorption spectra. We will show that the photophysics and the efficiency of the system are completely controlled by the relationship between the reaction path and the degeneracy-lifting coordinates at an S_0/S_1 MECI. Figure 17 shows a cartoon of the dithienylethene S_0 and S_1 PESs that can be derived from the static and dynamics computations reported in reference [92]. There is a ground-state thermal reaction path involving a transition state TS connecting the closed-ring isomer (DTE_c) to the open-ring isomer (DTE_o). In addition, there is an adiabatic reaction path on the excited state involving a closed-ring minimum (DTE_c*), a transition state TS*, and an open-ring minimum (DTE_o*). Finally, a conical intersection seam, S_0/S_1 CI, runs along the reaction path as a result of the orthogonal character of the reaction coordinate with the branching space. Thus, decay to S_0 is controlled by motion orthogonal to the reaction path and dynamics simulations are necessary to explain why the conical intersection is accessible. Furthermore, the transition state (TS*) is a narrow bottleneck. Just because the system has enough energy to get over the transition state does not mean that it will find it. In fact, passing through the transition state will be a rare event: not only the energy needs to be sufficient, but also it needs to be distributed in exactly the right mode (i.e., the transition vector). A trajectory started at the Franck-Condon structure on the DTE_o side of the reaction will remain in the DTE_o* minimum for a "long" time and will not necessarily find the transition state. By contrast, the conical intersection is a many-dimensional hypersurface, and consequently more accessible. It is not a dynamical bottleneck in the same way as a transition state. Once the crossing seam is reached, decay to S_0 is immediate.

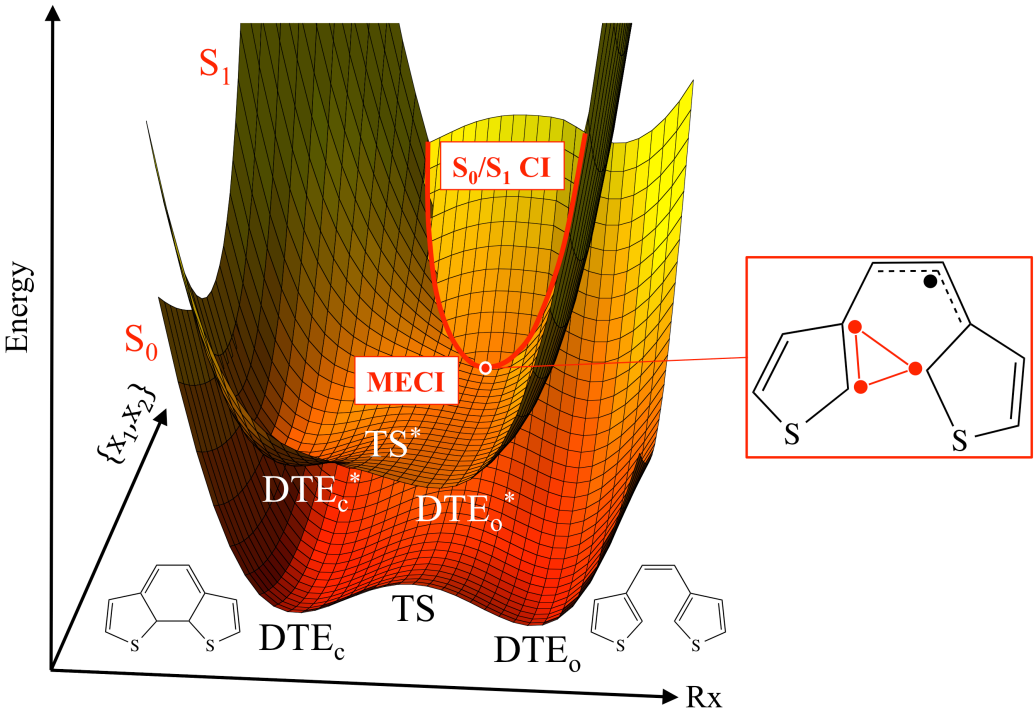

Figure 17. S_0 and S_1 potential energy landscape along the reaction path corresponding to the $DTE_c \rightarrow DTE_o$ photoisomerization. The reaction coordinate Rx is orthogonal to the branching space and the conical intersection appears as a seam running along Rx. The S_0/S_1 MECI structure is shown on the right.

The MECI on the conical intersection hyperline is shown in Figure 17. While it appears quite close to the transition state on the excited state, it is actually on the DTE_o side of the barrier. In the dynamics computations,[92] a typical trajectory (as shown in Figure 18) started from the Franck-Condon region on the DTE_o side of the reaction path lives in the DTE_o* minimum for almost two picoseconds, until a vibration that has enough energy inside the branching space (i.e., orthogonal to the reaction coordinate) drives it towards the CI seam and decay takes place to the ground state. The central point is that knowledge of the excited-state reaction path does not yield an understanding of the photochromism of this system. Simply finding the conical intersection points does not yield a complete picture, because they do not lie on the reaction path (note that the situation was different in DHA/VHF, as the intersection seam was intercepted by the reaction path). Indeed, a large segment of the intersection seam in this region is energetically accessible. However, to demonstrate and understand this, dynamics simulations need to be performed. Moreover, the MD simulations confirm that the crossing seam is reached before finding the "bottleneck" formed by the transition structure TS* on S_1. These simulations confirm the highly effective and ultrafast cyclization reaction.

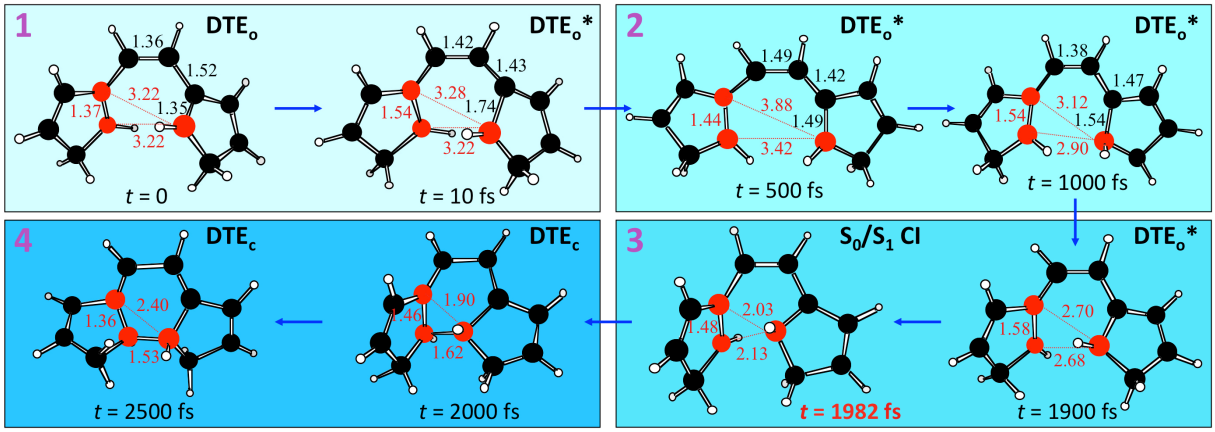

Figure 18. Description of the four phases in a typical MMVB trajectory on a prototype hydrocarbon model system started on the DTE_o side: 1) ultrafast relaxation to DTE_o*, 2) motion on S_1 in the DTE_o* minimum well, 3) energy flowing in one of the degeneracy-lifting coordinates and system decaying at the S_0/S_1 CI, and 4) ring-closure on S_0.

Experimentally, one observes fluorescence that is red-shifted, confirming that the position of the minimum is different on the excited state, as shown in Figure 17. The cyclization quantum yield (DTE_o* to DTE_c) is high, which arises from the fact that a trajectory from DTE_o* can sample the whole intersection seam, at right angles to the reaction path. On the other hand, for a trajectory starting from DTE_c*, the probability of decay to S_0 is low, because the main locus of the conical intersection seam appears to be on the DTE_o* side of the transition state. Thus, to reach DTE_o from DTE_c*, the system has to pass through the transition state TS* on the adiabatic excited-state reaction path. Hence, there is a competition between passing through the transition state to reach the reactive conical intersection on the DTE_o* side of TS*, decay at a nearby crossing on the DTE_c* side of the transition state (not shown in Figure 17), which does not lead to any reaction, and fluorescence from DTE_c*. This accounts for the relatively low cycloreversion quantum yield and its temperature-dependent character.

Dihydropyrenes photochromism. Dihydropyrenes (DHPs) also belong to the diarylethene family. However, in contrast with DTEs, DHPs have the particularity to be negative photochromes, which makes them highly interesting because the thermally stable isomer is the more colored one, while positive photochromes such as DTEs have the more stable form colorless. The colored form bleaches upon exposure to visible light corresponding to the formation of the cyclophanediene (CPD) isomer and returns to the colored DHP isomer upon exposure to UV light or in some cases thermally (Scheme 5).[93] However, the low DHP to CPD isomerization quantum yields and a fast rate of thermal back reaction in these compounds were representing an obstacle for their use as efficient photochromic systems.

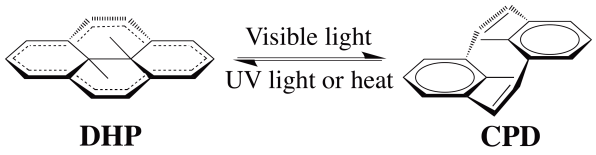

Scheme 5. The dimethyldihydropyrene (DHP) / cyclophanediene (CPD) photochromic system.

The reasons behind this lack of efficiency was rationalized based on an extensive CASSCF/CASPT2 ab initio study of the reference compound shown in Scheme 5.[94] The very low ring-opening quantum yield observed upon irradiation of DHP was explained by the quenching of the photoisomerization channel by internal conversion of the initially excited zwitterionic (Z) state to the lowest locally-excited (LE) state minimum (blue arrow, Figure 19), where the system can fluoresce or decay back to the ground state via another internal conversion. To undergo the DHP to CPD ring-opening reaction, the system needs to reach a biradical intermediate (correlating with the S_4 state at the Franck-Condon geometry denoted B state) via the population of a CPD precursor (CPD*) on S_2 followed by internal conversion at a conical intersection between the zwitterionic and biradicaloid states. Upon population of the biradical intermediate, the system can then decay to the ground state at a nearby conical intersection (photochemical funnel) leading to product formation. An elongated

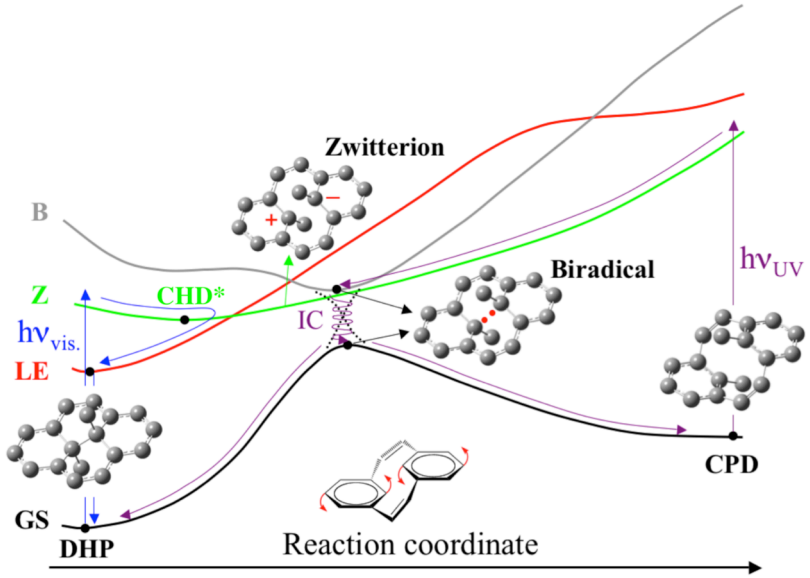

Figure 19. CASPT2 potential energy profiles of the relevant electronic states involved in the DHP / CPD photochromism. GS: ground state, LE: locally excited, Z: zwitterionic, B: biradicaloid, IC: internal conversion. A doubly-excited S_3 state quasi-degenerate with the B state at the FC geometry is not shown for simplicity.

transannular bond and a loss of planarity of the DHP core relative to the ground-state structure characterize the CPD precursor and represent the triggering process. On the other hand, irradiation of CPD leads to the formation of a biradical excited-state minimum along the ring-closure reaction path. Internal conversion back to the ground state can then occur at the same photochemical funnel, leading to the DHP photoproduct (purple arrows, Figure 19). Thus, our results point unambiguously towards a stepwise mechanism involving the formation of a biradical intermediate on a singlet excited state. The fact that this intermediate does not correspond to the lowest excited-state minimum is mainly responsible for the inefficiency of this system. The internal conversion mechanism responsible for the photochromic properties of these compounds is also controlled by the accessibility of a crossing seam, similar to the one found in dithienylethenes.[92] Based on our proposed mechanism, one could increase the efficiency of these systems by using substituents in order to energetically lower the biradical intermediate relative to the other excited-state minima and/or by suppressing the internal conversion of the initially excited Z state to the lowest LE state.

Attempts to synthesize more efficient DHP derivatives were successful using benzo[e]-fused-DHPs,[93] isobutenyl- and naphthoyl-DHPs,[95] and pyridinium-appended-DHPs.[96] We investigated theoretically the excited-state photoswitching mechanism in these improved DHP derivatives denoted DHP-**1** to DHP-**4**, respectively (Chart 1).[96,97] Because of the size of these derivatives, we did not use the highly accurate CASSCF/CASPT2 approach employed to study the reference compound. We used DFT and TD-DFT calculations instead. While the biradicaloid state cannot be described with TD-DFT because of the doubly-excited nature of this electronic state, TD-DFT is expected to describe the $S_2 \rightarrow S_1$ deactivation pathway, as both states results from single excitations. This was first verified for the reference compound. After validation of the description of the $S_2 \rightarrow S_1$ photophysical path at the TD-DFT level, we investigated the pathway leading to CPD* for the improved DHP derivatives **1** to **4** shown in Chart 1. In DHP-**1**, the efficient ring-opening reaction is made possible by the inversion of states occurring between S_1 and S_2. Thus, CPD* formation takes place directly on the lowest S_1 PES and no internal conversion with another excited state is involved (Figure 20a). In DHP-**2** and DHP-**3**, the S_1 and S_2 states are in the same order as in the reference DHP, but CPD* corresponds to the lowest minimum on the S_1 PES and the topology and accessibility of the S_2/S_1 conical intersection render CPD* formation efficient (Figure 20b). In DHP-**4**, the pyridinium electron withdrawing groups create excited states of charge transfer (CT) character and CPD* formation takes place directly on the lowest S_1 PES (Figure 20c).

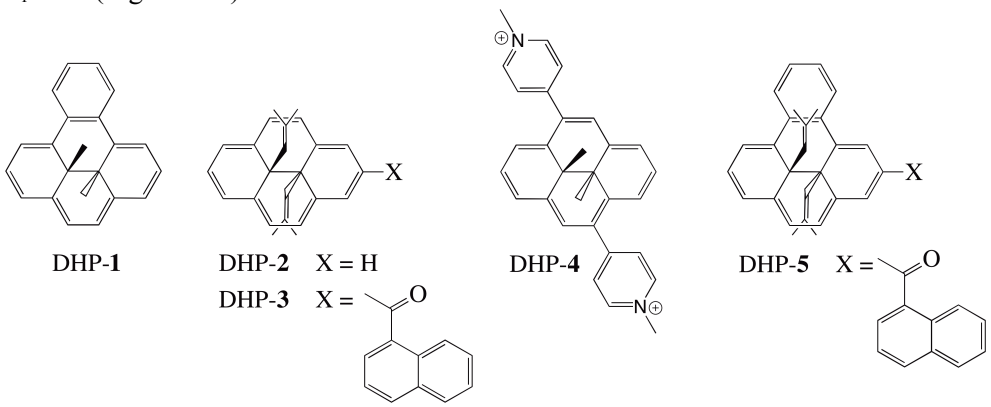

Chart 1. DHP derivatives investigated theoretically: benzo[e]-fused-DHP (DHP-**1**), isobutenyl-DHP (DHP-**2**), naphthoyl-DHP (DHP-**3**), pyridinium-appended-DHP (DHP-**4**) and benzo[e]-fused-naphthoyl-DHP (DHP-**5**).

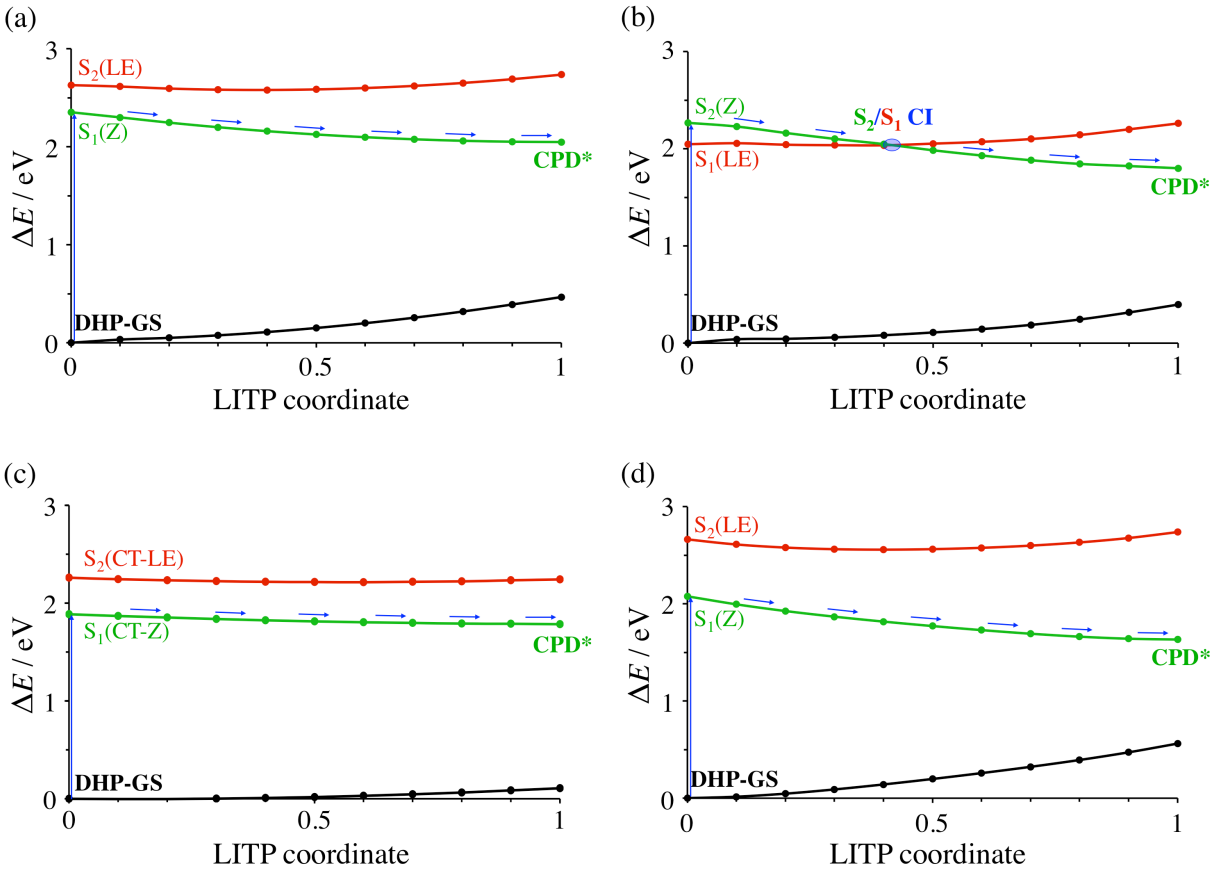

Figure 20. Computed photochemical pathways leading to CPD precursor (CPD*) formation in (a) DHP-**1**, (b) DHP-**3**, (c) DHP-**4**, and (d) DHP-**5**. Calculations performed at TD-DFT level using a linearly-interpolated transit path (LITP).

The previous results show that two distinct effects come into play in the improved efficiency of these DHP derivatives. In DHP-**1** and DHP-**4**, the inversion of electronic states between S_1 and S_2 is the main factor (with the subtlety that CT character is present in both states of DHP-**4**), allowing the efficient formation of CPD* directly on S_1. In DHP-**2** and DHP-**3**, no inversion between S_1 and S_2 is observed but the stabilization of CPD* on the S_1 PES in association with a more substantial elongation of the transannular bond is the key factor. A reasonable strategy to propose a rationally-designed improved system is to try combining both effects using a benzo[e]-fused version of DHP-**3**. The main result for the as yet unsynthesized benzo[e]-fused-naphthoyl-DHP (DHP-**5**, Chart 1) is presented in Figure 20d. It shows that we can combine the two effects separately responsible for improved ring-opening isomerization efficiency in DHP-**1**,**4** and DHP-**2**,**3**, i.e. i) having the zwitterionic state producing CPD* as the lowest excited state and ii) having CPD* as the lowest-lying S_1 minimum along with a substantial elongation of the transannular bond. We may thus anticipate an unprecedented efficiency for DHP-**5**. This is a nice illustration of the power of computational photochemistry to deliver guidelines for designing new chromophores with improved potentials.

4.1.3. *Intramolecular charge transfer.*

We now move to photoinduced charge transfer processes, which are of utmost importance in photochemistry. The example we will use is the intramolecular charge transfer (ICT) potentially occurring in aminobenzonitrile compounds (Scheme 6).[98] 4-Aminobenzonitrile (ABN) and 4-dimethylaminobenzonitrile (DMABN) will be used as prototype examples. In such compounds there

are two low-lying excited states: a locally excited (LE) state where the excitation is localized on the phenyl ring (anti-Kekule structure), and the intramolecular charge transfer (ICT) state, where there is a transfer of charge from the amino group to the benzene ring. The ICT state is thus similar (electronically) to a benzene radical anion. This zwitterionic state is characterized by a large dipole moment. In spectroscopy, with suitable substitution R and in the appropriate solvent, one can see emission from each state.[98] The mechanism accounting for the observation of this dual fluorescence is highly controversial and has been the subject of many experimental and theoretical studies. The central issues relate to i) the molecular and electronic structures of the emitting ICT species, ii) the nature of the adiabatic reaction pathway which connects the LE species to the ICT emitting state, and iii) the nature of the nonadiabatic reaction path via a conical intersection which connects the FC structure on S_2 to the LE and ICT species which emit from S_1.[99] Regarding the first issue, the lowest energy equilibrium geometry of the ICT state is usually assumed to be twisted; hence the acronym TICT (Scheme 6), but other ICT structures have been proposed such as a planar ICT (PICT) structure which have long been debated in the literature. Since one can observe dual fluorescence, there must be two S_1 minima, associated with the LE and ICT electronic structures. An adiabatic reaction path must therefore connect these two electronic structures on S_1. Thus, there is an adiabatic reaction coordinate associated with the electron transfer process. This is related to the second issue. However, the absorption from the ground state to the LE state in the Franck–Condon region is "forbidden". Rather the absorption takes place to S_2, which is the ICT state at the Franck–Condon geometry. Thus, there is also a nonadiabatic ICT process associated with the radiationless decay from S_2(ICT) to S_1(LE). This is the third aspect that we need to investigate.

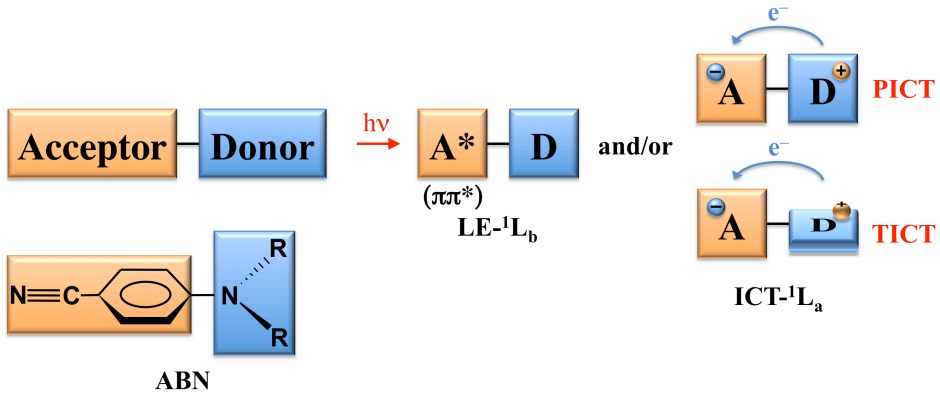

Scheme 6. Schematic representation of the ICT process and the generation of LE, PICT or TICT states.

The problematics just discussed above can be summarized in the potential energy profile shown in Figure 21a. From this figure it is clear that the (adiabatic) state labels S_1 and S_2 and the (diabatic) structure labels ICT or LE are independent. The adiabatic reaction path (solid arrow), involving a transition state (i.e., avoided crossing) appears to be associated with the real crossing. The TICT coordinate (amino group torsion) is assumed to be the reaction path. The transition state on this reaction path is associated with a state change from LE to ICT. This state change can also be associated with the nonadiabatic process via the real crossing. However, the real crossing and the nature of the branching space and its relationship to the adiabatic reaction path can be understood only by moving to higher dimensions and by consideration of the relationship between the branching space

coordinates and the torsion coordinate. In other words, we need to consider the PES model including the reaction path and the branching space coordinates. This is shown in Figure 21b for the particular case of ABN.

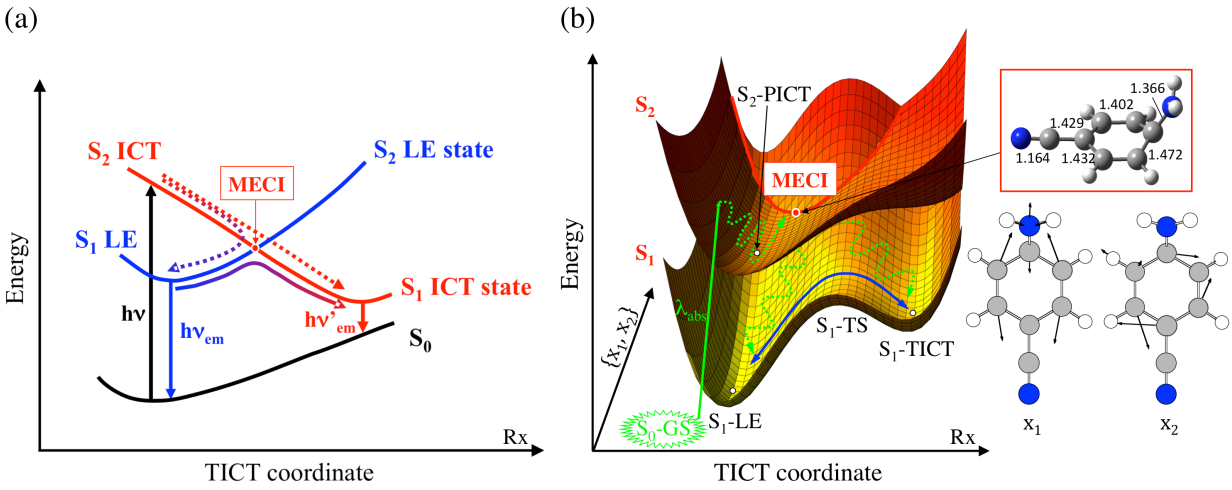

Figure 21. Adiabatic and nonadiabatic reaction profiles for the TICT process. (a) Schematic potential energy profiles represented along the reaction coordinate (mainly amino group torsion). (b) Schematic potential energy landscape represented in the space that includes the reaction coordinate and one of the two branching space coordinates, along with the S_1/S_2 MECI (distances in Å) and the associated branching space coordinates. The dotted arrows show the nonadiabatic pathways. The solid arrow shows the adiabatic pathway. In (b), the S_1-TICT minimum is represented higher in energy than the S_1-LE minimum, as this potential energy landscape is based on calculations in the gas phase of ABN.

In Figure 21b, we show the geometry of the S_1/S_2 LE/ICT MECI, together with the degeneracy-lifting coordinates $\mathbf{x_1}$ and $\mathbf{x_2}$ in ABN. The crossing occurs between the LE and ICT quinoid structures. The most important point about the geometry is that the amino group is not twisted. The directions $\mathbf{x_1}$ and $\mathbf{x_2}$ are mainly skeletal deformations of the phenyl ring and do not involve the amino group torsion. This is completely consistent with the fact that the LE and ICT quinoid structures differ essentially only in the phenyl ring (Figure 22). A local minimum for the ICT quinoid structure is found on S_2 with a planar conformation (S_2-PICT, Figures 21b and 22) and the system can access the S_1/S_2 conical intersection seam from this minimum. Thus, we have established that the nonadiabatic decay does not necessarily involve the amino group torsion, since the directions $\mathbf{x_1}$ and $\mathbf{x_2}$ exclude this coordinate.

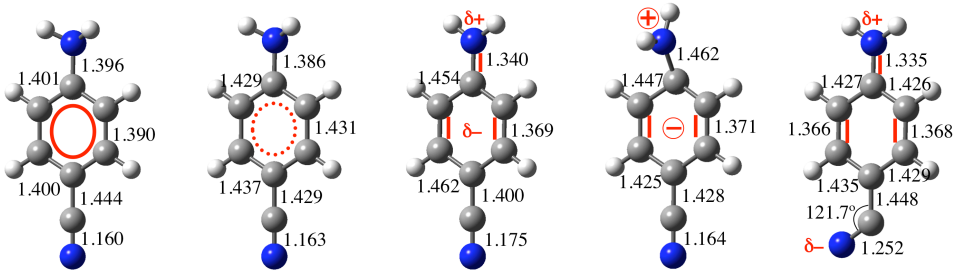

S_0-GS μ = 5.5 D | S_1-LE μ = 5.4 D | S_2-PICT μ = 12.1 D | S_1-TICT μ = 11.7 D | S_1-RICT μ = 13.8 D

Figure 22. CASSCF geometries, electronic structures (in red) and dipole moments (μ) of the ground state (GS), LE, PICT, TICT, and RICT minima in ABN. All bond lengths are in Å.

Thus, the ICT mechanism in ABN and DMABN can be summarized as follows. After excitation to the S_2 state, the system relaxes quickly to a shallow S_2-PICT minimum. No significant barrier occurs between S_2-PICT and the S_1/S_2 MECI. Because of the extended conical intersection seam, ultrafast nonradiative $S_2 \rightarrow S_1$ decay can take place at various torsion angles of the amino group leading to either S_1-LE or S_1-TICT geometries (green dotted arrows in Figure 21b). Experimentally, the ultrafast decay through the S_1/S_2 CI leads to both LE and TICT simultaneously.[100] The branching at the CI favors the formation of the LE state because the lowest energy point on the crossing seam is not twisted. Equilibration can then occur on S_1 so the dual fluorescence is controlled by the S_1-LE and S_1-TICT adiabatic reaction path. In ABN, because the equilibrium is displaced towards the LE minimum, the S_1-TICT minimum is not populated, and fluorescence occurs only from the S_1-LE state (no ICT reaction). For DMABN, population of LE and TICT can occur since the two species have similar stabilities. This explains why dual fluorescence can be observed in DMABN but not in ABN. Our mechanistic picture derived from static calculations has recently been confirmed by semi-classical and quantum dynamics simulations.[101,102]

4.2. Photobiochemistry

4.2.1. *Photostability and photodamage in DNA*. Deoxyribonucleic acid (DNA) carries the genetic information of all cellular forms of life. DNA is usually found as a double helix, in which the nucleoside bases of the single strands are stacked upon each other, forming strong hydrogen bonds with the bases in the complementary strand (Watson-Crick configuration).[103] Due to the absorbance of the bases in the harmful UV region of the spectrum (wavelength < 400 nm), DNA is vulnerable to photochemical damage. To protect the genetic information, highly elaborate mechanisms have evolved to repair damaged DNA. More important, however, is the robustness of DNA with respect to UV damage. Indeed, when arranged in the Watson-Crick configuration, the isolated base pairs have an extremely short excited-state lifetime,[104] suggesting a very high photostability. Excited-state decay

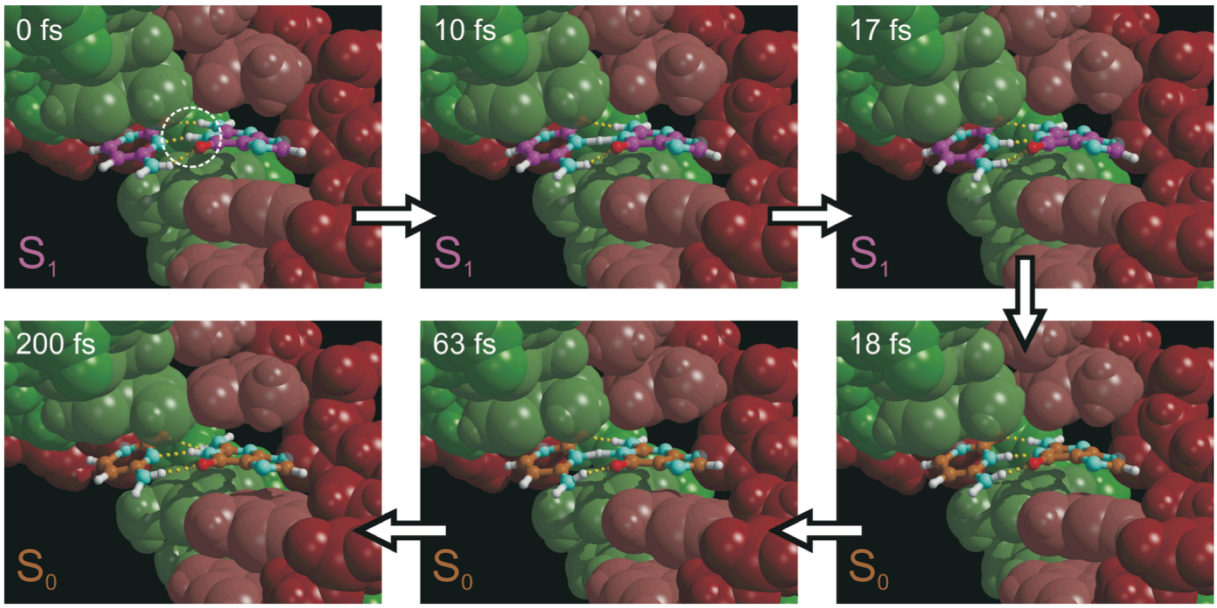

Figure 23. Illustration of the excited-state dynamics of a Watson-Crick cytosine-guanine base pair after light absorption. The snapshots show the light-induced transfer of the central proton from a guanine to a cytosine. After this transfer, a radiationless transition to the ground state takes place (18 fs). The proton then rapidly returns to the guanine, restoring the Watson-Crick base pair (200 fs).

measurements of bases and model base pairs suggest a subpicosecond repopulation of the ground state.[104,105] Experimental evidences indicate that the excited state of an isolated cytosine-guanine (C-G) base pair has a lifetime in the order of a few tens of femtoseconds.[106] Quantum chemistry calculations on the isolated C-G suggested that this ultrafast deactivation may be triggered by a barrierless single proton transfer in the excited state.[107] We investigated the photostability of C-G both in the gas phase and embedded in DNA.[108] This study provided detailed structural and dynamical insights into the ultrafast radiationless deactivation mechanism.

Figure 23 shows the sequence of events that follows excitation of a C-G base pair in DNA. According to our QM/MM simulations, photon absorption induces the transfer of a proton from the guanine to the cytosine. This proton transfer enhances ultrafast decay of the excited state. After the radiationless transition to the ground state, the original Watson-Crick configuration is quickly restored. The entire photochemical reaction is completed within about 200 fs. The absorbed energy is converted into heat and therefore does not lead to structural damage. These findings have been corroborated by experimental observations.[109] The existence of such ultrafast deactivation channel confirmed the static picture provided by ab initio calculations performed in the gas phase.[107] We investigated in detail the potential energy landscape of the electronic states involved in this mechanism and the results are summarized in Figure 24. Radiationless decay occurs along an extended crossing seam that lies parallel to the proton transfer coordinate in the vicinity the excited-state minimum. The gradient difference vector $\mathbf{x_1}$ and the derivative coupling vector $\mathbf{x_2}$ are collinear and thus span a one-dimensional branching space. The seam is displaced from the proton path along a skeletal deformation of the bases. Decay can thus occur anywhere along the proton transfer coordinate, accounting for the remarkably short lifetime of the excited base pair.[109] Note that during the dynamics the system can encounter the seam more than once and recrossings between the excited and ground

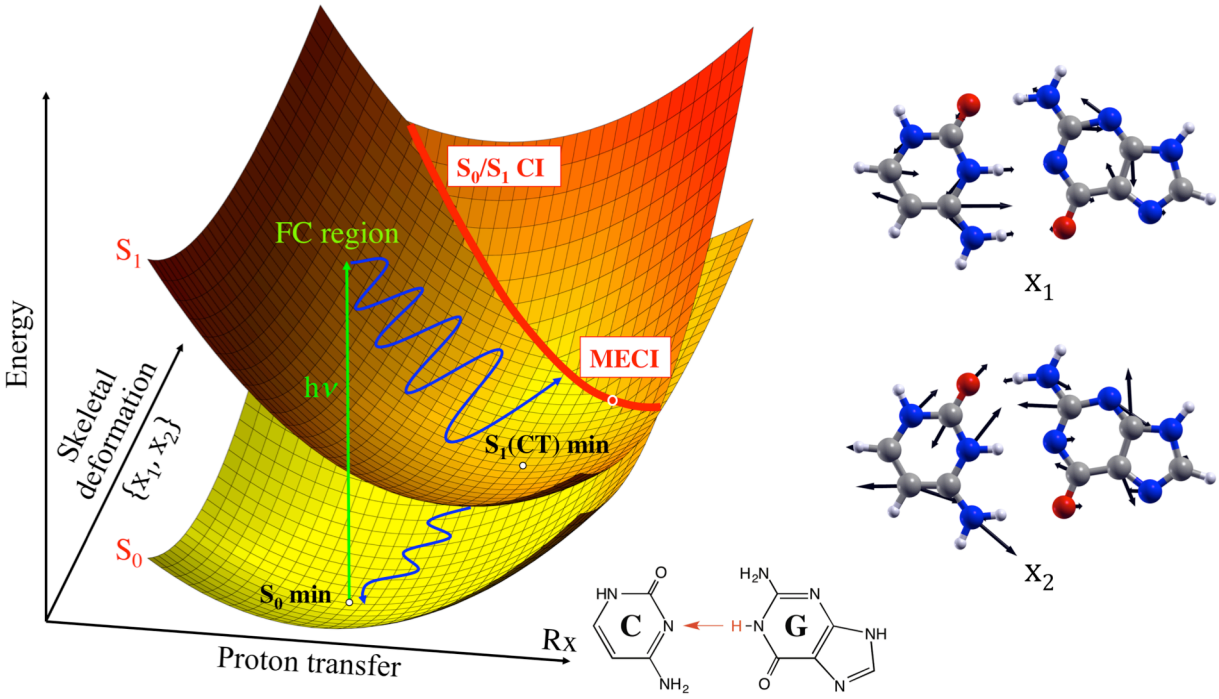

Figure 24. S_0 and S_1 potential energy landscape of the cytosine-guanine (C-G) base pair along the proton transfer reaction coordinate (Rx) and skeletal deformations of the bonds corresponding to the collinear branching space coordinates $\mathbf{x_1}$ and $\mathbf{x_2}$. Motion along the proton transfer coordinate connects the Franck-Condon (FC) geometry to the minimum of the S_1 charge transfer (CT) state. Nonradiative decay occurs along the intersection seam between the surfaces.

states can occur repeatedly due to the unusual (n-1) dimensional seam with a sloped topology. Another important point is that in the gas phase decay occurs after a complete proton transfer, whereas in DNA, decay can also occur much earlier. The origin of this effect lies in a temporal electrostatic stabilization of the dipole in the excited charge transfer state by the solvated DNA environment.

One important question that we still need to answer is the origin of the driving force for such excited-state proton transfer mechanism. A useful insight can be obtained from the various valence bond structures (Scheme 7) involved along the reaction coordinate. According to our calculations, photoexcitation to the CT state induces an electron transfer from guanine to cytosine giving rise to a zwitterionic structure (a→d, Scheme 7) in which guanine is positively charged and cytosine is negatively charged. This charge separation is the main driving force for the proton transfer from guanine to cytosine giving rise to a photoinduced proton-coupled electron transfer process. Upon the central proton transfer, the CT state is stabilized by restoring a non-zwitterionic electronic structure (d→d', Scheme 7). Along this relaxation coordinate, the ground-state structure is destabilized by acquiring a zwitterionic character (a', Scheme 7) in which guanine is negatively charged and cytosine is positively charged this time. Thus, this opposite charge transfer provides the driving force for the central proton to return to guanine (a'→a, Scheme 7) after $S_1 \rightarrow S_0$ nonradiative decay. Note that there are low-lying locally excited (LE) states in the Franck-Condon region (b and c, Scheme 7) but these states are destabilized upon the central proton transfer coordinate giving rise to low-lying conical intersections between the LE states and the CT state.

To conclude, understanding the dynamics of the ultrafast deactivation processes in the C-G base pair represents a major challenge. Here we demonstrated that, by using a combined static and dynamical study of the system in the gas phase and in its biological environment, it is possible not only to reproduce the experimental excited-state lifetime, but also to provide detailed mechanistic

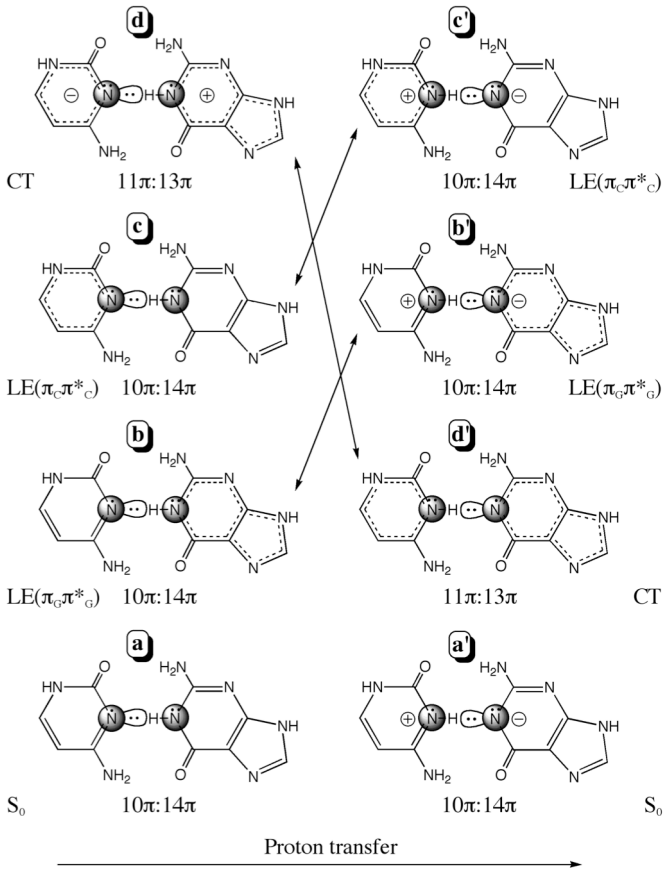

Scheme 7. Valence bond representations of the C-G base pair in the relevant electronic states.

insights into the deactivation process.

Intrastrand thymine photodimerization (Figure 25a) is recognized as the most common process leading to DNA damage under UV irradiation.[110] The formation of thymine dimers has potentially important physiological consequences. This mutagenic photoproduct can disrupt the function of DNA and thereby trigger complex biological responses, including apoptosis, immune suppression, and carcinogenesis.[111]

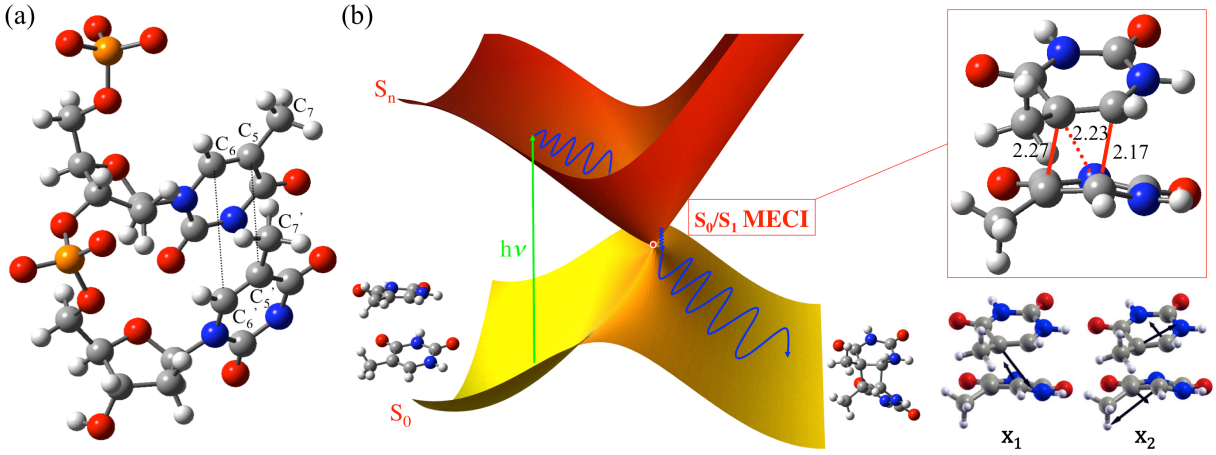

Figure 25. (a) Stacked thymines in DNA. (b) CASSCF potential energy landscape for the photochemical [2+2] cycloaddition of two stacked thymines along with the structure of the S_0/S_1 MECI. Gradient difference ($\mathbf{x_1}$) and derivative coupling ($\mathbf{x_2}$) vectors forming the branching space are shown. Interatomic distances are given in Å.

A recent study based on femtosecond time-resolved infrared spectroscopy showed that thymine dimers are fully formed around 1 ps after UV excitation.[112] The authors concluded that this ultrafast photolesion rate points to an excited-state reaction that is nearly barrierless for bases that are properly oriented at the instant of light absorption. It was suggested that the low quantum yield of this photoreaction results from infrequent conformational states in the unexcited system. However, this study did not provide a mechanistic picture of the photoactivated thymine dimerization process. Our theoretical investigation was aimed at finding the photochemical pathway leading to the formation of the thymine dimer in the gas phase and characterizing the funnel required for this ultrafast process.[113]

The mechanistic picture is summarized in Figure 25b. Unlike the ground-state reaction pathway, which involves a highly activated stepwise process, the excited-state photochemical [2+2] cycloaddition takes place through a concerted mechanism. The process is barrierless and leads to a low-lying minimum energy conical intersection, S_0/S_1 MECI, where ultrafast nonradiative decay to the ground state is extremely efficient. Such a nonadiabatic pathway is reminiscent of the one found in the ethylene-ethylene photochemical cycloaddition.[63a,114] The peaked topology of the CI suggests that upon decay to the ground state at S_0/S_1 MECI the system can either evolve to the dimeric photoproduct or reverse back to the original reactant. It has been suggested that photodimer formation occurs with a quantum yield close to unity when the molecule is excited in a favorable conformation, while in the more common unfavorable conformations the excited state will be unreactive.[112] The very low overall quantum yield of the thymine photodimerization can be mainly explained by the fact that the photoreactive state is not easily accessible at the Franck-Condon geometry (it corresponds to state S_6 with a weaker oscillator strength than lower LE states at CASPT2 level)[115] and its population

requires excitation of the stacked thymines at favorable but rare conformations where the two bases are close to each other as in the funnel region.

4.2.2. *Photoisomerizations in proteins*. In this subsection, we give a brief overview of our work on the photoisomerization in the photoactive yellow protein (PYP). Our choice for this system is motivated by the fact that the photochemistry of this protein and of its chromophore has been extensively studied by both experiments and computations, so that there is a wealth of data to compare the outcome of our calculations to. PYP is known to be the primary photoreceptor for the photoavoidance of the salt-tolerant bacterium *Halorhodospira halophila*. It contains a deprotonated 4-hydroxy-cinnamic acid (or *p*-coumaric acid, *p*CA, Scheme 8) chromophore that is covalently linked to the γ-sulfur atom of a cysteine amino acid (Cys^{69}) via a thioester bond. Upon absorbing a blue-light photon, PYP undergoes a complete photocycle involving several intermediates on timescales ranging from a few hundred femtoseconds to seconds.[116] Our focus is on the primary photochemical event, which involves a *trans*-to-*cis* photoisomerization of the chromophore.

To understand how the protein mediates the photoisomerization of the chromophore, we have performed atomistic simulations of the chromophore and related analogues in various molecular environments.[117,118] The results of these computations not only provided a detailed mechanistic picture of the isomerization process, but also revealed the influence of the interactions with the environment. With such detailed information new experiments can be designed, which will ultimately enhance our understanding of the photochemistry of PYP.

Isolated chromophore. To investigate the intrinsic excited-state dynamics of the deprotonated chromophore, we performed MD simulations of two isolated chromophore analogues (thiomethyl *para*-coumaric acid, thio-*p*CA^-, and *para*-coumaric-ketone, *p*CK^-, Scheme 8). Because the chromophore is deprotonated in the protein, we focused our attention on the anionic species. Note that these anionic chromophores in isolation are autoionizing (i.e., unstable with respect to electron detachment) upon electronic excitation. As our aim is to understand the effect of different molecular environments on the photoisomerization processes, we need to study these hypothetical chromophore models in vacuum as a reference.

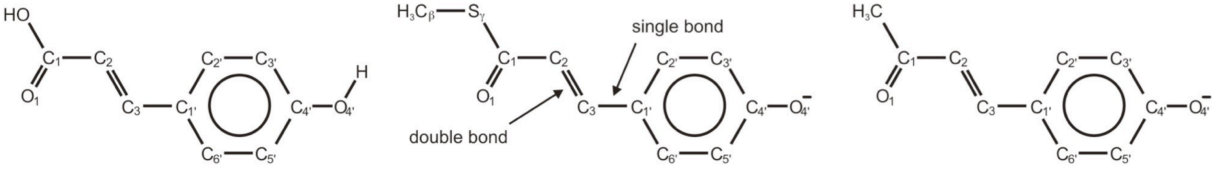

*p*CA thio-*p*CA^- *p*CK^-

Scheme 8. Schematic drawings of the *p*-coumaric acid (*p*CA) chromophore and the two analogues used in our study.

After vertical excitation to S_1, both chromophores rapidly relax from the Franck–Condon region by twisting around the formal single bond adjacent to the chromophore ring (Scheme 8). After reaching a single-bond-twisted minimum, no decay to the ground state occurred within 5 ps, which was the total time of our MD simulations. The observation of a fast vibrational relaxation into the single-bond-twisted S_1 minimum for both thio-*p*CA^- and *p*CK^- is consistent with the topology of the excited-state PES for these chromophores. Indeed, the topology of the S_1 PES reveals that in both

chromophores there are two minima on S_1, associated with bond twisting: the single-bond-twisted minimum, in which the bond adjacent to the phenol ring is rotated by 90° (Figure 26a), and the double-bond-twisted minimum, in which the ethylenic bond is twisted by 90° (Figure 26b). In the isolated chromophores, there is no barrier for reaching the single-bond-twisted S_1 minimum from the Franck–Condon region, whereas there is a significant barrier to double-bond rotation (9.4 kJ/mol for *p*CK$^-$ and 14.0 kJ/mol for thio-*p*CA$^-$ at the CASSCF level). Thus, in agreement with the MD simulations, the main initial relaxation channel after excitation should involve rotation of the single bond to 90°. Furthermore, we found that the S_0/S_1 CI seam lies rather far away from the single-bond-twisted minimum. The seam can be accessed only upon rotation of the double bond. Based on these findings we suggest that radiationless decay is not very efficient in vacuum. This observation is in line with the relatively long excited-state lifetime of 52 ps for the isolated *p*CK$^-$ chromophore, measured by means of time-resolved photoelectron spectroscopy.[119] In the following, we have probed the effect of different environments on the photochemistry of the chromophore.

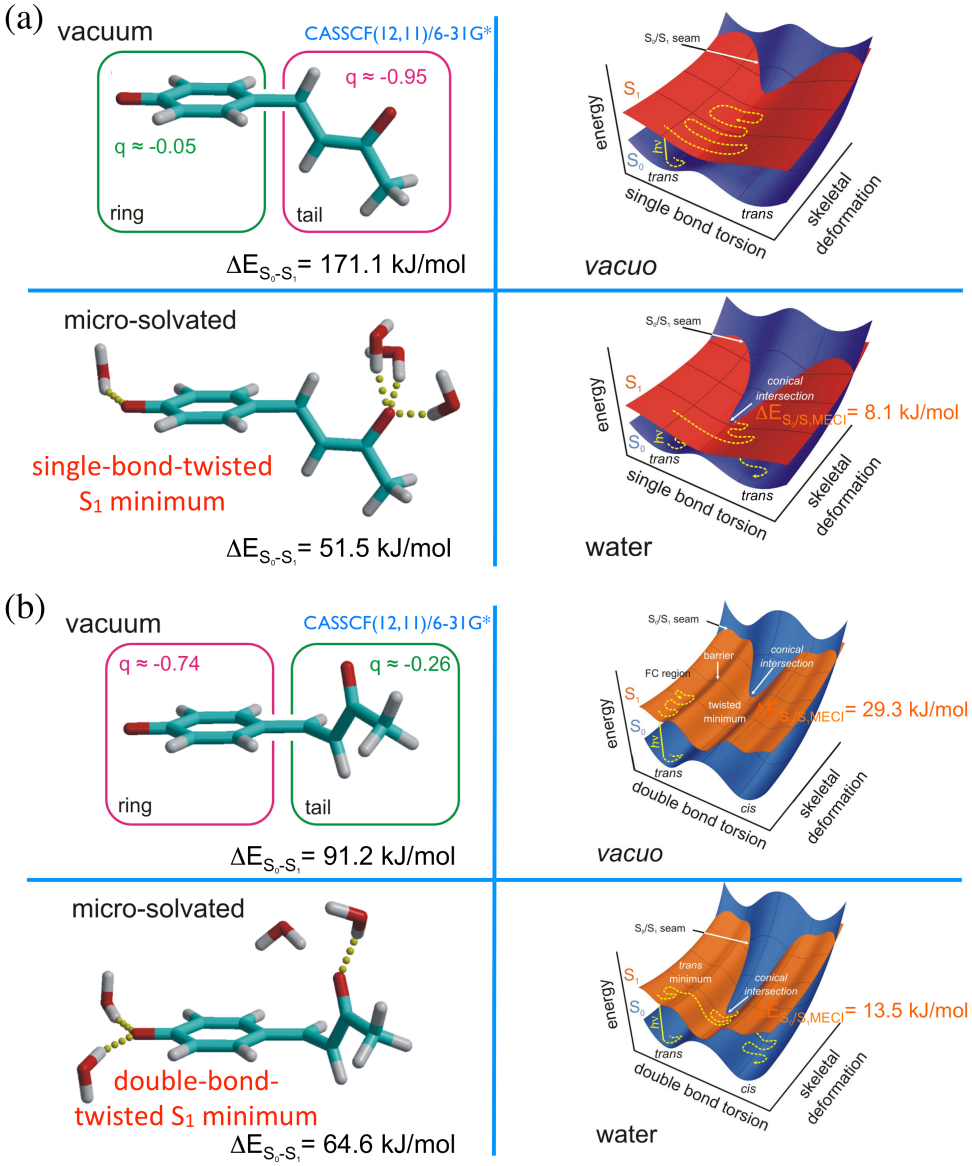

Figure 26. Schematic overview of the S_0 and S_1 potential energy landscape along the (a) single-bond and (b) double-bond torsion coordinates in the gas phase and in a micro-solvated environment.

Structures of the single-bond-twisted and double-bond-twisted S_1 minima are shown along with the corresponding S_1 charge distributions. S_0-S_1 energy gaps at these minima and activation energies to reach the S_0/S_1 MECI are also indicated.

Chromophore in water. To examine the effect of an aqueous environment, we have investigated the excited-state dynamics of the deprotonated *p*CK$^-$ chromophore analogue in water using QM/MM excited-state MD.[118a] The *p*CK$^-$ chromophore was chosen because experimental data are available both in the gas phase[119] and in water.[120] Static calculations were also performed in order to investigate the change in the PES landscape brought by the aqueous environment. Thus, we have computed the PESs for the micro-solvated chromophore, including explicit water molecules at key positions (based on the MD simulations) in the CASSCF calculations.

The results of the simulations demonstrate that radiationless decay is very efficient in water. The predominant excited-state decay channel involves twisting of the single bond (88%) rather than twisting of the double bond (12%), as illustrated in Figure 27. In contrast to the gas phase simulations, decay takes place very near these minima. Inspection of the trajectories revealed that decay is mediated by specific hydrogen-bond interactions with water molecules. These hydrogen bonds are different for the single- and double-bond-twisted S_1 minima. This reflects the difference in charge distribution of the electronic structures at these minima. In the single-bond-twisted S_1 minimum, the negative charge resides on the alkene moiety of the chromophore (Figure 26a). Thus, it corresponds to a twisted-intramolecular charge transfer (TICT) state. Three strong hydrogen bonds to the carbonyl oxygen stabilize this charge distribution to such an extent that the crossing seam becomes accessible from the single-bond-twisted S_1 minimum (Figure 26a): the S_0/S_1 MECI presents a single-bond-twisted structure lying only 8.1 kJ/mol above this minimum. In the double-bond-twisted S_1 minimum, the negative charge is localized on the phenolate ring (Figure 26b). Transient stabilization of this charge distribution by two or more strong hydrogen bonds to the phenolate oxygen brings the seam much closer to this S_1 minimum (Figure 26b): the activation energy to reach the S_0/S_1 MECI with a double-bond-twisted structure from this S_1 minimum decreases from 29.3 kJ/mol in the gas phase to 13.5 kJ/mol in water. Thus, in water the ultrafast excited-state decay is clearly mediated by hydrogen bonds. Note that among the 12% of trajectories that show twisting of the double bond, the chromophore continued isomerizing towards the *cis* configuration after decay to S_0 in just over half the trajectories. In the other simulations, the *trans* configuration was restored.

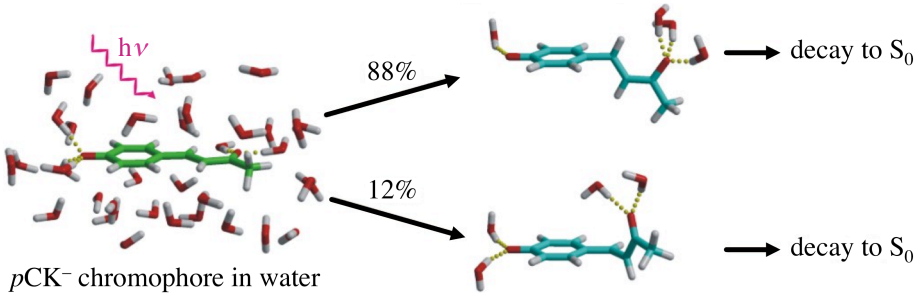

Figure 27. In water, *p*CK$^-$ undergoes both single- (88%) and double-bond (12%) photoisomerizations. Excited-state decay from the corresponding twisted minima is very efficient due to the stabilization of the S_1 charge distribution of the chromophore by specific hydrogen bond interactions.

To summarize, the predominant excited-state relaxation process of *p*CK$^-$ in water involves a rotation of the single bond, adjacent to the phenolate ring, rather than rotation of the ethylenic double bond. In the gas phase, only the double-bond torsion can lead to radiationless decay, whereas in water, both channels lead to decay. This decay becomes ultrafast in water because of the proximity of the S_0/S_1 intersection seam with the photochemical pathway. Because single-bond photoisomerization is strongly favored over double-bond photoisomerization for *p*CK$^-$ in water, the probability of finding the chromophore in the *cis* configuration is very low. This result is in good agreement with the observed ultrashort excited-state lifetime of *p*CK$^-$ in water (~1 ps) and a negligible *trans*-to-*cis* photoisomerization quantum yield.[120]

Effect of the protein environment. By displacing the S_0/S_1 crossing seam very close to the S_1 minima, hydrogen-bond interactions between the chromophore and water molecules enhance excited-state decay in water.[118a] Yet, the major decay channel involves torsion around the single bond, rather than torsion around the double bond of the chromophore. To find out the effect of the protein environment on the excited-state dynamics of the chromophore, QM/MM MD simulations of the wild-type PYP, as well as on the Arg52Gln mutant, were carried out.[117]

Figure 28 shows the primary events after photoexcitation in the simulation of the wild-type PYP.[117a] In the majority of the trajectories the chromophore rapidly decays to the ground state via a 90° torsion around the double bond. During this photoisomerization process, the hydrogen bonds between the phenolate oxygen atom of the thio-*p*CA$^-$ chromophore and the side chains of the highly conserved tyrosine (Tyr^{42}) and glutamic acid (Glu^{46}) residues remain intact. Just as in water, these hydrogen bonds are essential to promote excited-state decay from the double-bond-twisted S_1 minimum (Figure 26b). Upon returning to the ground state, the chromophore either relaxes back to the original *trans* conformation (70% of the trajectories) or it continues isomerizing to a *cis* conformation (remaining 30%). In the latter case, the relaxation also involves a flip of the thioester linkage, which causes the carbonyl group to rotate by 180°. During this rotation, the hydrogen bond between the carbonyl oxygen and the Cys^{69} backbone amino group is broken (Figure 28). The loss of this hydrogen bond has been observed in time-resolved infrared spectroscopy[121] as well as in time-resolved Laue crystallography studies.[122]

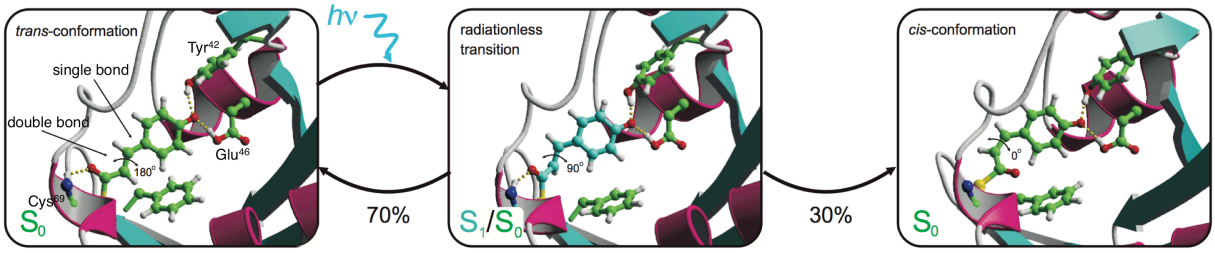

Figure 28. Snapshots from QM/MM MD simulations of wild-type PYP, showing the thio-*p*CA$^-$ chromophore in the active site pocket. The first snapshot is at the excitation. The second shows the configuration at the $S_1 \rightarrow S_0$ radiationless transition. The third snapshot shows the photoproduct, in which the carbonyl oxygen of the thioester linkage has flipped and is no longer hydrogen bonded to the backbone of Cys^{69}.

Although the number of trajectories is too small (only 14 QM/MM MD simulations could be run back in 2004) to rule out that single-bond isomerization could also occur in the wild-type protein, no

single-bond isomerization was observed.[117a] Because in water single-bond isomerization is the main decay channel, the latter observation implies that the protein not only provides the hydrogen bonds required for ultrafast decay, but also controls which of the chromophore bonds isomerizes upon photoexcitation. It was speculated at the time that a positive guanidinium moiety of an arginine amino acid (Arg^{52}) located just above the chromophore ring, acts as the 'catalytic' residue that enforces double-bond isomerization. This hypothesis was tested by removing the charge from the Arg^{52} side chain in a snapshot taken at the $S_1 \rightarrow S_0$ hop, and recalculating the energy gap. The gap increased by 40 kJ/mol.[117a] This result suggested that a preferential electrostatic stabilization of the double-bond twisted S_1 minimum by the positive Arg^{52} favors double-bond isomerization over single-bond isomerization in the wild-type protein. Recent theoretical works on an isolated *p*CK^- chromophore in the presence of an external electric field confirms that the photoisomerization can indeed be controlled by electrostatic interactions.[123]

To elucidate the role of Arg^{52} in the activation process in more detail, we investigated the excited-state dynamics of the Arg52Gln mutant of PYP (R52Q), in which the positively charged Arg^{52} has been replaced by a neutral glutamine (Gln^{52}) residue.[117b] Such PYP mutant can still enter the photocycle, albeit with lower rate and quantum yield.[124] Without the positive Arg^{52}, the predominant photochemical reaction path in the simulations involved isomerization of the single bond in the chromophore, rather than isomerization of the double bond (Figure 29).[117b] Although the latter was also observed in one of the trajectory, it is a minor decay channel. Again, the number of trajectories (a few tens) is too low to make quantitative predictions. Nevertheless, the R52Q mutant simulations confirm that within our model the role of Arg^{52} is to steer the initial events after photon absorption to ensure rotation of the double bond rather than that of the single bond in the chromophore.

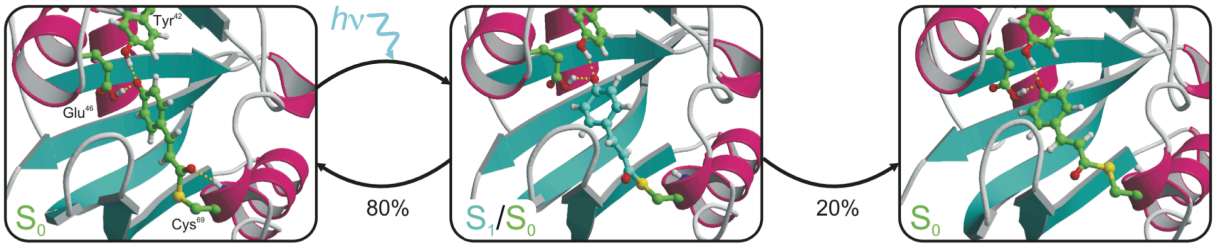

Figure 29. Snapshots from QM/MM MD simulations of Arg52Gln mutant of PYP (R52Q), showing the thio-*p*CA^- chromophore in the active site pocket. The first snapshot is at the excitation. The second shows the configuration at the $S_1 \rightarrow S_0$ radiationless transition. The third snapshot shows the photoproduct. In this mutant, isomerization takes place around the single-bond. Like in the wild-type protein, the carbonyl oxygen of the thioester linkage flips, causing the break of the hydrogen bond to the backbone of Cys^{69} (20% of the trajectories).

Remarkably, the hydrogen-bonding interactions play also an essential role in the decay process of the mutant. During rotation of the single bond, the hydrogen bond between the carbonyl oxygen and the Cys^{69} backbone amino group is broken. In contrast to the wild-type, the rupture of this bond occurs before the decay. Therefore this may seem at conflict with the observation that in water three hydrogen bonds at the carbonyl group are required to make the S_0/S_1 crossing seam accessible from the single-bond-twisted minimum. However, as shown in Figure 30, new hydrogen bonds are rapidly formed between the carbonyl oxygen atom and the backbone amino groups of Tyr^{98} and Asp^{97}. A water molecule enters the chromophore pocket to donate a third hydrogen bond. This is possible

because the chromophore pocket has become more exposed to the solvent due to the replacement of the rather bulky arginine side chain by the much smaller glutamine side chain. With these three hydrogen bonds stabilizing the negative charge on the alkene moiety, the chromophore rapidly decays to S_0. Thus, the decay mechanisms in the Arg52Gln mutant and in water are essentially the same in our simulations.

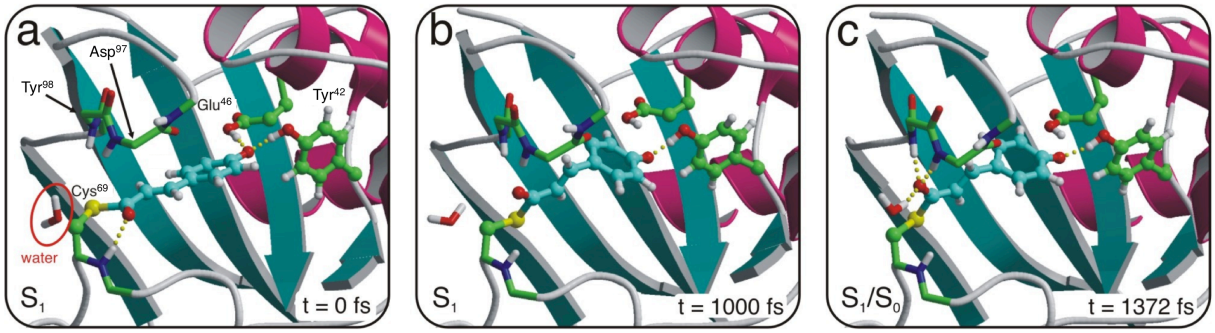

Figure 30. Snapshots from an excited-state trajectory of the Arg52Gln mutant of PYP (R52Q), demonstrating that three hydrogen bonds to the carbonyl moiety are essential for $S_1 \rightarrow S_0$ radiationless decay near the single-bond-twisted minimum. The first snapshot (a) is at the excitation to S_1. The second snapshot (b) shows the twisted configuration without hydrogen bonds to the carbonyl. The gap between S_1 and S_0 is far too high for decay at this configuration. However, as the third snapshot (c) shows, two backbone amino groups and a bulk water that has moved into the chromophore pocket during the excited-state dynamics donate the three hydrogen bonds that are required for efficient decay from the S_1 minimum.

Although single-bond isomerization does not result in the formation of the *cis* chromophore, a 180° flip of the thioester group and a rupture of the hydrogen bond to Cys^{69} were observed in 20% of the trajectories (Figure 29). Together with the experimental observation that the mutant can still enter the photocycle, this suggests that the key step to enter the photocycle may be the carbonyl flip rather than the double-bond isomerization. This suggestion is further supported by the observation that when the protein is reconstituted with chromophore analogues that cannot isomerize,[125] PYP can still enter the photocycle.[126] In these chromophores the isomerization is prevented by either a covalent bridge that blocks both single- and double-bond rotations, or by oxidation of the double bond to a triple bond. However, since *trans*-to-*cis* isomerization of the double bond was also observed in R52Q, we cannot rule out the possibility that only the latter process is responsible for photoactivation and that the single-bond isomerization pathway is a dead-end in the process, responsible for the lower activation yield in the mutant. Support for the involvement of the double-bond photoisomerization comes from time-resolved absorption spectroscopy measurements that show the appearance of the *cis* photoproduct on a sub-picosecond timescale in this mutant.[127] In these experiments, the lower quantum yield and slower deactivation dynamics as compared to the wild-type PYP were attributed to a lower structural integrity of the chromophore pocket. Based on our simulations, however, we would attribute the difference in efficiency to the involvement of the single-bond isomerization channel.

To summarize, the simulations have provided detailed structural and dynamical information at a resolution well beyond that achievable by other means. From the simulations, we have identified key amino acids and the mechanism by which they control the primary events in the photocycle of PYP. These are i) the *trans*-to-*cis* photoisomerization around the double bond and ii) the break of a

hydrogen bond between the chromophore and the protein backbone. These events trigger a proton transfer from the protein to the chromophore, which ultimately leads to the signaling state of PYP.[128]

4.3. Inorganic photochemistry

One of my main research line is devoted to the study of polypyridine ruthenium complexes. Such complexes are extensively studied in coordination chemistry, material science and biochemistry due to their remarkable photophysical and photochemical properties.[129,130] In particular, ligands can be chosen to tune these properties in order to design for example new photoluminescent or photovoltaic systems with the aim to improve lighting devices[131] or solar cells.[132]

In order to rationalize theoretically the photophysical and photochemical properties of such metal complexes, it is important to understand the nature of the electronic states involved in the various photoinduced processes. Our first studies were aimed at describing and characterizing the various electronic excited states of archetypal ruthenium polypyridine complexes.[133] As shown by the simplified Jablonski diagram in Scheme 9, upon initial photoexcitation to singlet metal-to-ligand charge transfer (^{1}MLCT) states, the system relaxes to lower triplet states of either metal-to-ligand charge transfer character (^{3}MLCT states) or metal centered character (^{3}MC state, also known as ligand-field state or *d-d* state). This is made possible by the efficient intersystem crossing (ISC) encountered in these 2nd row metal complexes for which spin-orbit coupling (SOC) is significant.[134] The photophysical properties and photochemical reactivity are largely governed by the position of the lowest ^{3}MLCT state relative to that of the ^{3}MC state and the associated equilibration pathway between these states on the lowest triplet PES. While ^{1}MLCT states are very short lived (fs timescale) because of efficient ISC and mainly permit ultrafast electron transfer processes (e.g., such as the injection of an electron in the conduction band of a semi-conductor in dye-sensitized solar cells[132]), ^{3}MLCT states have substantially longer lifetimes (ps up to μs timescale). For most polypyridine Ru(II) complexes, the lowest ^{3}MLCT state undergoes relatively slow radiationless transitions and thus exhibits fairly long lifetime and intense luminescence.[129] This state is also responsible for photoinduced electron transfer reactions and photoreactivity with biomolecules (e.g., DNA and polypeptides).[130a] In contrast, ^{3}MC states are short lived due to efficient radiationless transitions back to the ground state.[129,134] The dissociative character encountered in these ^{3}MC states[133] also allows for photoinduced ligand dissociation, *trans*-to-*cis* photoisomerization and photosubstitution.[135] In the following, we will

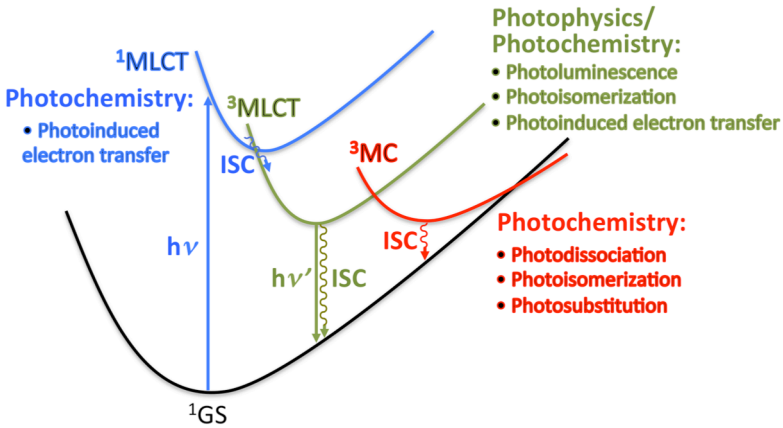

Scheme 9. Simplified Jablonski diagram indicating the main electronic states involved in various photophysical and photochemical processes of the studied polypyridine ruthenium complexes. MLCT: metal-to-ligand charge transfer, MC: metal centered, ISC: intersystem crossing.

present our main contribution as regard to designing efficient photoluminescent polypyridine ruthenium complexes and understanding the linkage photoisomerization mechanisms in ruthenium photochromic compounds.

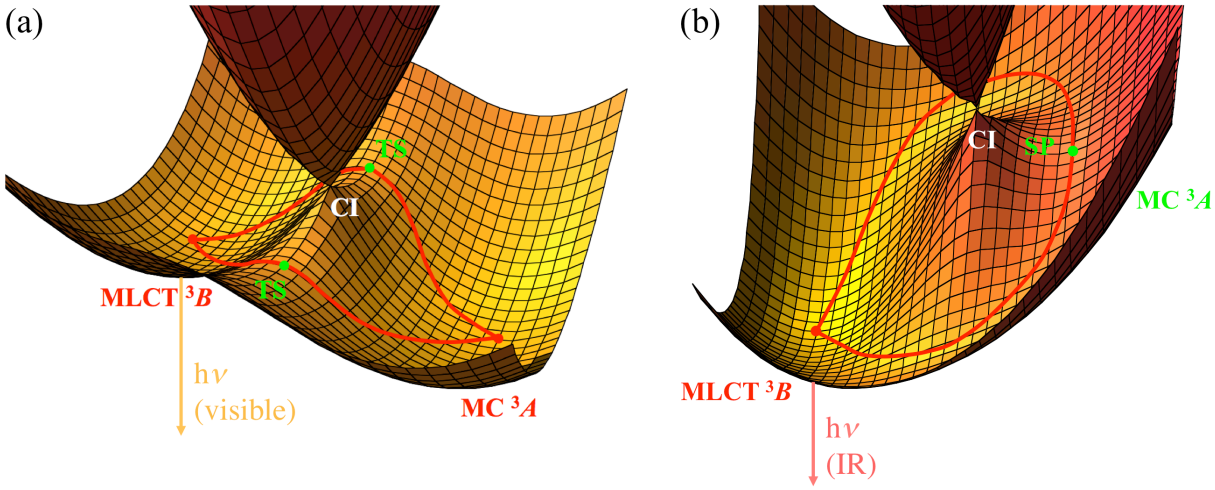

Figure 31. Potential energy landscape of the triplet PES: comparison between (a) $[Ru(bpy)_3]^{2+}$ and (b) $[Ru(bpy)_2(HN{=}\ CH{-}CH{=}NH)]^{2+}$. Red lines correspond to MEPs between ^{3}MLCT and ^{3}MC states belonging to the C_2 point group. CI: conical intersection, TS: transition state, SP: saddle point. Solid arrows indicate the emission process from the ^{3}MLCT state.

4.3.1. *Photophysical properties of ruthenium complexes*. As explained above, the lowest ^{3}MLCT state is responsible for the observation of luminescence in polypyridine ruthenium complexes provided that its lifetime is sufficiently long to undergo a radiative transition. One of the main reasons for luminescence quenching is the depopulation of the ^{3}MLCT in favor of a non-luminescent low-lying ^{3}MC state,[129,134] as illustrated in Figure 31a. Thus, the excited-state lifetime of the ^{3}MLCT state is largely governed by the ^{3}MLCT↔^{3}MC equilibration pathway on the lowest triplet PES. To design a long-lived photoluminescent candidate, one has to find a ruthenium complex with a ^{3}MLCT state sufficiently lower in energy than the ^{3}MC state to improve the emission quantum yield. Two strategies can be contemplated to increase the stability of the ^{3}MLCT state relative to the ^{3}MC state. One can either use strong π-accepting ligands that will stabilize the ^{3}MLCT state, or use strong σ-donating ligands that will destabilize the ^{3}MC state. These are the two strategies that we followed.

First, we used strong π-accepting acyclic α-diimine ligands such as 1,4-diaza-1,3-butadiene (HN=CH–CH=NH). We substituted the 2,2'-bipyridine (bpy) ligands of the reference $[Ru(bpy)_3]^{2+}$ complex and investigated the effects of successive substitutions by this diazabutadiene ligand (Figure 32). We have investigated the absorption properties of these systems and the triplet potential energy

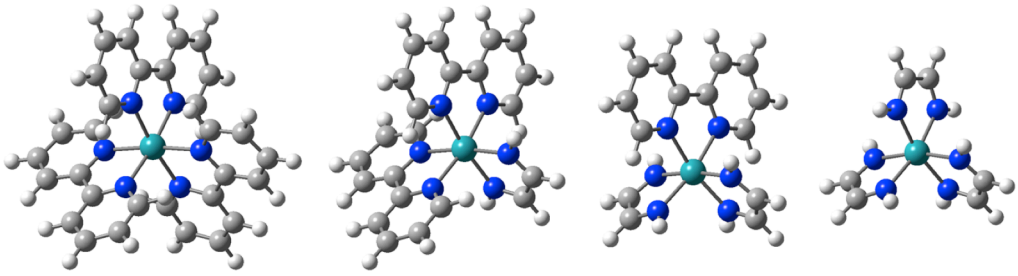

Figure 32. Series of $[Ru(bpy)_n(HN{=}CH{-}CH{=}NH)_{3-n}]^{2+}$ (n=0–3) studied complexes.

landscape along the ^{3}MLCT↔^{3}MC equilibration path.[136] This study showed a high stabilization of the MLCT state due to the presence of the strong π-accepting diazabutadiene ligands, making these complexes luminescent in the IR region (Figure 31b). In addition, the ^{3}MC state became unstable on the triplet PES, as the corresponding stationary point corresponds to a first-order saddle-point (Figure 31b). Thus, the ^{3}MLCT→^{3}MC deactivation pathway is efficiently suppressed in these complexes.[137]

Following the second strategy, strong σ-donating ligands were used in order to destabilize the lowest ^{3}MC state. To achieve this goal, we resorted to original organophosphorus ligands. Most examples of Ru(II) complexes combining polypyridine and phosphorus ligands make use of phosphine ligands.[138] Here, we investigated polypyridine ruthenium complexes incorporating aminophosphine and phosphoryl ligands, which displayed unprecedented luminescent properties for polypyridine Ru(II) organophosphorus complexes.[139,140] More precisely, we studied the following complexes: $[Ru(bpy)(tpy)(R_2P–N=CH–N(i\text{-}Pr)_2)]^{2+}$ (tpy = 2,2':6',2"-terpyridine, R = i-Pr, Ph) denoted [Ru-P(N)]$^{2+}$ and $[Ru(bpy)(tpy)(PPh_2O)]^+$, denoted [RuPO]$^+$. The use of an aminophosphine ligand on the one hand and of a phosphoryl ligand on the other hand proved largely successful to destabilize the ^{3}MC state. Indeed, room-temperature luminescence in the visible range was observed for the complex [Ru-P(N)]$^{2+}$ (R = i-Pr), which was the first account of such photoluminescent behavior in the $[Ru(bpy)(tpy)(L)]^{2+}$ family of complexes.[139] The [RuPO]$^+$ complex synthesized subsequently proved to be the complex with the longer emission lifetime at room temperature (57 ns),[140] whereas it was only 1.2 ns in [Ru-P(N)]$^{2+}$.

In order to rationalize these results, we performed calculations of the Gibbs energy profiles corresponding to the lowest triplet excited state along the ^{3}MLCT↔^{3}MC equilibration pathway for [Ru-P(N)]$^{2+}$ (R = Ph), [RuPO]$^+$ and compared these to the one of the reference $[Ru(bpy)(tpy)(PPh_2H)]^{2+}$ complex, denoted [Ru-PH]$^{2+}$. Figure 33 collects these results and clearly shows that the ^{3}MC state has been destabilized relative to the ^{3}MLCT state by substitution of an –H by the $–N=CH–N(i\text{-}Pr)_2$ group, and even more so by substitution with the anionic group $–O^-$. In the case of the [RuPO]$^+$ complex, the minimum of the ^{3}MC state becomes even higher in energy than the minimum of the ^{3}MLCT state. In addition, the ^{3}MLCT→^{3}MC activation energy increases substantially in the following order [Ru-PH]$^{2+}$ < [Ru-P(N)]$^{2+}$ < [RuPO]$^+$. This means that from a kinetic point of view, we expect a longer ^{3}MLCT excited-state lifetime in [RuPO]$^+$ compared to that of [Ru-P(N)]$^{2+}$,

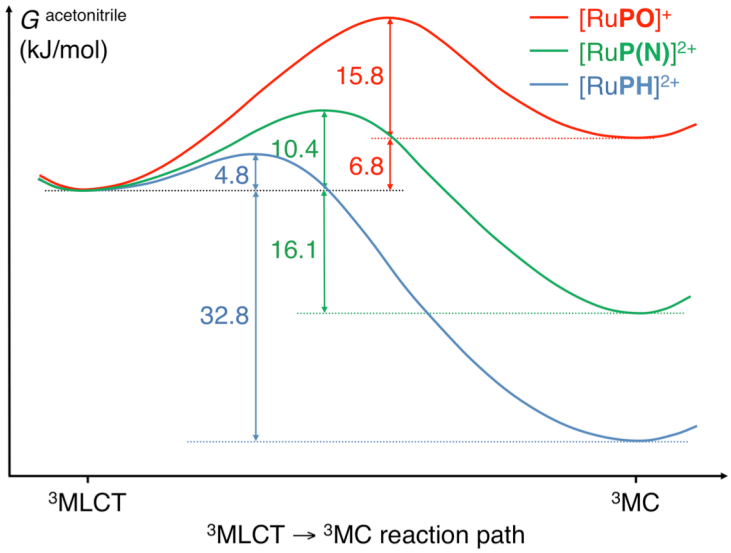

Figure 33. Schematic Gibbs energy profiles computed using DFT in acetonitrile at 298 K for the three complexes [Ru-PH]$^{2+}$, [Ru-P(N)]$^{2+}$ and [RuPO]$^+$. ^{3}MLCT states are set at the same energy for clarity.

being itself longer than that of $[Ru\text{-}PH]^{2+}$. At low temperature (77 K), the three complexes are photoluminescent because the system can remain trapped in the ^{3}MLCT well for a long enough time to undergo radiative decay. At room temperature, the system disposes of more vibrational kinetic energy to overcome the ^{3}MLCT→^{3}MC barrier. The $[Ru\text{-}PH]^{2+}$ complex becomes non-luminescent, as only a small energy barrier has to be crossed to undergo ^{3}MLCT→^{3}MC deactivation. In $[Ru\text{-}P(N)]^{2+}$ and $[RuPO]^{+}$, this barrier is increased significantly and provides a rationale for explaining the increased ^{3}MLCT excited-state lifetime along with the room-temperature emission. Thus, these calculations accounted for the substitution effects on the evolution of the photoluminescent behaviors at room temperature in this series of complexes. Both favorable thermodynamic and kinetic factors are responsible for the remarkable room-temperature luminescence properties of the phosphoryl complex.

4.3.2. *Photochromic ruthenium complexes*. Although transition metal complexes represent a relatively small fraction within the realm of photochromic compounds, they offer a large flexibility to tune the photochemical and photophysical properties with the use of different ligands. These systems are often based on linkage isomerizations between the metal center, M, and various ambidentate ligands. There are three main groups of inorganic compounds that are commonly used in photochromic materials: nitrosyl (M-NO),[141] sulfoxide (M-SO)[142] and sulfur dioxide ($M\text{-}SO_2$)[143] complexes. First, we will focus on the photoisomerization mechanism in photochromic polypyridine ruthenium sulfoxide complexes, which have attracted considerable interest over the past fifteen years or so. An intriguing complex, $[Ru(bpy)_2(OSO)]^+$ (OSO = 2-methylsulfinylbenzoate, Scheme 10), for which nonadiabatic photoisomerization via a conical intersection was deduced from the absence of spectroscopic and kinetic signatures of an O-bonded ^{3}MLCT state, has recently been synthesized.[144] The photoisomerization was suspected to occur nonadiabatically from an S-bonded ^{3}MLCT state or from an η^2-sulfoxide excited-state species. Further support of a nonadiabatic mechanism comes from the fast timescale of the isomerization (124 ps) and time-resolved transient absorption spectroscopy.[145]

Our theoretical study of this compound focused on characterizing both the adiabatic and nonadiabatic pathways for the S→O linkage photoisomerization on the lowest triplet PES.[146] The results are synthesized in Figure 34. The adiabatic route requires a multistep process involving both ^{3}MLCT and ^{3}MC states. The nonadiabatic mechanism was characterized by locating minimum energy crossing points (MECPs) between the lowest triplet state and the singlet ground state. We know that, at these critical points, efficient intersystem crossing due to significant spin-orbit interactions will take place.[134] The most important conclusions we can infer from Figure 34 are the following: i) the ^{3}MC states play a crucial role in the adiabatic mechanism: the isomerization route on the triplet PES going from the S-bonded isomer to the O-bonded isomer can only proceed through the population of ^{3}MC states for which decoordination of S and O from the metal center are favorable energetically. The critical step involving the rotation of the sulfoxide group to get from an S-bonded structure to an O-bonded structure occurs via a transition state (*SO*-MC-TS, Figure 34) of ^{3}MC character and with an η^2

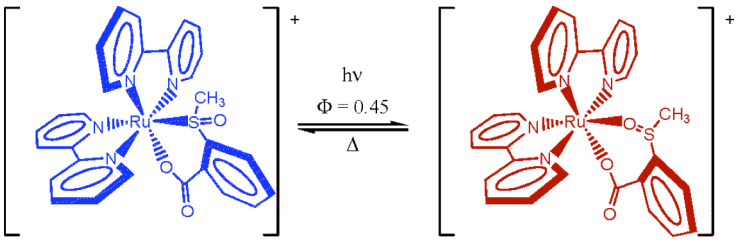

Scheme 10. Illustration of the $[Ru(bpy)_2(OSO)]^+$ photochromic system.

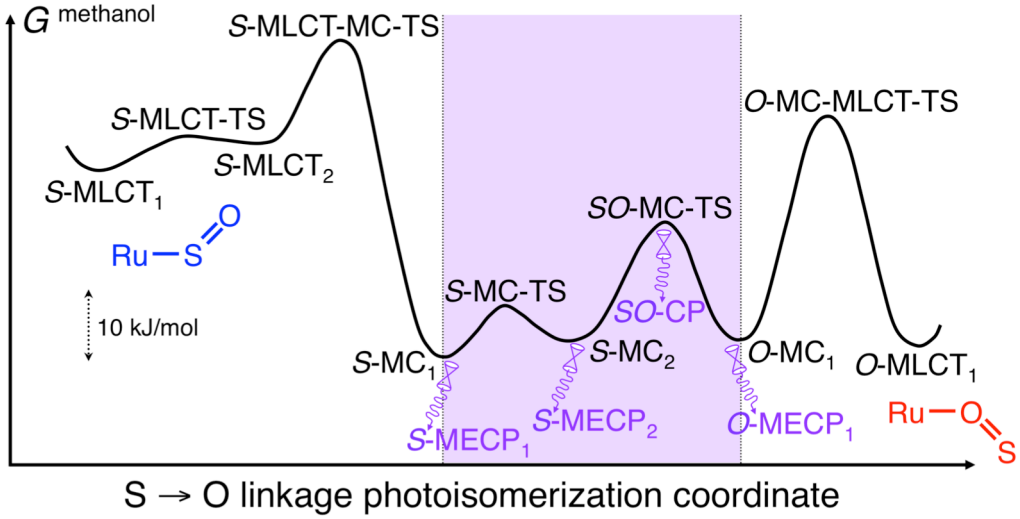

Figure 34. Schematic representation of the lowest triplet excited-state Gibbs energy profile of $[Ru(bpy)_2(OSO)]^+$ in methanol at 298 K for the S→O linkage photoisomerization path. The adiabatic pathway is shown as a black line. The region where nonadiabatic transitions can occur is represented by a purple shaded area, and funnels for such transitions are shown as double cone pictograms.

coordination; ii) the ^{3}MC states also play a critical role in the nonadiabatic mechanism: the funnels (conical intersections) for efficient triplet to singlet nonradiative decay (ISC) were all located in the region of the ^{3}MC states on the lowest triplet PES; iii) the nonadiabatic pathways are kinetically more favorable than the adiabatic path: the activation energies required to access the funnels from the respective nearby ^{3}MC minima are lower than the barrier associated with the transition states on the adiabatic triplet PES (in particular for the formation of the O-bonded ^{3}MLCT state, *O*-MLCT$_1$ in Figure 34). All these results are in agreement with the experimental observations that no O-bonded ^{3}MLCT state is formed and that the mechanism is taking place nonadiabatically through a conical intersection. However, the calculations also demonstrate that the photoisomerization will involve an excursion on the triplet PES in the region of ^{3}MC states, which was not inferred from the reported experimental observations.[142,144,145]

We then studied the $[Ru(bpy)_2(DMSO)_2]^{2+}$ (DMSO = dimethyl sulfoxide) complex[147] in order to investigate the photoisomerization mechanisms of the DMSO ligands in the *cis* and *trans* isomers (Scheme 11). When the DMSO ligands are in the *cis* position in the ground state, the stable species corresponds to two S-bonded DMSO ligands (*cis*-SS). Upon photoexcitation, the *cis*-SS isomer is converted into a species with two O-bonded DMSO ligands (*cis*-OO).[147,148] The *cis*-OO isomer is metastable and thermally reverts back to the *cis*-SS isomer. The thermal OO→SS linkage

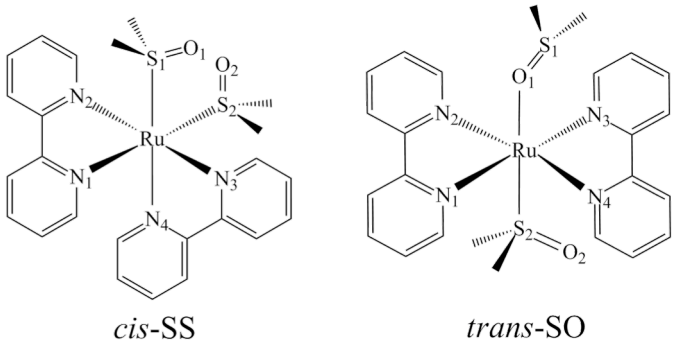

Scheme 11. Schematic representation of the *cis*- and *trans*-$[Ru(bpy)_2(DMSO)_2]^{2+}$ complexes.

isomerization occurs through a two-step process with the formation of an intermediate species with one S-bonded DMSO and one O-bonded DMSO (*cis*-SO). For the *trans* complex, it is the *trans*-SO isomer that is observed experimentally as a stable species, and its photoexcitation leads to the formation of the *trans*-OO isomer.[148] Our theoretical investigation aimed at elucidating the double linkage photoisomerization mechanism in the *cis* complex (*cis*-SS→*cis*-OO) and the single linkage photoisomerization mechanism in the trans complex (*trans*-SO→*trans*-OO).[149]

For the *cis* complex, reaction pathways that allow the adiabatic SS → OO isomerization on the lowest triplet excited PES were identified. Along these paths, the S→O linkage isomerization of the two S-bonded DMSO ligands occurs sequentially following one-photon excitation of the *cis*-SS isomer and is thermodynamically allowed throughout. As for the linkage photoisomerization of the bidentate OSO ligand in $[Ru(bpy)_2(OSO)]^+$, following the population of the lowest ^{3}MLCT state that already elongates the Ru−S bond, the intervention of highly distorted ^{3}MC states is required to allow the large structural rearrangements occurring during the linkage isomerization of DMSO ligands.[146] The two possible adiabatic routes are i) SS-^{3}MLCT→SO-^{3}MC→OO-^{3}MC→OO-^{3}MLCT, or ii) SS-^{3}MLCT→SO-^{3}MLCT→OO-^{3}MC→OO-^{3}MLCT (Figure 35a). In addition, some nonradiative deactivations toward the ground state are favorable from ^{3}MC states, especially after the linkage isomerization of the first DMSO ligand, due to the presence of singlet/triplet conical intersections. In this nonadiabatic scenario, the SO-bonded ground state is populated and a second photoexcitation is required to isomerize the second S-bonded DMSO ligand, which results in a proposed two-photon mechanism (Figure 35b).

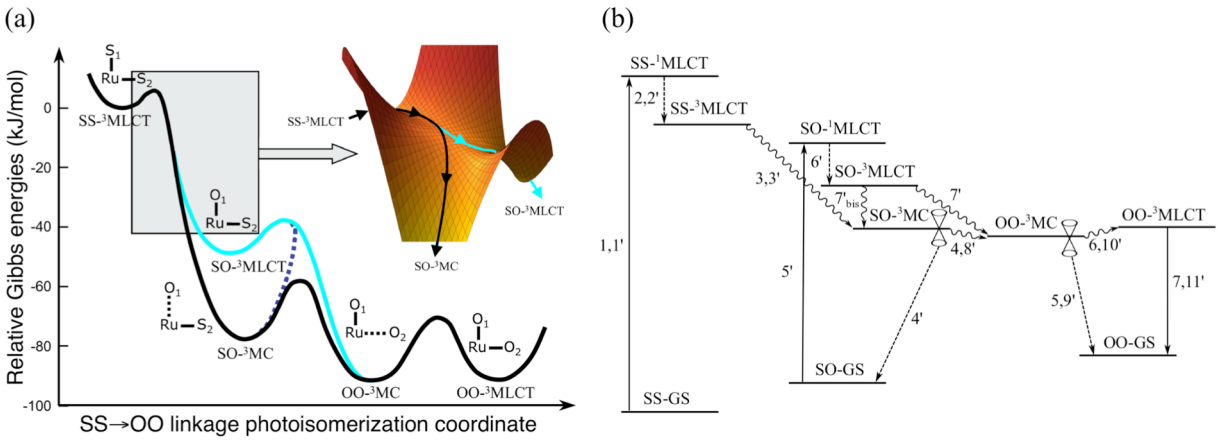

Figure 35. (a) Gibbs energy profile of *cis*-$[Ru(bpy)_2(DMSO)_2]^{2+}$ in DMSO at 298 K for the adiabatic *cis*-SS → *cis*-OO photoisomerization paths. The Gibbs energies are arbitrarily given relative to the SS-^{3}MLCT state. The black line represents the lowest energy reaction path and the cyan line, an alternative path. The inset schematically shows a possible bifurcation occurring after the first transition state encountered along the back path. (b) Schematic depiction of the major events involved in the stepwise *cis*-SS → *cis*-OO double photoisomerization mechanism. The various steps are labeled sequentially for the one-photon mechanism (1−7) and the two-photon mechanism (1′−11′). Solid arrows are used for absorption and emission, dashed arrows for intersystem crossings and curly arrows for adiabatic processes.

For the *trans* complex, the mechanism is far simpler. As summarized in Figure 36, upon photoexcitation, the system relaxes to the OO-^{3}MC species leading to the ground-state photoproduct OO-GS following nonradiative decay (ISC at a funnel near OO-^{3}MC). This process is barrierless (no

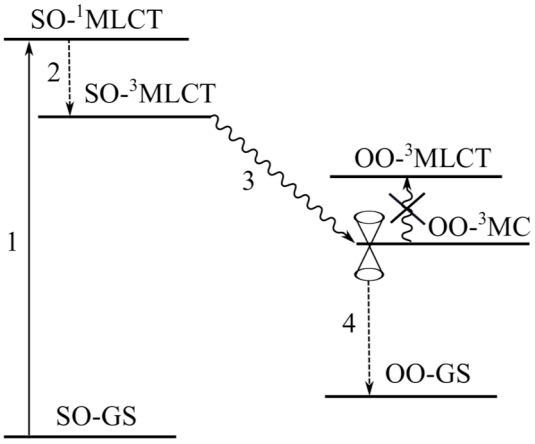

Figure 36. Schematic depiction of the SO→OO photoisomerization mechanism of *trans*-$[Ru(bpy)_2(DMSO)_2]^{2+}$. The various steps, which result in the population of the OO-GS state, are labeled sequentially (1−4) and their nature is specified using the same code as in Figure 35.

minimum corresponding to the SO-^{3}MLCT species) and population of the OO-^{3}MLCT is highly unlikely due to its high energy relative to the funnel near OO-^{3}MC. This peculiarity implies that the *trans* complex has probably the same behavior at room temperature and at low temperature, namely the absence of emission from the SO-^{3}MLCT state and a photochromic behavior.

Our interest in using organophosphorus ligand to tune the photophysical properties of polypyridine ruthenium complexes (see subsection 4.3.1) also incited us to use this type of ligands to design original photoswitchable and possibly photochromic complexes. While the aminophosphine and phosphoryl ambidentate ligands reported above were successful in improving the luminescence efficiency of polypyridine ruthenium complexes, they did not confer any photoisomerizable properties to these systems. However, the phosphinidene oxide ligand (R-P=O) proved to be a completely different story. We performed a DFT-based computational study in the gas phase and in acetonitrile on the yet to be synthesized $[Ru(tpy)(bpy)(POPh)]^{2+}$ (Ru–P, Figure 37a) and $[Ru(tpy)(bpy)(OPPh)]^{2+}$ (Ru-O, Figure 37a) complexes and predicted that they would constitute a prototype for a new family of inorganic photochromic systems.[150]

The computed P→O linkage photoisomerization pathways are schematized in Figure 37b. The P-bonded isomer (Ru–P) and the O-bonded isomer (Ru–O) are characterized by distinct UV-visible

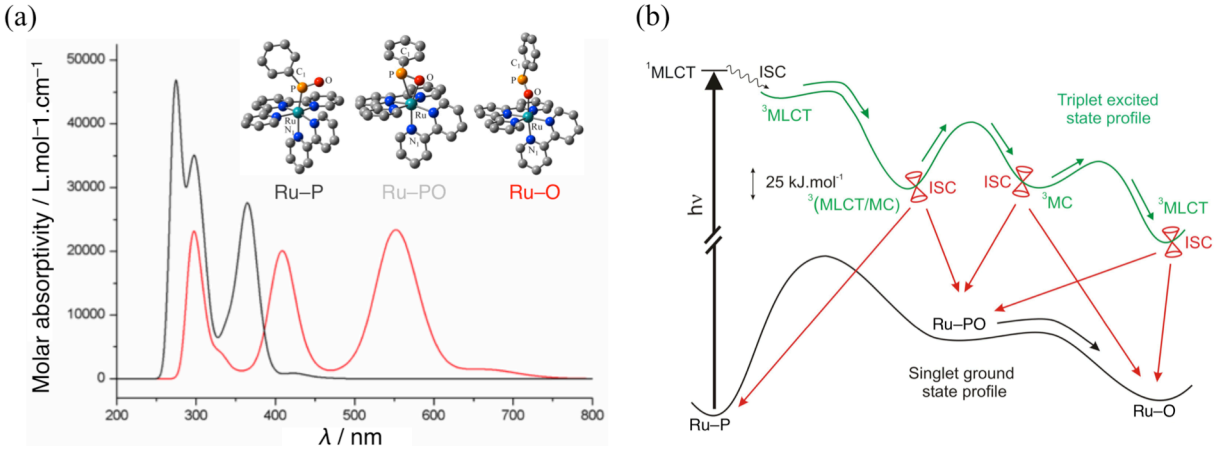

Figure 37. (a) UV-visible absorption spectra of Ru–P and Ru–O linkage isomers of $[Ru(tpy)(bpy)(POPh)]^{2+}$ computed by TD-DFT. (b) Schematic representation of the adiabatic (green line) and nonadiabatic (red line) mechanisms of the Ru–P → Ru–O photoisomerization process. Triplet/singlet funnels are represented by double cone pictograms.

absorption spectra (Figure 37a): Ru–P is expected to be colorless, while Ru–O should be colored. The main result is that the thermal isomerization is both kinetically and thermodynamically unfavorable, whereas photoisomerization can readily take place either by adiabatic or nonadiabatic routes (Figure 37b). The adiabatic mechanism is based on a triplet potential energy profile that connects various excited states of the two isomers. Although this mechanism can lead to the photoproduct formation, the location of triplet/singlet funnels in the vicinity of the lowest energy minima along the excited-state profile will favor the nonadiabatic pathways. We have shown that upon nonradiative decay (ISC) at these funnels, the photoisomerization can complete on the ground state PES. Another consequence of the presence of these funnels will be the absence of luminescence in this system. The reverse RuO to RuP isomerization was found to be achievable only thermally. The backward isomerization barrier is relatively large allowing the photoproduct to be long-lived (several hours), as found for example in ruthenium sulfoxide complexes.[151] Thus, the predicted bistability of the complex, the different absorption properties (different colors) of the two isomers and their photoswitching properties make this complex a promising candidate for photochromic devices.

5. Perspectives

5.1. Electronic energy transfer

Electronic energy transfer (EET) between chromophores is an important process in biology and chemistry. In photosynthesis special antennae complexes harvest light, but the absorbed energy must be transferred into another part of the system to be used. A famous example of EET is fluorescence resonance energy transfer (FRET), where light is absorbed in one part of the system and emitted in another part. FRET has become one of the most important tools for studying structure and dynamics of biological systems.[152] However, our understanding of how energy transfer occurs at the molecular level is still rather limited and mostly based upon empirical theories, such as Förster theory[153] and Dexter theory[154] that are of limited use to design new systems.

Our plan is to provide a general theoretical framework to rationalize EET processes at the molecular level. We will use *ab initio* quantum chemistry approaches in combination with on-the-fly nonadiabatic MD simulations to provide evidence for an EET mechanism that is based on chemical reaction pathways on nonadiabatically coupled PESs. Our investigation will focus on a bridged bichromophoric system[155] shown in Figure 38. This dyad consists of a cyclic α-diketone incorporating a para-substituted benzene ring. Upon photoexcitation to the (π,π^*) state on benzene, EET takes place to the (n,π^*) state on the α-diketone moiety. By varying the length of the linkers connecting the two chromophore units, Speiser and coworkers were able to control the distance and relative orientation

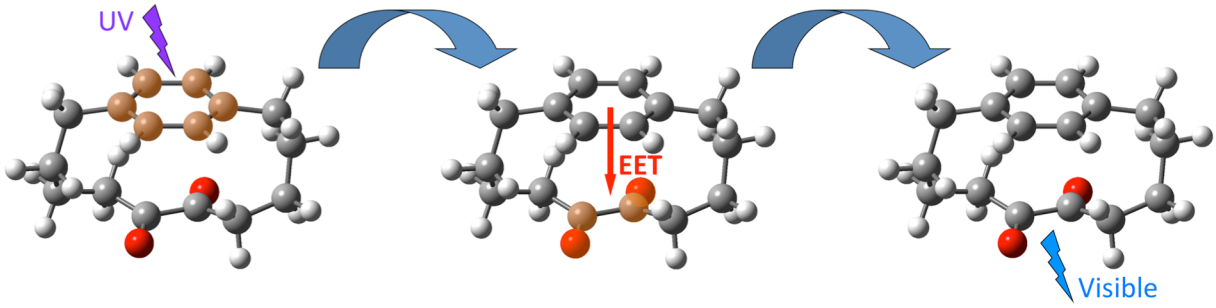

Figure 38. Illustration of EET in the P_{44} bichromophore.

between the chromophores. In the smallest dyad, with four aliphatic carbon atoms in both linkers (denoted P_{44}), excitation of benzene at 268 nm induces fluorescence of α-diketone at 480 nm with a 100% efficiency.[155] We will thus try to understand the EET mechanism in P_{44} and account for the very efficient energy transfer process that occurs in this bichromophoric system. We will also attempt to rationalize the decrease of EET efficiency upon increasing the length of the aliphatic bridges by studying the P_{55} and P_{66} systems.

5.2. Photoswitchable systems

5.2.1. *Organic photoswitches*. Another aspect that I would like to investigate in organic photochromic systems is the improvement of photoisomerization efficiency with the use of multiphoton excitation. For example, while DHA to VHF photoconversion is highly efficient in the first electronic excited state, the backward isomerization can only take place thermally or via two-photon excitation.[90] The mechanistic picture obtained from our theoretical study back in 2002 provided an explanation for the forbidden VHF to DHA photoisomerization in the S_1 state (see section 4.1.2).[91] However, no investigation of the higher excited states has been performed to rationalize the results from the two-pulse experiments.[90c] Similarly, dithienylethene photochromism has been extensively studied both experimentally and theoretically. Our theoretical contribution provided a detailed mechanistic picture for the cyclization and cycloreversion reactions in the first electronic state.[92] However, no theoretical data are available to interpret the recently observed increase of the cycloreversion quantum yield following sequential two-photon excitation.[156] One objective could be to extend our theoretical studies to the excited states involved in these multiphoton excitation experiments and rationalize the experimental data. Following this line of thought, we could also consider whether the use of nonlinear optical processes (two-photon excitations) can improve the DHP to CPD photoizomerization efficiency.

5.2.2. *Reversibly switchable fluorescent proteins*. Reversibly switchable fluorescent proteins (RSFPs) are proteins homologous to the Green Fluorescent Protein (GFP) developed over the last decade, that can be switched back and forth between a fluorescent state (ON state) and a non-fluorescent state (OFF state) by irradiation at appropriate wavelengths (see Figure 39 for examples).

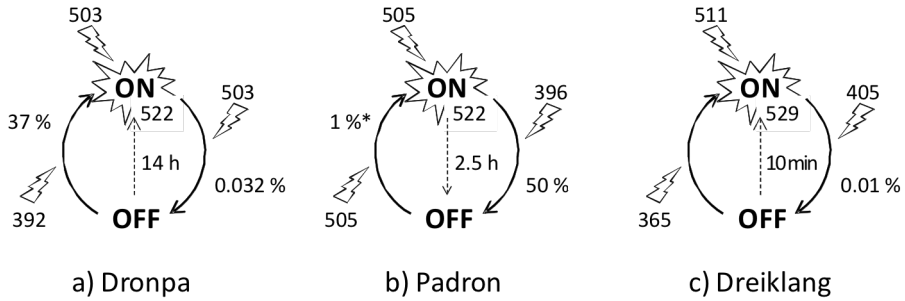

Figure 39. Schematic representation of the reversible thermal and photoinduced transitions of the RSFP variants to be investigated: a) Dronpa, b) Padron and c) Dreiklang. The wavelengths driving the different photoinduced processes are written at the end of the excitation flashes, and the associated quantum yields on the side of the arrows. The emission wavelengths of the ON forms are indicated at the lower right edge of the explosion pictograms symbolizing fluorescence. The half-lives of the metastable forms are given at the right of the dashed arrows representing thermal recovery reactions.

The number of ON-OFF cycles that can actually be achieved varies from one RSFP to the other. It is determined by the competition between reversible ON-OFF switching and irreversible photoreactions equivalent to those responsible for the photobleaching of conventional fluorescent proteins.[157] In addition to the photoinduced transitions, RSFPs exhibit a thermal recovery reaction, which spontaneously restores the most stable form (ON or OFF depending on the protein).

Thanks to their reversible photoconversion properties, RSFPs show great promise for numerous new imaging techniques, in particular in the field of super-resolution imaging. As an example, in PALM (photoactivation and localization microscopy) super-resolution imaging, a sparse subset of RSFPs are switched ON, localized with subdiffraction spatial precision by fitting of the diffraction-limited spots corresponding to single molecules, and then switched OFF.[158] This process is repeated many times, and the position information from all sequentially photoactivated subsets is assembled into a super-resolution image.

One of the main drawbacks of available RSFPs is their low photoswitching quantum yields. Higher photoswitching efficiencies would increase the number of achievable ON-OFF cycles, by favoring reversible photoswitching over irreversible photoreactions. The ability to perform a high number of ON-OFF cycles is important for applications (e.g., in PALM, it would increase the duration of the super-resolution movies that can be acquired). Higher photoswitching efficiencies would moreover decrease the irradiation time and/or power needed to drive the ON-OFF transitions.

It would be highly desirable to establish detailed models of the photophysics and photochemistry of RSFPs, aimed in particular at understanding why some photoswitching quantum yields are so low. It could then be used to rationally design new mutants with increased efficiency. For this purpose, we would like to investigate both reactive processes leading to the photoswitched state and competitive nonreactive excited-state relaxation processes leading back to the initial ground state in three RSFPs named Dronpa, Padron and Dreiklang (Figure 39). As far as the photoswitching process is concerned, X-ray crystallography studies revealed two types of mechanisms: the photoswitching of Dronpa[159] and Padron[160] consists in cis/trans isomerization of the chromophore double bond and protonation/deprotonation of its phenol group, while Dreiklang[161] exhibits a completely different photoswitching mechanism based on the reversible addition of a water molecule on the C-N double bond of the imidazolinone ring (Figure 40).

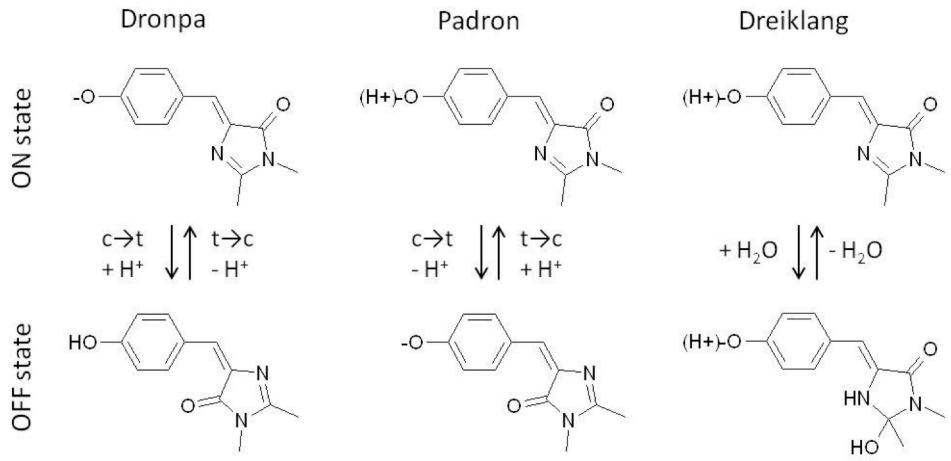

Figure 40. Chromophore states in the ON and OFF forms of Dronpa, Padron and Dreiklang. The molecular changes associated with the photoswitching reactions at chromophore level are indicated on the side of the corresponding arrows. c and t stand for cis and trans, respectively.

Computational photochemistry is a formidable help to understand and interpret the extremely complex time-resolved experimental data on such biological photoactive systems. To systematically exploit the potential of such photoswitchable proteins and to enable rational improvements to their properties require a detailed understanding of the molecular switching mechanism, which is still largely unknown. In the past, we were able to unravel the photoswitching mechanism in asFP595 based on extensive CASSCF calculations and QM/MM excited-state MD simulations.[162] Using a similar strategy, our goal here will be to get insight into the nature of the intermediate states leading to the final products identified by X-ray crystallography and to identify the amino acids that are transiently involved in the photoswitching mechanism of these three RSFPs. We might then be in a position to propose new variants of Dronpa, Padron and Dreiklang with increased photoswitching quantum yields by mutagenesis at rationally selected amino acid positions. It is important to note that, considering the complexity of the processes involved, this kind of studies can only be successful if a close partnership between experiment and theory is established.

5.2.3. *Inorganic photochromes*. As mentioned in section 4.3.2, there exist inorganic photochromic compounds which typically involve optical switching of an ambidentate ligand such as NO^+, SO_2 or RR'S=O. Two families of complexes will be the center of my interest in the next future. First, ruthenium nitrosyl complexes have found utility in a variety of applications, such as optical switches and data storage,[163] or medicine.[164] Depending on the ancillary ligands, environment, and irradiation wavelength, these complexes can undergo either intramolecular N→O linkage photoisomerization[141,165] or NO photorelease[166] (Figure 41). A recent theoretical study has investigated the initial part of the NO photorelease mechanism,[167] but so far the mechanistic picture associated with the intramolecular N→O linkage photoisomerization remains unclear. Our main objective will be to investigate the photoreactivity of ruthenium nitrosyl complexes in realistic conditions in order to understand the factors that govern the competition between intramolecular N→O linkage photoisomerization and NO photorelease.

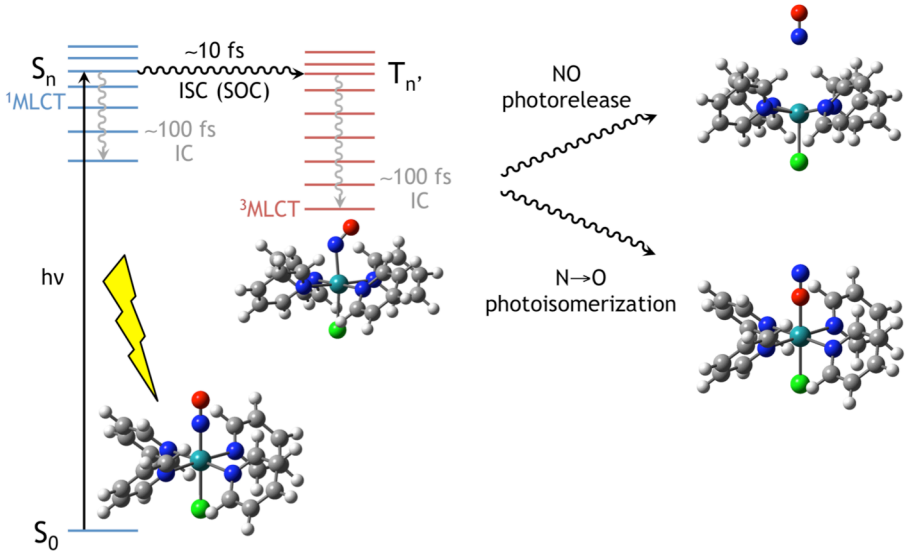

Figure 41. Illustration of the competing photoisomerization and photorelease mechanisms taking place in the triplet states of a ruthenium nitrosyl complex. IC: internal conversion, ISC: intersystem crossing, SOC: spin-orbit coupling.

Another family of inorganic photochromic complexes which we are interested in is the sulfoxide (RR'S=O) family. Our recent theoretical studies of ruthenium sulfoxide complexes[146,149] have revealed the involvement of ^{3}MC states in the nonadiabatic S→O linkage photoisomerization mechanism, which was not inferred from the experimental observations.[142] One of the reasons was that osmium sulfoxide complexes can also undergo S→O linkage photoisomerization despite the fact that these MC states are inaccessible for third-row transition metals.[168] Thus, I will investigate theoretically the S→O linkage photoisomerization in osmium sulfoxide complexes for which I expect to find a different mechanism compared to their ruthenium counterparts.

5.2.4. *Hybrid photochromes*. In the context of elaborating multifunctional materials, two main strategies can be followed. The first one consists in combining several photochromic units onto a single molecule to allow for multiswitchable systems.[89a,169] This approach has been successfully applied for the first time between dihydroazulene and diarylethene chromophores.[170] The second promising approach is to covalently link organic photochromic derivatives with metal complexes.[171] An example is the bridging of bisterpyridine ruthenium complexes with DHP/CPD photochromes.[172] One strategy we are considering is the possibility to merge these two distinct approaches by linking DHP/CPD photochromes to photochromic ruthenium nitrosyl or sulfoxide complexes (Scheme 12 for an illustration using ruthenium nitrosyl complexes). To our knowledge, it would be the first attempt to attach an organic negative photochrome to an inorganic positive photochrome. We anticipate that from the Ru-NO/DHP stable ground-state isomer, we may be able to control the reversible transformation to the metastable states Ru-ON/DHP and Ru-NO/CPD. These two states should have distinct optical signatures and we will investigate whether the Ru-ON/CPD isomer formation can be controlled, providing an original cyclic multistep switch. In the case of ruthenium nitrosyl complexes, it will also be interesting to verify if the NO photorelease properties is modulated by the presence of the organic photochrome.

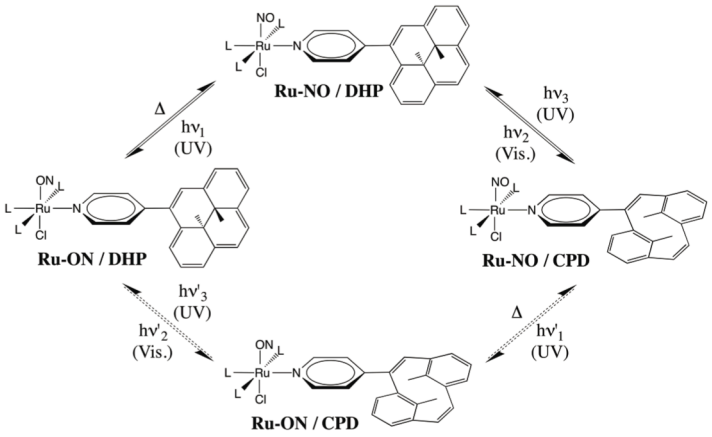

Scheme 12. Example of a hybrid multiswitchable system based on ruthenium nitrosyl complexes linked with DHP/CPD photochromes.

5.3. SOC nonadiabatic dynamics in transition metal complexes

So far, all our theoretical studies of ruthenium complexes have been limited to the exploration of the excited-state PESs to rationalize their photochemical and photophysical properties. The static

information gained from these calculations has been enlightening (see section 4.3). Two main hypotheses were made to derive the mechanistic features from the excited-state potential energy landscapes: i) we assumed that the photochemical and photophysical properties of the studied complexes could be rationalized based only on the population of the lowest triplet excited state, and ii) nonradiative deactivations by ISC were assumed to take place at singlet/triplet crossings only. While it is reasonable to think that the lowest excited state will eventually be populated, the relaxations pathways from the initially excited singlet states and their possible deactivation to higher triplet states by ISC have been ignored. In other words, the initial part of the photochemical path is completely overlooked and assumed to lead to the lowest excited state on an ultrafast timescale. Moreover, while we know that efficient ISC will take place at singlet/triplet crossings, SOC will also allow ISC to take place away from the crossing regions. It would therefore be desirable to go beyond the "simple" static approach and investigate the photochemistry of these systems from the initially excited singlet states to the final photoproducts using a dynamical strategy which allows the computation of the nonadiabatic transition probabilities between singlet and triplet states like in the case of internal conversion (see section 3.2).

The TSH method[74] was originally formulated to consider only nonadiabatic couplings between electronic states of the same spin multiplicity and has been therefore extensively used to describe nonadiabatic excited-state dynamics involving internal conversion. By introducing SOC in the surface hopping procedure, dynamical studies can be extended to describe ISC. Several approaches of increasing complexity have been proposed to achieve this purpose. On the simplest level, hopping between states of different spin multiplicity is performed "manually". This can be done by exploring first the deactivation mechanism within, for example, the singlet manifold with conventional TSH and then identifying singlet/triplet crossings, where ISC is assumed to occur, along these trajectories. These regions then serve as starting points for independent simulations (a procedure known as *spawning*) in the triplet manifold. This oversimplified approach was first used by Warshel and Karplus[173] in the 70s but is still considered a viable option to treat complex systems (see reference [167] for example). On the next level of sophistication, conventional TSH is applied between states of different spin multiplicity by computing hopping probabilities only at crossing points based on Landau-Zener theory.[71,72] In this approach, internal conversions and intersystem crossings are treated inconsistently. A more reliable way to treat ISC is to properly include SOC in the equation of motion which governs the evolution of the electronic populations and hence the hopping probabilities. Thus, ISC can occur in principle at every time step of the simulation and not just at singlet/triplet crossings. Two alternative approaches can be considered. In the case of weak SOC, *spin-diabatic* states can be used[174] but the more reliable approach consists in using *spin-adiabatic* (or *spin-coupled*) states which are eigenstates of the total electronic Hamiltonian including SOC.[174,175,176]

I would like to apply this type of methods to study the photodynamics of ruthenium nitrosyl complexes in order to describe the competition between intramolecular N→O linkage photoisomerization and NO photorelease. While the static approach can provide useful information about the most likely photochemical pathways for these two processes, simulating the competition between them requires a dynamical approach in order to understand the factors favoring one process over the other. This project will involve designing model systems small enough to apply nonadiabatic on-the-fly SOC dynamics. The reason is that the evaluation of the energy and forces on-the-fly is very time-consuming even for relatively small ruthenium complexes.

6. Conclusion

In this manuscript, I have tried to convince the reader that computational photochemistry is a powerful tool to investigate the underlying mechanisms of photochemical reactions that determine the fate of a molecular system from energy absorption to photoproduct formation. I hope that, through the different studies I have participated in, I have provided evidence that conical intersections and their associated crossing seams were playing a central role in these mechanisms. Research performed in computational photochemistry in recent years has made it evident that these extended crossing seams are key mechanistic features of excited-state mechanisms.[1,9,12,13,177] In this manuscript, I have given examples in the fields of organic photochemistry (photoswitching mechanisms of organic photochromic systems, photostability of PAHs, photoinduced intramolecular charge transfer in donor-acceptor systems), photobiochemistry (photoisomerization of a protein, photostability and photodamage in DNA) and inorganic photochemistry (photoswitching mechanisms of photochromic ruthenium complexes). These studies rely on exploring the relevant PESs involved in the investigated photochemical processes, including the characterization of the all-important conical intersections accessible along the photochemical path(s). This (or these) photochemical path(s) is (are) determined by a series of minimum energy path calculations allowing the connection of the excited reactant (Franck-Condon point on the corresponding excited-state PES) to the ground-state photoproduct(s). Based on this static information, one can already obtain a detailed insight into the mechanistic picture of the photochemistry and/or photophysics of the system. These studies can sometimes be complemented by a dynamical approach. The underlying molecular mechanisms of light-driven processes are typically governed by sub-picosecond atomic motions. Mechanisms on such ultrafast timescales are very challenging to probe by experiment, in particular in complex systems like proteins. Thus, molecular dynamics simulations have become an invaluable tool to understand such processes in atomic detail. In addition, I have shown that, depending on the orientation of the photochemical reaction path with the branching space coordinates, the extended crossing seam may require vibrational motion within the branching space to be accessed. Only a dynamical investigation can then determine if the seam is really accessible and on which timescale. Also, these seams may play the role of reactive or quenching funnels depending on the local topology of the PESs at the crossing region. Dynamics can then help to determine quantum yields and branching ratios provided that one properly samples the initial conditions and performs enough simulations to analyze the results on a statistical basis.

Any mechanistic study undertaken using quantum chemistry methods requires considerable physical and chemical insight. Thus, for a thermal reaction, there is no method that will generate automatically all the possible mechanistic pathways that might be relevant. Rather, one still needs to apply skills of chemical intuition and make sensible hypotheses that can then be explored computationally. In excited-state chemistry, these problems are even more difficult, and I hope the examples given in this manuscript are a step in providing this required insight. In addition to the conceptual and physical problems associated with mechanistic studies in photochemistry, the actual computations are technically difficult to carry out. Whether the calculations are aimed at obtaining static or dynamical information on the photochemical process, I believe that only a well-trained scientist in computational photochemistry can be in a position to perform these calculations and interpret their results with a critical viewpoint.

To finish, it is clear that we are now living a new era where experimental and theoretical chemistry can talk to each other on an equal footing. I have been privileged to work on fascinating systems, which I would never have studied without the efforts of experimental groups to synthesize these systems and without their willingness to understand how their systems physically operate. The work I have carried out with my coworkers was often the outcome of a constructive interplay between the experimental and theoretical viewpoints, and has been rewarding in many different ways as a result.

7. References

[1] (a) A. G. Kutateladze (Ed.), Computational Methods in Photochemistry, CRC Press, 2005. (b) M. Olivucci (Ed.), Computational Photochemistry, Elsevier, 2005.

[2] I. J. Palmer, I. N. Ragazos, F. Bernardi, M. Olivucci, M. A. Robb, An MC-SCF study of the S_1 and S_2 photochemical reactions of benzene, *J. Am. Chem. Soc.* 115 (**1993**) 673–682.

[3] W. T. A. M. van der Lugt, L. J. Oosterhoff, Symmetry control and photoinduced reactions, *J. Am. Chem. Soc.* 91 (**1969**) 6042–6049.

[4] (a) H. E. Zimmerman, On molecular orbital correlation diagrams, the occurrence of Möbius systems in cyclization reactions, and factors controlling ground- and excited-state reactions. I, *J. Am. Chem. Soc.* 88 (**1966**) 1564–1565. (b) H. E. Zimmerman, Molecular orbital correlation diagrams, Möbius systems, and factors controlling ground- and excited-state reactions. II, *J. Am. Chem. Soc.* 88 (**1966**) 1566–1567.

[5] E. Teller, Internal conversion in polyatomic molecules, *Isr. J. Chem.* 7 (**1969**) 227–235.

[6] (a) J. Michl, Photochemical reactions of large molecules. I. A simple physical model of photochemical reactivity, *Mol. Photochem.* 4 (**1972**) 243–255. (b) J. Michl, *Topics Curr. Chem.* 46 (**1974**) 1. (c) J. Michl, Model calculations of photochemical reactivity, *Pure App. Chem.* 41 (**1975**) 507–534.

[7] E. Teller, The crossing of potential energy surfaces, *J. Phys. Chem.* 41 (**1937**) 109–116.

[8] G. Herzberg, H. C. Longuet-Higgins, Intersection of potential energy surfaces in polyatomic molecules, *Disc. Faraday Soc.* 35 (**1963**) 77–82.

[9] M. A. Robb, F. Bernardi, M. Olivucci, Conical intersections as a mechanistic feature of organic photochemistry, *Pure App. Chem.* 67 (**1995**) 783–789.

[10] F. Bernardi, M. Olivucci, M. A. Robb, Potential energy surface crossings in organic photochemistry, *Chem. Soc. Rev.* 25 (**1996**) 321–328.

[11] F. Bernardi, M. Olivucci, J. Michl, M. A. Robb, Conical intersections in the theory of organic singlet photochemistry, *The Spectrum* 9 (**1996**) 1–6.

[12] M. A. Robb, M. Garavelli, M. Olivucci, F. Bernardi, A computational strategy for organic photochemistry, *Rev. Comp. Chem.* 15 (**2000**) 87–146.

[13] M. J. Bearpark, M. A. Robb, Conical intersection species as reactive intermediates, in *Reviews of reactive intermediate chemistry*, Eds. M. S. Platz, R. A. Moss, M. Jones Jr., Wiley, New Jersey, 2007, pp. 379–414.

[14] C. A. Mead, The "noncrossing" rule for electronic potential energy surfaces: The role of time-reversal invariance, *J. Chem. Phys.* 70 (**1979**) 2276–2283.

[15] (a) C. A. Mead, D. G. Truhlar, On the determination of Born-Oppenheimer nuclear motion wave functions including complications due to conical intersections and identical nuclei, *J. Chem. Phys.* 70 (**1979**) 2284–2296. (b) C. A. Mead, D. G. Truhlar, Erratum: On the determination of Born-Oppenheimer nuclear motion wave functions including complications due to conical intersections and identical nuclei, *J. Chem. Phys.* 78 (**1983**) 6344.

[16] (a) D. R. Yarkony, Diabolical conical intersections, *Rev. Mod. Phys.* 68 (**1996**) 985–1013. (b) D. R. Yarkony, Conical intersections: diabolical and often misunderstood, *Acc. Chem. Res.* 31 (**1998**) 511–518.

[17] M. Baer, Beyond Born-Oppenheimer: Electronic nonadiabatic coupling terms and conical intersections, Wiley, New York, 2006, pp. 1–234.

[18] D. G. Truhlar, C. A. Mead, Relative likelihood of encountering conical intersections and avoided intersections on the potential energy surfaces of polyatomic molecules, *Phys. Rev. A* 68 (**2003**) 032501.

[19] V. I. Baranovskii, Photochemistry of XXI century: Paradigm change, *Russ. J. Gen. Chem.* 80 (**2010**) 1586–1592.

[20] (a) A. L. Sobolewski, W. Domcke, The chemical physics of the photostability of life, *Europhysics News* 37 (**2006**) 20–23. (b) A. L. Sobolewski, W. Domcke, Molecular mechanisms of the photostability of life, *Phys. Chem. Chem. Phys.* 12 (**2010**) 4897–4898. (c) B. G. Levine, T. J. Martínez, Isomerization through conical intersections, *Annu. Rev. Phys. Chem.* 58 (**2007**) 613–634. (d) T. J. Martínez, Seaming is believing, *Nature* 467 (**2010**) 412–413. (e) D. Polli, P. Altoè, O. Weingart, K. M. Spillane, C. Manzoni, D. Brida, G. Tomasello, G. Orlandi, P. Kukura, R. A. Mathies, M. Garavelli, G. Cerullo, Conical intersection dynamics of the primary photoisomerization event in vision, *Nature* 467 (**2010**) 440–443. (f) S. Matsika, P. Krause, Nonadiabatic events and conical intersections, *Annu. Rev. Phys. Chem.* 62 (**2011**) 621–643. (g) W. Domcke, D. R. Yarkony, Role of conical intersections in molecular spectroscopy and photoinduced chemical dynamics, *Annu. Rev. Phys. Chem.* 63 (**2012**) 325–352.

[21] We only address in this manuscript the case of conical intersections between two electronic states. Three-state degeneracies also exist, particularly in the context of Jahn-Teller problems, but are less common when accidental crossings are considered.

[22] J. von Neumann, E. P. Wigner, On the behaviour of eigenvalues in adiabatic processes, *Phys. Z.* 30 (**1929**) 467–470.

[23] G. J. Atchity, S. S. Xantheas, K. Ruedenberg, Potential energy surfaces near intersections, *J. Chem. Phys.* 95 (**1991**) 1862–1876.

[24] I. N. Ragazos, M. A. Robb, F. Bernardi, M. Olivucci, Optimization and characterization of the lowest energy point on a conical intersection using an MC-SCF Lagrangian, *Chem. Phys. Lett.* 197 (**1992**) 217–223.

[25] M. J. Bearpark, M. A. Robb, H. B. Schlegel, A direct method for the location of the lowest energy point on a potential surface crossing, *Chem. Phys. Lett.* 223 (**1994**) 269–274.

[26] G. A. Worth, M. J. Bearpark, M. A. Robb, Semiclassical nonadiabatic trajectory computations in photochemistry: Is the reaction path enough to understand a photochemical reaction mechanism?, in *Computational Photochemistry*, Ed. M. Olivucci, Elsevier, Amsterdam, 2005, pp. 171–190.

[27] G. A. Worth, L. S. Cederbaum, Beyond Born-Oppenheimer: Molecular dynamics through a conical intersection, *Annu. Rev. Phys. Chem.* 55 (**2004**) 127–158.

[28] G. A. Worth, M. A. Robb, Applying direct molecular dynamics to non-adiabatic systems, *Adv. Chem. Phys.* 124 (**2002**) 355–431.

[29] G. A. Worth, P. Hunt, M. A. Robb, Nonadiabatic dynamics: A comparison of surface hopping direct dynamics with quantum wavepacket calculations, *J. Phys. Chem. A* 107 (**2003**) 621–631.

[30] B. Lasorne, G. A. Worth, M. A. Robb, Excited-state dynamics, *WIREs Comput. Mol. Sci.* 1 (**2011**) 460–475.

[31] M. Barbatti, Nonadiabatic dynamics with trajectory surface hopping method, *WIREs Comput. Mol. Sci.* 1 (**2011**) 620–633.

[32] M. W. Schmidt, M. S. Gordon, The construction and interpretation of MCSCF wavefunctions, *Annu. Rev. Phys. Chem.* 49 (**1998**) 233–266.

[33] V. Veryazov, P. Å. Malmqvist, B. O. Roos, How to select active space for multiconfigurational quantum chemistry?, *Int. J. Quantum Chem.* 111 (**2011**) 3329–3338.

[34] W. T. Borden, E. R. Davidson, The importance of including dynamic electron correlation in *ab initio* calculations, *Acc. Chem. Res.* 29 (**1996**) 67–75.

[35] K. Andersson, P. Å. Malmqvist, B. O. Roos, A. J. Sadlej, K. Wolinski, Second-order perturbation theory with a CASSCF reference function, *J. Phys. Chem.* 94 (**1990**) 5483–5488.

[36] M. Garavelli, Computational organic photochemistry: strategy, achievements and perspectives, *Theor. Chem. Acc.* 116 (**2006**) 87–105.

[37] D. Roca-Sanjuán, F. Aquilante, R. Lindh, Multiconfiguration second-order perturbation theory approach to strong electron correlation in chemistry and photochemistry, *WIREs Comput. Mol. Sci.* 2 (**2012**) 585–603.

[38] M. Boggio-Pasqua, M. J. Bearpark, M. A. Robb, Photostability via a sloped conical intersection: a CASSCF and RASSCF study of pyracylene, *J. Phys. Chem. A* 109 (**2005**) 8849–8856.

[39] M. Boggio-Pasqua, M. J. Bearpark, M. Klene, M. A. Robb, A computational strategy for geometry optimization of ionic and covalent excited states, applied to butadiene and hexatriene, *J. Chem. Phys.* 120 (**2004**) 7849–7860.

[40] M. Boggio-Pasqua, G. Groenhof, On the use of reduced active space in CASSCF calculations, *Comput. Theor. Chem.* 1040–1041 (**2014**) 6–13.

[41] K. K. Baeck, T. J. Martínez, Ab initio molecular dynamics with equation-of-motion coupled-cluster theory: electronic absorption spectrum of ethylene, *Chem. Phys. Lett.* 375 (**2003**) 299–308.

[42] (a) I. Tavernelli, U. F. Röhrig, U. Rothlisberger, Molecular dynamics in electronically excited states using time-dependent density functional theory, *Mol. Phys.* 103 (**2005**) 963–981. (b) E. Tapavicza, I. Tavernelli, U. Rothlisberger, C. Filippi, M. E. Casida, Mixed time-dependent density-functional theory/classical trajectory surface hopping study of oxirane photochemistry, *J. Chem. Phys.* 129 (**2008**) 124108. (c) B. F. E. Curchod, U. Rothlisberger, I. Tavernelli, Trajectory-based nonadiabatic dynamics with time-dependent density functional theory, *Chem. Phys. Chem.* 14 (**2013**) 1314–1340.

[43] A. Dreuw, M. Head-Gordon, Single-reference ab initio methods for the calculation of excited states of large molecules, *Chem. Rev.* 105 (**2005**) 4009–4037.

[44] B. G. Levine, C. Ko, J. Quenneville, T. J. Martínez, Conical intersections and double excitations in time-dependent density functional theory, *Mol. Phys.* 104 (**2006**) 1039–1051.

[45] F. Cordova, L. J. Doriol, A. Ipatov, M. E. Casida, C. Filippi, A. Vela, Troubleshooting time-dependent density-functional theory for photochemical applications: Oxirane, *J. Chem. Phys.* 127 (**2007**) 164111.

[46] (a) M. E. Casida, M. Huix-Rotllant, Progress in time-dependent density-functional theory, *Annu. Rev. Phys. Chem.* 63 (**2012**) 287–323. (b) M. Huix-Rotllant, M. Filatov, S. Gozem, I. Schapiro, M. Olivucci, N. Ferré, Assessment of density functional theory for describing the correlation effects on the ground and excited state potential energy surfaces of a retinal chromophore model, *J. Chem. Theory Comput.* 9 (**2013**) 3917–3932. (c) M. Huix-Rotllant, N. Ferré, Triplet state photochemistry and the three-state crossing of acetophenone within time-dependent density-functional theory, *J. Chem. Phys.* 140 (**2014**) 134305.

[47] G. Granucci, M. Persico, A. Toniolo, Direct semiclassical simulation of photochemical processes with semiempirical wave functions, *J. Chem. Phys.* 114 (**2001**) 10608.

[48] A. Koslowski, M. E. Beck, W. Thiel, Implementation of a general multireference configuration interaction procedure with analytic gradients in a semiempirical context using the graphical unitary group approach, *J. Comput. Chem.* 24 (**2003**) 714.

[49] F. Bernardi, M. Olivucci, M. A. Robb, Simulation of MC-SCF results on covalent organic multi-bond reactions: Molecular mechanics with valence bond (MM-VB), *J. Am. Chem. Soc.* 114 (**1992**) 1606–1616.

[50] P. W. Anderson, New approach to the theory of superexchange interactions, *Phys. Rev.* 115 (**1959**) 2–13.

[51] N. L. Allinger, Calculation of molecular structure and energy by force-field methods, *Adv. Phys. Org. Chem.* 13 (**1976**) 1–82.

[52] M. J. Bearpark, M. A. Robb, F. Bernardi, M. Olivucci, Molecular mechanics valence bond methods for large active spaces. Application to conjugated polycyclic hydrocarbons, *Chem. Phys. Lett.* 217 (**1994**) 513–519.

[53] M. J. Bearpark, M. Boggio-Pasqua, Excited states of conjugated hydrocarbon radicals using the molecular mechanics – valence bond (MMVB) method, *Theor. Chem. Acc.* 110 (**2003**) 105–114.

[54] M. J. Bearpark, M. Boggio-Pasqua, M. A. Robb, F. Ogliaro, Excited states of conjugated hydrocarbons using the molecular mechanics – valence bond (MMVB) method: conical intersections and dynamics, *Theor. Chem. Acc.* 116 (**2006**) 670–682.

[55] M. J. Bearpark, F. Ogliaro, T. Vreven, M. Boggio-Pasqua, M. J. Frisch, S. M. Larkin, M. Morrison, M. A. Robb, CASSCF calculations for photoinduced processes in large molecules: Choosing when to use the RASSCF, ONIOM and MMVB approximations, *J. Photochem. Photobiol. A* 190 (**2007**) 207–227.

[56] (a) G. Groenhof, L. V. Schäfer, M. Boggio-Pasqua, M. A. Robb, Excited state dynamics in biomolecules, in *Handbook of Molecular Biophysics*, Ed. H. Bohr, Wiley-VCH, Weinheim, **2009**, pp. 93–134. (b) G. Groenhof, M. Boggio-Pasqua, L. V. Schäfer, M. A. Robb, Computer simulations of photobiological processes: The effect of the protein environment, *Adv. Quantum Chem.* 59 (**2010**) 181–212.

[57] M. Boggio-Pasqua, C. F. Burmeister, M. A. Robb, G. Groenhof, Photochemical reactions in biological systems: probing the effect of the environment by means of hybrid quantum chemistry/molecular mechanics simulations, *Phys. Chem. Chem. Phys.* 14 (**2012**) 7912–7928.

[58] (a) K. Fukui, The path of chemical reactions – The IRC approach, *Acc. Chem. Res.* 14 (**1981**) 363–368. (b) C. Gonzalez, H. B. Schlegel, Reaction path following in mass-weighted internal coordinates, *J. Phys. Chem.* 94 (**1990**) 5523–5527.

[59] M. R. Manaa, D. R. Yarkony, On the intersection of two potential energy surfaces of the same symmetry. Systematic characterization using a Lagrange multiplier constrained procedure, *J. Chem. Phys.* 99 (**1993**) 5251–5256.

[60] C. Ciminelli, G. Granucci, M. Persico, The photoisomerization mechanism of azobenzene: a semiclassical simulation of nonadiabatic dynamics, *Chem. Eur. J.* 10 (**2004**) 2327–2341.

[61] M. J. Frisch, G. W. Trucks, H. B. Schlegel, G. E. Scuseria, M. A. Robb, J. R. Cheeseman, G. Scalmani, V. Barone, B. Mennucci, G. A. Petersson, H. Nakatsuji, M. Caricato, X. Li, H. P. Hratchian, A. F. Izmaylov, J. Bloino, G. Zheng, J. L. Sonnenberg, M. Hada, M. Ehara, K. Toyota, R. Fukuda, J. Hasegawa, M. Ishida, T. Nakajima, Y. Honda, O. Kitao, H. Nakai, T. Vreven, J. A. Montgomery, Jr., J. E. Peralta, F. Ogliaro, M. Bearpark, J. J. Heyd, E. Brothers, K. N. Kudin, V. N. Staroverov, R. Kobayashi, J. Normand, K. Raghavachari, A. Rendell, J. C. Burant, S. S. Iyengar, J. Tomasi, M. Cossi, N. Rega, J. M. Millam, M. Klene, J. E. Knox, J. B. Cross, V. Bakken, C. Adamo, J. Jaramillo, R. Gomperts, R. E. Stratmann, O. Yazyev, A. J. Austin, R. Cammi, C. Pomelli, J. W. Ochterski, R. L. Martin, K. Morokuma, V. G. Zakrzewski, G. A. Voth, P. Salvador, J. J. Dannenberg, S. Dapprich, A. D. Daniels, Ö. Farkas, J. B. Foresman, J. V. Ortiz, J. Cioslowski, D. J. Fox, Gaussian 09, Revision D.01, Gaussian, Inc., Wallingford CT, 2009.

[62] H.-J. Werner, P. J. Knowles, G. Knizia, F. R. Manby, M. Schütz, P. Celani, T. Korona, R. Lindh, A. Mitrushenkov, G. Rauhut, K. R. Shamasundar, T. B. Adler, R. D. Amos, A. Bernhardsson, A. Berning, D. L. Cooper, M. J. O. Deegan, A. J. Dobbyn, F. Eckert, E. Goll, C. Hampel, A. Hesselmann, G. Hetzer, T. Hrenar, G. Jansen, C. Köppl, Y. Liu, A. W. Lloyd, R. A. Mata, A. J. May, S. J. McNicholas, W. Meyer, M. E. Mura, A. Nicklaß, D. P. O'Neill, P. Palmieri, D. Peng, K. Pflüger, R. Pitzer, M. Reiher, T. Shiozaki, H. Stoll, A. J. Stone, R. Tarroni, T. Thorsteinsson, M. Wang, MOLPRO, version 2012.1, a package of ab initio programs, see http://www.molpro.net.

[63] (a) P. Celani, M. A. Robb, M. Garavelli, F. Bernardi, M. Olivucci, Geometry optimisation on a hypersphere. Application to finding reaction paths from a conical intersection, *Chem. Phys. Lett.* 243 (**1995**) 1–8. (b) M. Garavelli, P. Celani, M. Fato, M. J. Bearpark, B. R. Smith, M. Olivucci, M. A. Robb, Relaxation paths from a conical intersection: The mechanism of product formation in the cyclohexadiene/hexatriene photochemical interconversion, *J. Phys. Chem. A* 101 (**1997**) 2023–2032.

[64] R. Kosloff, Time-dependent quantum-mechanical methods for molecular dynamics, *J. Phys. Chem.* 92 (**1988**) 2087–2100.

[65] (a) H.-D. Meyer, U. Manthe, L. S. Cederbaum, The multi-configurational time-dependent Hartree approach, *Chem. Phys. Lett.* 165 (**1990**) 73–78. (b) M. H. Beck, A. Jäckle, G. A. Worth, H.-D. Meyer, The multiconfiguration time-dependent Hartree (MCTDH) method: A highly efficient algorithm for propagating wavepackets, *Phys. Rep.* 324 (**2000**) 1–105.

[66] D. Mendive-Tapia, B. Lasorne, G. A. Worth, M. A. Robb, M. J. Bearpark, Towards converging non-adiabatic direct dynamics calculations using frozen-width variational Gaussian product basis functions, *J. Chem. Phys.* 137 (**2012**) 22A548.

[67] G. A. Worth, M. A. Robb, B. Lasorne, Solving the time-dependent Schrödinger equation for nuclear motion in one step: Direct dynamics of non-adiabatic systems, *Mol. Phys.* 106 (**2008**) 2077–2091.

[68] A. Bjerre, E. E. Nikitin, Energy transfer in collisions of an excited sodium atom with a nitrogen molecule, *Chem. Phys. Lett.* 1 (**1967**) 179–181.

[69] J. C. Tully, R. K. Preston, Trajectory surface hopping approach to nonadiabatic molecular collisions: The reaction of H^+ with D_2, *J. Chem. Phys.* 55 (**1971**) 562–572.

[70] (a) M. F. Hermann, Dynamics by semiclassical methods, *Ann. Rev. Phys. Chem.* 45 (**1994**) 83–111. (b) S. Chapman, The classical trajectory surface hopping approach to charge transfer processes, *Adv. Chem. Phys.* 82 (**1992**) 423–483. (c) M. Barbatti, Nonadiabatic dynamics with trajectory surface hopping method, *WIREs Comput. Mol. Sci.* 1 (2011) 620–633.

[71] L. D. Landau, On the theory of transfer of energy at collisions II, *Phys. Z. USSR* 2 (**1932**) 46–51.

[72] C. Zener, Non-adiabatic crossing of energy levels, *Proc. R. Soc. Lond. A* 137 (**1932**) 696–702.

[73] M. Desouter-Lecomte, J. Lorquet, Nonadiabatic interactions in unimolecular decay. IV. Transition probability as a function of the Massey parameter, *J. Chem. Phys.* 71 (**1979**) 4391–4403.

[74] (a) J. C. Tully, Molecular dynamics with electronic transitions, *J. Chem. Phys.* 93 (**1990**) 1061–1071. (b) J. C. Tully, Nonadiabatic molecular dynamics, *Int. J. Quantum Chem.* 40 (**1991**) 299–309.

[75] (a) F. Salama, G. A. Galazutdinov, J. Krelowski, L. J. Allamandola, F. A. Musaev, Polycyclic aromatic hydrocarbons and the diffuse interstellar bands: A survey, *Astrophys. J.* 526 (**1999**) 265–273. (b) W. W. Duley, Polycyclic aromatic hydrocarbons, carbon nanoparticles and the diffuse interstellar bands, *Faraday Discuss.* 133 (**2006**) 415–425.

[76] H. W. Jochims, H. Baumgärtel, S. Leach, Structure-dependent photostability of polycyclic aromatic hydrocarbon cations: Laboratory studies and astrophysical implications, *Astrophys. J.* 512 (**1999**) 500–510.

[77] L. Zhao, R. Lian, I. A. Shkrob, R. A. Crowell, S. Pommeret, E. L. Chronister, A. D. Liu, A. D. Trifunac, Ultrafast studies on the photophysics of matrix-isolated radical cations of polycyclic aromatic hydrocarbons, *J. Phys. Chem. A* 108 (**2004**) 25–31.

[78] K. F. Hall, M. Boggio-Pasqua, M. J. Bearpark, M. A. Robb, Photostability via sloped conical intersections: a computational study of the excited states of the naphthalene radical cation, *J. Phys. Chem. A* 110 (**2006**) 13591–13599.

[79] A. M. Tokmachev, M. Boggio-Pasqua, M. J. Bearpark, M. A. Robb, Photostability via sloped conical intersections: a computational study of the pyrene radical cation, *J. Phys. Chem. A* 112 (**2008**) 10881–10886.

[80] A. M. Tokmachev, M. Boggio-Pasqua, D. Mendive-Tapia, M. J. Bearpark, M. A. Robb, Fluorescence of the perylene radical cation and an inaccessible D_0/D_1 conical intersection: An MMVB, RASSCF and TD-DFT computational study, *J. Chem. Phys.* 132 (**2010**) 044306.

[81] (a) M. Stockburger, H. Gattermann, W. Klusmann, Spectroscopic studies on naphthalene in the vapor phase. I. Fluorescence spectra from single vibronic levels, *J. Chem. Phys.* 63 (**1975**) 4519–4528. (b) S. M. Beck, J. B. Hopkins, D. E. Powers, R. E. Smalley, Jet-cooled naphthalene. II. Single vibronic level fluorescence spectra, *J. Chem. Phys.* 74 (**1981**) 43–52. (c) C. Reylé, P. Bréchignac, Fluorescence of jet-cooled naphthalene: Emission spectra, lifetimes and quantum yields, *Eur. Phys. J. D* 8 (**2000**) 205–210.

[82] (a) F. Salama, L. J. Allamandola, Is a pyrene-like molecular ion the cause of the 4,430 Å diffuse interstellar absorption band?, *Nature* 358 (**1992**) 42–43. (b) O. Parisel, G. Berthier, Y. Ellinger, New clues for ionized polycyclic aromatic hydrocarbons as possible carriers of diffuse interstellar bands, *Astron. Astrophys.* 266 (**1992**) L1–L4. (c) F. Salama, L. J. Allamandola, Neutral and ionized polycyclic aromatic hydrocarbons, diffuse interstellar bands and the ultraviolet extinction curve, *J. Chem. Soc. Faraday Trans.* 89 (**1993**) 2277–2284. (d) J. Szczepanski, M. Vala, Laboratory evidence for ionized polycyclic aromatic hydrocarbons in the interstellar medium, *Nature* 363 (**1993**) 699–701.

[83] J.-C. Gumy, E. Vauthey, Investigation of the excited-state dynamics of radical ions in the condensed phase using the picosecond transient grating technique, *J. Phys. Chem. A* 101 (**1997**) 8575–8580.

[84] P. Brodard, A. Sarbach, J.-C. Gumy, T. Bally, E. Vauthey, Excited-state dynamics of organic radical ions in liquids and in low-temperature matrices, *J. Phys. Chem. A* 105 (**2001**) 6594–6601.

[85] (a) C. Joblin, F. Salama, L. Allamandola, Photoinduced fluorescence from the perylene cation isolated in Ne and Ar matrices, *J. Chem. Phys.* 102 (**1995**) 9743–9745. (b) X. D. F. Chillier, B. M. Stone, C. Joblin, F. Salama, L. J. Allamandola, $D_1(^2B_{2g})\rightarrow D_0(^2A_u)$ fluorescence from the matrix-isolated perylene cation following laser excitation into the $D_5(^2B_{3g})$ and $D_2(^2B_{3g})$ electronic states, *J. Chem. Phys.* 116 (**2002**) 5725–5730.

[86] C. Moutou, L. Verstraete, P. Bréchignac, S. Piccirillo, A. Léger, Laser induced fluorescence spectroscopy of jet-cooled molecular species: a tool to identify diffuse interstellar band carriers, *Astron. Astrophys.* 319 (**1997**) 331–339.

[87] (a) H. Dürr, H. Bouas-Laurent (Eds.), Photochromism, molecules and systems, Elsevier, Amsterdam, 1990. (b) H. Bouas-Laurent, H. Dürr, Organic Photochromism, *Pure Appl. Chem.* 73 (**2001**) 639–665. (c) J. C. Crano, R. J. Guglielmetti (Eds.), Organic Photochromic and Thermochromic Compound, Plenum Press: New York and London, 1998.

[88] (a) M. Irie, Diarylethenes for memories and switches, *Chem. Rev.* 100 (**2000**) 1685–1716. (b) G. Berkovic, V. Krongauz, V. Weiss, Spiropyrans and spirooxazines for memories and switches, *Chem. Rev.* 100 (**2000**) 1741–1753. (c) Y. Yokoyama, Fulgides for memories and switches, *Chem. Rev.* 100 (**2000**) 1717–1739.

[89] (a) K. Szacilowski, Digital information processing in molecular systems, *Chem. Rev.* 108 (**2008**) 3481–3548. (b) J. Andréasson, U. Pischel, Smart molecules at work-mimicking advanced logic operations, *Chem. Soc. Rev.* 39 (**2010**) 174–188.

[90] (a) J. Daub, T. Knöchel, A. Mannschreck, Photosensitive dihydroazulenes with chromogenic properties, *Angew. Chem. Int. Ed.* 23 (**1984**) 960–961. (b) J. Ern, M. Petermann, T. Mrozek, J. Daub, K. Kuldová, C. Kryschi, Dihydroazulene/vinylheptafulvene photochromism: dynamics of the photochemical ring-opening reaction, *Chem. Phys.* 259 (**2000**) 331–337. (c) V. De Waele, U. Schmidhammer, T. Mrozek, J. Daub, E. Riedle, Ultrafast bidirectional dihydroazulene/vinylheptafulvene (DHA/VHF) molecular switches: Photochemical ring closure of vinylheptafulvene proven by a two-pulse experiment, *J. Am. Chem. Soc.* 124 (**2002**) 2438–2439.

[91] M. Boggio-Pasqua, M. J. Bearpark, P. A. Hunt, M. A. Robb, Dihydroazulene/vinylheptafulvene photochromism: A model for one-way photochemistry via a conical intersection, *J. Am. Chem. Soc.* 124 (**2002**) 1456–1470.

[92] M. Boggio-Pasqua, M. Ravaglia, M. J. Bearpark, M. Garavelli, M. A. Robb, Can diarylethene photochromism be explained by a reaction path alone? A CASSCF study with model MMVB dynamics, *J. Phys. Chem. A* 107 (**2003**) 11139–11152.

[93] M. A. L. Sheepwash, R. H. Mitchell, C. Bohne, Mechanistic insights into the photochromism of *trans*-10b,10c-dimethyl-10b-10c-dihydropyrene derivatives, *J. Am. Chem. Soc.* 124 (**2002**) 4693–4700.

[94] M. Boggio-Pasqua, M. J. Bearpark, M. A. Robb, Towards a mechanistic understanding of the photochromism of dimethyldihydropyrenes, *J. Org. Chem.* 72 (**2007**) 4497–4503.

[95] K. Ayub, R. Li, C. Bohne, R. V. Williams, R. H. Mitchell, Calculation driven synthesis of an excellent dihydropyrene negative photochrome and its photochemical properties, *J. Am. Chem. Soc.* 133 (**2011**) 4040–4045.

[96] D. Roldan, S. Cobo, F. Lafolet, N. Vilà, C. Bochot, C. Bucher, E. Saint-Aman, M. Boggio-Pasqua, M. Garavelli, G. Royal, A multi-addressable switch based on the dimethyldihydropyrene photochrome with remarkable proton-triggered photo-opening efficiency, *Chem. Eur. J.* 21 (**2015**) 455–467.

[97] M. Boggio-Pasqua, M. Garavelli, Rationalization and design of enhanced photoinduced cycloreversion in photochromic dimethyldihydropyrenes by theoretical calculations, *J. Phys. Chem. A*., DOI: 10.1021/jp5118773.

[98] Z. R. Grabowski, K. Rotkiewicz, W. Rettig, Structural changes accompanying intramolecular electron transfer: Focus on twisted intramolecular charge-transfer states and structures, *Chem. Rev.* 103 (**2003**) 3899–4031.

[99] I. Gómez, M. Reguero, M. Boggio-Pasqua, M. A. Robb, Intramolecular charge transfer in 4-aminobenzonitriles does not necessarily need the twist, *J. Am. Chem. Soc.* 127 (**2005**) 7119–7129.

[100] W. Fuß, K. K. Pushpa, W. Rettig, W. E. Schmid, S. A. Trushin, Ultrafast charge transfer *via* a conical intersection in dimethylaminobenzonitrile, *Photochem. Photobiol. Sci.* 1 (**2002**) 255–262.

[101] M. A. Kochman, A. Tajti, C. A. Morrison, R. J. D. Miller, Early events in the nonadiabatic relaxation dynamics of 4-(*N*,*N*-dimethylamino)benzonitrile, *J. Chem. Theory Comput.* 11 (**2015**) 1118–1128.

[102] A. Perveaux, P. J. Castro, D. Lauvergnat, M. Reguero, B. Lasorne, Intramolecular charge transfer in 4-aminobenzonitrile does not need the twist and may not need the bend, *J. Phys. Chem. Lett.* 6 (**2015**) 1316–1320.

[103] J. D. Watson, F. H. C. Crick, Molecular structure of nucleic acids: A structure for deoxyribose nucleic acid, *Nature* 171 (**1953**) 737–738.

[104] C. E. Crespo-Hernández, B. Cohen, P. M. Hare, B. Kohler, Ultrafast excited-state dynamics in nucleic acids, *Chem. Rev.* 104 (**2004**) 1977–2019.

[105] J. Peon, A. H. Zewail, DNA/RNA nucleotides and nucleosides: Direct measurement of excited-state lifetimes by femtosecond fluorescence up-conversion, *Chem. Phys. Lett.* 348 (**2001**) 255–262.

[106] A. Abo-Riziq, L. Grace, E. Nir, M. Kabelac, P. Hobza, M. S. de Vries, Photochemical selectivity in guanine-cytosine base-pair structures, *Proc. Natl. Ac. Sci. U. S. A.* 102 (**2005**) 20–23.

[107] (a) A. L. Sobolewski, W. Domcke, Ab initio studies on the photophysics of the guanine–cytosine base pair, *Phys. Chem. Chem. Phys*. 6 (**2004**) 2763–2771. (b) T. Schultz, E. Samoylova, W. Radloff, I. V. Hertel, A. L. Sobolewski, W. Domcke, Efficient deactivation of a model base pair via excited-state hydrogen transfer, *Science* 306 (**2004**) 1765–1768. (c) A. L. Sobolewski, W. Domcke, C. Hättig, Tautomeric selectivity of the excited-state lifetime of guanine/cytosine base pairs: The role of electron-driven proton-transfer processes, *Proc. Natl. Ac. Sci. U. S. A.* 102 (**2005**) 17903–17906.

[108] G. Groenhof, L. V. Schäfer, M. Boggio-Pasqua, M. Goette, H. Grubmüller, M. A. Robb, Ultrafast deactivation of an excited cytosine-guanine base pair in DNA, *J. Am. Chem. Soc.* 129 (**2007**) 6812–6819.

[109] (a) F.-A. Miannay, A. Bányász, T. Gustavsson, D. Markovitsi, Ultrafast excited-state deactivation and energy transfer in guanine–cytosine DNA double helices, *J. Am. Chem. Soc.* 129 (**2007**) 14574–14575. (b) N. K. Schwalb, F. Temps, Ultrafast electronic relaxation in guanosine is promoted by hydrogen bonding with cytidine, *J. Am. Chem. Soc.* 129 (**2007**) 9272–9273.

[110] J. Cadet, P. Vigny, The photochemistry of nucleic acids, In *Bioorganic Photochemistry*, Ed. H. Morrison, Wiley, New York, 1990, pp 1–272.

[111] (a) J.-S. Taylor, Unraveling the molecular pathway from sunlight to skin cancer, *Acc. Chem. Res.* 27 (**1994**) 76–82. (b) A. A. Vink, L. Roza, Biological consequences of cyclobutane pyrimidine dimers, *J. Photochem. Photobiol. B* 65 (**2001**) 101–104.

[112] W. J. Schreier, T. E. Schrader, F. O. Koller, P. Gilch, C. E. Crespo-Hernández, V. N. Swaminathan, T. Carell, W. Zinth, B. Kohler, Thymine dimerization in DNA is an ultrafast photoreaction, *Science* 315 (**2007**) 625–629.

[113] M. Boggio-Pasqua, G. Groenhof, L. V. Schäfer, H. Grubmüller, M. A. Robb, Ultrafast deactivation channel for thymine dimerization, *J. Am. Chem. Soc.* 129 (**2007**) 10996–10997.

[114] (a) F. Bernardi, S. De, M. Olivucci, M. A. Robb, Mechanism of ground-state-forbidden photochemical pericyclic reactions: Evidence for real conical intersections, *J. Am. Chem. Soc.* 112 (**1990**) 1737–1744. (b) F. Bernardi, M. Olivucci, M. A. Robb, Predicting forbidden and allowed cycloaddition reactions: Potential surface topology and its rationalization, *Acc. Chem. Res.* 23 (**1990**) 405–412.

[115] L. Blancafort, A. Migani, Modeling thymine photodimerizations in DNA: Mechanism and correlation diagrams, *J. Am. Chem. Soc.* 129 (**2007**) 14540–14541.

[116] K. J. Hellingwerf, J. Hendriks, T. Gensch, Photoactive yellow protein, a new type of photoreceptor protein: Will this "yellow lab" bring us where we want to go?, *J. Phys. Chem. A* 107 (**2003**) 11082–1094.

[117] (a) G. Groenhof, M. Bouxin-Cademartory, B. Hess, S. P. de Visser, H. J. C. Berendsen, M. Olivucci, A. E. Mark, M. A. Robb, Photoactivation of the photoactive yellow protein: Why photon absorption triggers a trans-to-cis isomerization of the chromophore in the protein, *J. Am. Chem. Soc.* 126 (**2004**) 4228–4233. (b) G. Groenhof, L. V. Schäfer, M. Boggio-Pasqua, H. Grubmüller, M. A. Robb, Arginine52 controls the photoisomerization process in photoactive yellow protein, *J. Am. Chem. Soc.* 130 (**2008**) 3250–3251.

[118] (a) M. Boggio-Pasqua, M. A. Robb, G. Groenhof, Hydrogen bonding controls excited-state decay of the photoactive yellow protein chromophore, *J. Am. Chem. Soc.* 131 (**2009**) 13580–13581. (b) M. Boggio-Pasqua, G. Groenhof, Controlling the photoreactivity of the photoactive yellow protein chromophore by substituting at the *p*-coumaric acid group, *J. Phys. Chem. B* 115 (**2011**) 7021–7028.

[119] I. Lee, W. Lee, A. H. Zewail, Primary steps of the photoactive yellow protein: Isolated chromophore dynamics and protein directed function, *Proc. Natl. Acad. Sci. U. S. A.* 103 (**2006**) 258–262.

[120] A. Espagne, D. H. Paik, P. Changenet-Barret, P. Plaza, M. M. Martin, A. H. Zewail, Ultrafast light-induced response of photoactive yellow protein chromophore analogues, *Photochem. Photobiol. Sci.* 6 (**2007**) 780–787.

[121] (a) K. Heyne, O. F. Mohammed, A. Usman, J. Dreyer, E. T. J. Nibbering, M. A. Cusanovich, Structural evolution of the chromophore in the primary stages of trans/cis isomerization in photoactive yellow protein, *J. Am. Chem. Soc.* 127 (**2005**) 18100–18106. (b) L. J. G. W. van Wilderen, M. A. van der Horst, I. H. M. van Stokkum, K. J. Hellingwerf, R. van Grondelle, M. L. Groot, Ultrafast infrared spectroscopy reveals a key step for successful entry into the photocycle for photoactive yellow protein, *Proc. Natl. Acad. Sci. U. S. A.* 103 (**2006**) 15050–15055.

[122] H. Ihee, S. Rajagopal, V. Srajer, R. Pahl, S. Anderson, M. Schmidt, F. Schotte, P. A. Anfinrud, M. Wulff, K. Moffat, Visualizing reaction pathways in photoactive yellow protein from nanoseconds to seconds, *Proc. Natl. Acad. Sci. U. S. A.* 102 (**2005**) 7145–7150.

[123] (a) C. Ko, A. M. Virshup, T. J. Martínez, Electrostatic control of photoisomerization in the photoactive yellow protein chromophore: Ab initio multiple spawning dynamics, *Chem. Phys. Lett.* 460 (**2008**) 272–277. (b) F. Knoch, D. Morozov, M. Boggio-Pasqua, G. Groenhof, Steering the excited state dynamics of a photoactive yellow protein chromophore analogue with external electric fields, *Comput. Theor. Chem.* 1040–1041 (**2014**) 120–125.

[124] K. Takeshita, Y. Imamoto, M. Kataoka, K. Mihara, F. Tokunaga, M. Terazima, Structural change of site-directed mutants of PYP: New dynamics during pR state, *Biophys. J.* 83 (**2002**) 1567–1577.

[125] (a) M. Vengris, M. A. van der Horst, G. Zgrablic, I. H. M. van Stokkum, S. Haacke, M. Chergui, K. J. Hellingwerf, R. van Grondelle, D. S. Larsen, Contrasting the excited-state dynamics of the photoactive yellow protein chromophore: Protein versus solvent environments, *Biophys. J.* 87 (**2004**) 1848–1857. (b) M. Vengris, D. S. Larsen, M. A. van der Horst, O. F. A. Larsen, K. J. Hellingwerf, R. van Grondelle, Ultrafast dynamics of isolated model photoactive yellow protein chromophores: "Chemical perturbation theory" in the laboratory, *J. Phys. Chem. B* 109 (**2005**) 4197–4208.

[126] R. Cordfunke, R. Kort, A. Pierik, B. Gobets, G.-J. Koomen, J. W. Verhoeven, K. J. Hellingwerf, *trans*/*cis* (*Z*/*E*) photoisomerization of the chromophore of photoactive yellow protein is not a prerequisite for the initiation of the photocycle of this photoreceptor protein, *Proc. Natl. Acad. Sci. U. S. A.* 95 (**1998**) 7396–7401.

[127] P. Changenet-Barret, P. Plaza, M. M. Martin, H. Chosrowjan, S. Taniguchi, N. Mataga, Y. Imamoto, M. Kataoka, Role of arginine 52 on the primary photoinduced events in the PYP photocycle, *Chem. Phys. Lett.* 434 (2007) 320–325.

[128] (a) A. H. Xie, W. D. Hoff, A. R. Kroon, K. J. Hellingwerf, Glu46 donates a proton to the 4-hydroxycinnamate anion chromophore during the photocycle of photoactive yellow protein, *Biochemistry* 35 (**1996**) 14671–14678. (b) G. Groenhof, M. F. Lensink, H. J. C. Berendsen, A. E. Mark, Signal transduction in the photoactive yellow protein. II. Proton transfer initiates conformational changes, *Proteins* 48 (**2002**) 212–219.

[129] (a) A. Juris, V. Balzani, F. Barigelletti, S. Campagna, P. Belser, A. von Zelewsky, Ru(II) polypyridine complexes: Photophysics, photochemistry, electrochemistry, and chemiluminescence, *Coord. Chem. Rev.* 84 (**1988**) 85–277. (b) S. Campagna, F. Puntoriero, F. Nastasi, G. Bergamini, V. Balzani, Photochemistry and photophysics of coordination compounds: Ruthenium, *Top. Curr. Chem.* 280 (**2007**) 117–214.

[130] (a) L. Herman, S. Ghosh, E. Defrancq, A. Kirsch-De Mesmaeker, Ru(II) complexes and light: Molecular tools for biomolecules, *J. Phys. Org. Chem.* 21 (**2008**) 670–681. (b) H. Dürr, S. Bossmann, Ruthenium polypyridine complexes. On the route to biomimetic assemblies as models for the photosynthetic reaction center, *Acc. Chem. Res.* 34 (**2001**) 905–917.

[131] (a) R. C. Evans, P. Douglas, C. J. Winscom, Coordination complexes exhibiting room-temperature phosphorescence: Evaluation of their suitability as triplet emitters in organic light emitting diodes, *Coord. Chem. Rev.* 250, **2006**, 2093–2126. (b) Y. Chi, P.-T. Chou, Contemporary progresses on neutral, highly emissive Os(II) and Ru(II) complexes, *Chem. Soc. Rev.* 36, **2007**, 1421–1431.

[132] (a) M. Grätzel, Dye-sensitized solar cells, *J. Photochem. Photobiol. C* 4 (**2003**) 145–153. (b) M. K. Nazeeruddin, S. M. Zakeeruddin, J.-J. Lagref, P. Liska, P. Comte, C. Barolo, G. Viscardi, K. Schenk, M. Grätzel, Stepwise assembly of amphiphilic ruthenium sensitizers and their applications in dye-sensitized solar cell, *Coord. Chem. Rev.* 248 (**2004**) 1317–1328. (c) G. C. Vougioukalakis, A. I. Philippopoulos, T. Stergiopoulos, P. Falaras, Contributions to the development of ruthenium-based sensitizers for dye-sensitized solar cells, *Coord. Chem. Rev.* 255 (**2011**) 2602–2621. (d) A. Reynal, E. Palomares, Ruthenium polypyridyl sensitisers in dye solar cells based on mesoporous TiO_2, *Eur. J. Inorg. Chem.* (**2011**) 4509–4526. (e) J.-F. Yin, M. Velayudham, D. Bhattacharya, H.-C. Lin, K.-L. Lu, Structure optimization of ruthenium photosensitizers for efficient dye-sensitized solar cells – A goal toward a "bright" future, *Coord. Chem. Rev.* 256 (**2012**) 3008–3035.

[133] (a) F. Alary, J.-L. Heully, L. Bijeire, P. Vicendo, Is the ^{3}MLCT the only photoreactive state of polypyridyl complexes?, *Inorg. Chem.* 46 (**2007**) 3154–3165. (b) F. Alary, M. Boggio-Pasqua, J.-L. Heully, C. Marsden, P. Vicendo, Theoretical characterization of the lowest triplet excited states of the tris-(1,4,5,8-tetraazaphenanthrene) ruthenium dication complex, *Inorg. Chem.* 47 (**2008**) 5259–5266.

[134] J.-L. Heully, F. Alary, M. Boggio-Pasqua, Spin-orbit effects on the photophysical properties of $Ru(bpy)_3^{2+}$, *J. Chem. Phys.* 131 (**2009**) 184308.

[135] L. Ding, L. W. Chung, K. Morokuma, Excited-state proton transfer controls irreversibility of photoisomerization in mononuclear ruthenium(II) monoaquo complexes: A DFT study, *J. Chem. Theory Comput.* 10 (**2014**) 668–675.

[136] T. Guillon, M. Boggio-Pasqua, F. Alary, J.-L. Heully, E. Lebon, P. Sutra, A. Igau, Theoretical investigation on the photophysical properties of model ruthenium complexes with diazabutadiene ligands $[Ru(bpy)_{3-x}(dab)_x]^{2+}$ (x=1–3), *Inorg. Chem.* 49 (**2010**) 8862–8872.

[137] R. E. Piau, T. Guillon, E. Lebon, N. Perrot, F. Alary, M. Boggio-Pasqua, J.-L. Heully, A. Juris, P. Sutra, A. Igau, Photophysical and electrochemical properties of polypyridine imine ruthenium(II) complexes: A comparative experimental and theoretical study, *New J. Chem.* 36 (**2012**) 2484–2492.

[138] I. M. Dixon, E. Lebon, P. Sutra, A. Igau, Luminescent ruthenium–polypyridine complexes & phosphorus ligands: Anything but a simple story, *Chem. Soc. Rev.* 38 (**2009**) 1621–1634.

[139] E. Lebon, S. Bastin, P. Sutra, L. Vendier, R. E. Piau, I. M. Dixon, M. Boggio-Pasqua, F. Alary, J.-L. Heully, A. Igau, A. Juris, Can a functionalized phosphine ligand promote room temperature luminescence of the $[Ru(bpy)(tpy)]^{2+}$ core?, *Chem. Commun.* 48 (**2012**) 741–743.

[140] E. Lebon, R. Sylvain, R. E. Piau, C. Lanthony, J. Pilmé, P. Sutra, M. Boggio-Pasqua, J.-L. Heully, F. Alary, A. Juris, A. Igau, Phosphoryl group as a strong σ-donor anionic phosphine-type ligand: A combined experimental and theoretical study on long-lived room temperature luminescence of the $[Ru(tpy)(bpy)(Ph_2PO)]^{+}$ complex, *Inorg. Chem.* 53 (**2014**) 1946–1948.

[141] (a) P. Coppens, I. Novozhilova, A. Kovalevsky, Photoinduced linkage isomers of transition-metal nitrosyl compounds and related complexes, *Chem. Rev.* 102 (**2002**) 861–883. (b) T. E. Bitterwolf, Photochemical nitrosyl linkage isomerism/metastable states, *Coord. Chem. Rev.* 250 (**2006**) *250*, 1196–1207.

[142] (a) J. J. Rack, Electron transfer triggered sulfoxide isomerization in ruthenium and osmium complexes, *Coord. Chem. Rev.* 253 (**2009**) 78–85. (b) B. A. McClure, J. J. Rack, Isomerization in photochromic ruthenium sulfoxide complexes, *Eur. J. Inorg. Chem.* (**2010**) 3895–3904.

[143] S. O. Sylvester, J. M. Cole, P. G. Waddell, Photoconversion bonding mechanism in ruthenium sulfur dioxide linkage photoisomers revealed by in situ diffraction, *J. Am. Chem. Soc.* 134 (**2012**) 11860–11863.

[144] B. A. McClure, N. V. Mockus, D. P. Butcher Jr., D. A. Lutterman, C. Turro, J. L. Petersen, J. J. Rack, Photochromic ruthenium sulfoxide complexes: Evidence for isomerization through a conical intersection, *Inorg. Chem.* 48 (**2009**) 8084–8091.

[145] B. A. McClure, J. J. Rack, Ultrafast spectroscopy of a photochromic ruthenium sulfoxide complex, *Inorg. Chem.* 50 (**2011**) 7586–7590.

[146] A. J. Göttle, I. M. Dixon, F. Alary, J.-L. Heully, M. Boggio-Pasqua, Adiabatic versus nonadiabatic photoisomerization in photochromic ruthenium sulfoxide complexes: a mechanistic picture from density functional theory calculations, *J. Am. Chem. Soc.* 133 (**2011**) 9172–9174.

[147] M. K. Smith, J. A. Gibson, C. G. Young, J. A. Broomhead, P. C. Junk, F. R. Keene, Photoinduced ligand isomerization in dimethyl sulfoxide complexes of ruthenium(II), *Eur. J. Inorg. Chem.* (**2000**) 1365–1370.

[148] J. J. Rack, N. V. Mockus, Room-temperature photochromism in *cis*- and *trans*-$[Ru(bpy)_2(dmso)_2]^{2+}$, *Inorg. Chem.* 42 (**2003**) 5792–5794.

[149] A. J. Göttle, F. Alary, I. M. Dixon, J.-L. Heully, M. Boggio-Pasqua, Unravelling the S→O linkage photoisomerization mechanisms in *cis*- and *trans*-$[Ru(bpy)_2(DMSO)_2]^{2+}$ using density functional theory, *Inorg. Chem.* 53 (**2014**) 6752–6760.

[150] O. P. J. Vieuxmaire, R. E. Piau, F. Alary, J.-L. Heully, P. Sutra, A. Igau, M. Boggio-Pasqua, Theoretical investigation of phosphinidene oxide polypyridine ruthenium(II) complexes: toward the design of a new class of photochromic compounds, *J. Phys. Chem. A* 117 (**2013**) 12821–12830.

[151] V. Dieckmann, S. Eicke, J. J. Rack, T. Woike, M. Imlau, Pronounced photosensitivity of molecular $[Ru(bpy)_2(OSO)]^{+}$ solutions based on two photoinduced linkage isomers, *Opt. Express* 17 (**2009**) 15052–15060.

[152] (a) P. Wu, L. Brand, Resonance energy transfer: Methods and applications, *Anal. Biochem.* 218 (**1994**) 1–13. (b) R. M. Clegg, Fluorescence resonance energy transfer, *Curr. Opin. Biotechnol.* 6 (**1995**) 103–110.

[153] (a) Th. Förster, Zwischenmolekulare energiewanderung und fluoreszenz, *Ann. Phys.* 437 (**1948**) 55–75. (b) Th. Förster, Transfer mechanisms of electronic excitation, *Discuss. Faraday Soc.* 27 (**1959**) 7–17. (c) Th. Förster, Delocalized excitation and excitation transfer, in *Modern Quantum Chemistry*, Ed. O. Sinanoglu, Academic Press, New York, **1968**, pp. 93–137.

[154] D. L. Dexter, A theory of sensitized luminescence in solids, *J. Chem. Phys.* 21 (**1953**) 836–850.

[155] (a) S. Hassoon, H. Lustig, M. B. Rubin, S. Speiser, Molecular structure effects in intramolecular electronic energy transfer, *Chem. Phys. Lett.* 98 (**1983**) 345–348. (b) S. Speiser, J. Katriel, Intramolecular electronic energy transfer via exchange interaction in bichromophoric molecules, *Chem. Phys. Lett.* 102 (**1983**) 88–94. (c) S. Hassoon, H. Lustig, M. B. Rubin, S. Speiser, The mechanism of short-range intramolecular electronic energy transfer in bichromophoric molecules, *J. Phys. Chem. A* 88 (**1984**) 6367–6374.

[156] (a) C. L. Ward, C. G. Elles, Controlling the excited-state reaction dynamics of a photochromic molecular switch with sequential two-photon excitation, *J. Phys. Chem. Lett.* 3 (**2012**) 2995–3000. (b) C. L. Ward, C. G. Elles, Cycloreversion dynamics of a photochromic molecular switch via one-photon and sequential two-photon excitation, *J. Phys. Chem. A* 118 (**2014**) 10011–10019.

[157] N. C. Shaner, P. A. Steinbach, R. Y. Tsien, A guide to choosing fluorescent proteins, *Nature Methods* 2 (**2005**) 905–909.

[158] E. Betzig, G. H. Patterson, R. Sougrat, O. W. Lindwasser, S. Olenych, J. S. Bonifacino, M. W. Davidson, J. Lippincott-Schwartz, H. F. Hess, Imaging intracellular fluorescent proteins at nanometer resolution, *Science* 313 (**2006**) 1642–1645.

[159] M. Andresen, A. C. Stiel, S. Trowitzsch, G. Weber, C. Eggeling, M. C. Wahl, S. W. Hell, S. Jakobs, Structural basis for reversible photoswitching in Dronpa, *Proc. Nat. Acad. Sci. USA* 104 (**2007**) 13005–13009.

[160] T. Brakemann, G. Weber, M. Andresen, G. Groenhof, A. C. Stiel, S. Trowitzsch, C. Eggeling, H. Grubmüller, S. W. Hell, M. C. Wahl, S. Jakobs, Molecular basis of the light-driven switching of the photochromic fluorescent protein Padron, *J. Biol. Chem.* 285 (**2010**) 14603–14609.

[161] T. Brakemann, A. C. Stiel, G. Weber, M. Andresen, I. Testa, T. Grotjohann, M. Leutenegger, U. Plessmann, H. Urlaub, C. Eggeling, M. C. Wahl, S. W. Hell, S. Jakobs, A reversibly photoswitchable GFP-like protein with fluorescence excitation decoupled from switching, *Nature Biotech.* 29 (**2011**) 942–947.

[162] (a) L. V. Schäfer, G. Groenhof, A. R. Klingen, G. M. Ullmann, M. Boggio-Pasqua, M. A. Robb, H. Grubmüller, Photoswitching of the fluorescent protein asFP595: mechanism, proton pathways, and absorption spectra, *Angew. Chem. Int. Ed.* 46 (**2007**) 530–536. (b) L. V. Schäfer, G. Groenhof, M. Boggio-Pasqua, M. A. Robb, H. Grubmüller, Chromophore protonation state controls photoswitching of the fluoroprotein asFP595, *PLoS Comput. Biol.* 4 (**2008**) e1000034.

[163] M. Imlau, T. Bieringer, S. G. Odoulov, Th. Woike, Holographic data storage, in *Nanoelectronics and Information Technology*, Ed. R. Waser, Wiley-VCH, **2003**, pp. 659–686.

[164] (a) E. Culotta, D. E. Koshland Jr., NO news is good news, *Science* 258 (**1992**) 1862–1865. (b) J. S. Stamler, D. J. Singel, J. Loscalzo, Biochemistry of nitric oxide and its redox-activated forms, *Science* 258 (**1992**) 1898–1902.

[165] (a) B. Cormary, S. Ladeira, K. Jacob, P. G. Lacroix, Th. Woike, D. Schaniel, I. Malfant, Structural influence on the photochromic response of a series of ruthenium mononitrosyl complexes, *Inorg. Chem.* 51 (**2012**) 7492–7501. (b) J. Akl, C. Billot, P. G. Lacroix, I. Sasaki, S. Mallet-Ladeira, I. Malfant, R. Arcos-Ramos, M. Romero, N. Farfán, Molecular materials for switchable nonlinear optics in the solid state, based on ruthenium-nitrosyl complexes, *New J. Chem.* 37 (**2013**) 3518–3527.

[166] (a) N. L. Fry, P. K. Mascharak, Photoactive ruthenium nitrosyls as NO donors: How to sensitize them toward visible light, *Acc. Chem. Res.* 44 (**2011**) 289–298. (b) J. Akl, I. Sasaki, P. G. Lacroix, I. Malfant, S. Mallet-Ladeira, P. Vicendo, N. Farfán, R. Santillan, Comparative photo-release of nitric oxide from isomers of substituted terpyridinenitrosyl-ruthenium(II) complexes: experimental and computational investigations, *Dalton Trans.* 43 (**2014**) 12721–12733.

[167] L. Freitag, L. González, Theoretical spectroscopy and photodynamics of a ruthenium nitrosyl complex, *Inorg. Chem.* 53 (**2014**) 6415–6426.

[168] K. Garg, S. I. M. Paris, J. J. Rack, A flexible chelate leads to phototriggered isomerization in an osmium sulfoxide complex, *Eur. J. Inorg. Chem.* (**2013**) 1142–1148.

[169] (a) A. Perrier, F. Maurel, D. Jacquemin, Single molecule multiphotochromism with diarylethenes, *Acc. Chem. Res.* 45 (**2012**) 1173–1182. (b) A. Fihey, A. Perrier, W. R. Browne, D. Jacquemin, Multiphotochromic molecular systems, *Chem. Soc. Rev.* 44 (**2015**) 3719–3759.

[170] T. Mrozek, H. Görner, J. Daub, Multimode-photochromism based on strongly coupled dihydroazulene and diarylethene, *Chem. Eur. J.* 7 (**2001**) 1028–1040.

[171] S. Kume, H. Nishihara, Photochrome-coupled metal complexes: molecular processing of photon stimuli, *Dalton Trans.* (**2008**) 3260–3271.

[172] N. Vilà, G. Royal, F. Loiseau, A. Deronzier, Photochromic and redox properties of bisterpyridine ruthenium complexes based on dimethyldihydropyrene units as bridging ligands, *Inorg. Chem.* 50 (**2011**) 10581–10591.

[173] A. Warshel, M. Karplus, Semiclassical trajectory approach to photoisomerization, *Chem. Phys. Lett.* 32 (**1975**) 11–17.

[174] G. Granucci, M. Persico, G. Spighi, Surface hopping trajectory simulations with spin-orbit and dynamical couplings, *J. Chem. Phys.* 137 (**2012**) 22A501.

[175] (a) M. Richter, P. Marquetand, J. González-Vázquez, I. Sola, L. González, SHARC: ab initio molecular dynamics with surface hopping in the adiabatic representation including arbitrary couplings, *J. Chem. Theory Comput.* 7 (**2011**) 1253–1258. (b) S. Mai, P. Marquetand, L. González, A general method to describe intersystem crossing dynamics in trajectory surface hopping, *Int. J. Quantum Chem.* (**2015**) DOI: 10.1002/qua.24891.

[176] G. Cui, W. Thiel, Generalized trajectory surface-hopping method for internal conversion and intersystem crossing, *J. Chem. Phys.* 141 (**2014**) 124101.

[177] L. Blancafort, Photochemistry and photophysics at extended seams of conical intersection, *ChemPhysChem* 15 (**2014**) 3166–3181.

8. Curriculum Vitæ

Personal Information

Date of birth: 3 October 1973
Nationality: French

Status: Married, two children
Personal address: 10 rue Germaine Tillion
31400 Toulouse, France

Professional Experience

Permanent Researcher **2007–**

Employed as Chargé de Recherche 1st class (CR1) in CNRS working at Laboratoire de Chimie et Physique Quantiques – IRSAMC at Université Paul Sabatier (Toulouse, France) since 1st October 2007. Theme: Computational photochemistry of organic, inorganic and biological systems.

Associate Researcher **2000-2007**

Employed as a post-doctoral research associate at King's College London (4 years), then at Imperial College London (3 years) in the group of Prof. Mike Robb. Theme: Computational photochemistry of organic and biological systems.

Temporary Lecturer **1999-2000**

Employed as Attaché Temporaire à l'Enseignement et à la Recherche at Université Bordeaux 1.

Doctoral Fellowship and Instructor. **1996-1999**

Employed as a doctoral researcher and instructor for teaching chemistry at Université Bordeaux 1.

Academic Education

PhD **1996-1999**

Doctoral thesis in Physical Chemistry at Laboratoire de Physico-Chimie Moléculaire at Université de Bordeaux 1. Title of the thesis: Theoretical study of the reaction C+CH. Date of viva: 23rd November 1999. Grade Highly Honorable.

MSc **1994-1996**

Master of Science in Physical Chemistry obtained at Université de Bordeaux 1. Grade Very Good.

BSc **1991-1994**

Bachelor of Science in Physical Chemistry obtained at Université de Bordeaux 1. Grade Good.

Specific Skills

- Expert in computational photochemistry.
- In-depth knowledge of *ab initio* methods, in particular for electronic excited state calculations.
- Expert in the studies of reaction paths and topologies of potential energy surfaces of molecular systems (e.g., photochemical paths involving conical intersections).
- Experienced in semiclassical nonadiabatic molecular dynamics.
- Qualified user of quantum chemistry packages, in particular Gaussian and Molpro.
- Experienced in hybrid methods (MMVB, ONIOM and QM/MM)
- Experienced in teaching physical chemistry and supervising students.
- Fluent in English (more than 7 years spent in London)

Scientific Production

Peer-reviewed articles

1. Rationalization and design of enhanced photoinduced cycloreversion in photochromic dimethyldihydropyrenes by theoretical calculations

M. Boggio-Pasqua, M. Garavelli, *J. Phys. Chem. A*., DOI: 10.1021/jp5118773.

2. A multi-addressable switch based on the dimethyldihydropyrene photochrome with remarkable proton-triggered photo-opening efficiency

D. Roldan, S. Cobo, F. Lafolet, N. Vilà, C. Bochot, C. Bucher, E. Saint-Aman, **M. Boggio-Pasqua**, M. Garavelli, G. Royal, *Chem. Eur. J.* 21, **2015**, 455–467.

3. Probing the photophysical capability of mono and bis(cyclometallated) Fe(II) polypyridine complexes using inexpensive ground state DFT

I. M. Dixon, S. Khan, F. Alary, **M. Boggio-Pasqua**, J.-L. Heully, *Dalton Trans.* 43, **2014**, 15898–15905.

4. Unravelling the S→O linkage photoisomerization mechanisms in *cis*- and *trans*-$[Ru(bpy)_2(DMSO)_2]^{2+}$ using density functional theory

A. J. Göttle, F. Alary, I. M. Dixon, J.-L. Heully, **M. Boggio-Pasqua**, *Inorg. Chem.* 53, **2014**, 6752–6760.

5. Steering the excited state dynamics of a photoactive yellow protein chromophore analogue with external electric fields

F. Knoch, D. Morozov, **M. Boggio-Pasqua**, G. Groenhof, *Comput. Theor. Chem.* 1040–1041, **2014**, 120–125.

6. On the use of reduced active space in CASSCF calculations

M. Boggio-Pasqua, G. Groenhof, *Comput. Theor. Chem.* 1040–1041, **2014**, 6–13.

7. Phosphoryl group as a strong σ-donor anionic phosphine-type ligand: A combined experimental and theoretical study on long-lived room temperature luminescence of the $[Ru(tpy)(bpy)(Ph_2PO)]^+$ complex

E. Lebon, R. Sylvain, R. E. Piau, C. Lanthony, J. Pilmé, P. Sutra, **M. Boggio-Pasqua**, J.-L. Heully, F. Alary, A. Juris, A. Igau, *Inorg. Chem.* 53, **2014**, 1946–1948.

8. Enantiomerization pathway and atropochiral stability of the BINAP ligand: a density functional theory study

J. Sanz Garcia, C. Lepetit, Y. Canac, R. Chauvin, **M. Boggio-Pasqua**, *Chem. Asian J.* 9, **2014**, 462–465.

9. A roaming wavepacket in the dynamics of electronically excited 2-hydroxypyridine

L. Poisson, D. Nandi, B. Soep, M. Hochlaf, **M. Boggio-Pasqua**, J.-M. Mestdagh, *Phys. Chem. Chem. Phys.* 16, **2014**, 581–587.

10. Theoretical investigation of phosphinidene oxide polypyridine ruthenium(II) complexes: toward the design of a new class of photochromic compounds

O. P. J. Vieuxmaire, R. E. Piau, F. Alary, J.-L. Heully, P. Sutra, A. Igau, **M. Boggio-Pasqua**, *J. Phys. Chem. A* 117, **2013**, 12821–12830.

11. The $(N_4C_2)^{2-}$ donor set as promising motif for bis(tridentate) Fe(II) photoactive compounds

I. Dixon, F. Alary, **M. Boggio-Pasqua**, J.-L. Heully, *Inorg. Chem.* 52, **2013**, 13369–13374.

12. Giant Ising-type magnetic anisotropy in trigonal bipyramidal Ni(II) complexes: experiment and theory

R. Ruamps, R. Maurice, L. Batchelor, **M. Boggio-Pasqua**, R. Guillot, A. L. Barra, J. Liu, E.-E. Bendeif, S. Pillet, S. Hill, T. Mallah, N. Guihéry, *J. Am. Chem. Soc.* 135, **2013**, 3017–3026.

13. Photophysical and electrochemical properties of polypyridine imine ruthenium(II) complexes: a comparative experimental and theoretical study

R. E. Piau, T. Guillon, E. Lebon, N. Perrot, F. Alary, **M. Boggio-Pasqua**, J.-L. Heully, A. Juris, P. Sutra, A. Igau, *New J. Chem.* 36, **2012**, 2484–2492.

14. Photochemical reactions in biological systems: probing the effect of the environment by means of hybrid quantum chemistry/molecular mechanics simulations

M. Boggio-Pasqua, C. F. Burmeister, M. A. Robb, G. Groenhof, *Phys. Chem. Chem. Phys.* 14, **2012**, 7912–7928.

15. Can a functionalized phosphine ligand promote room temperature luminescence of the $[Ru(bpy)(tpy)]^{2+}$ core?

E. Lebon, S. Bastin, P. Sutra, L. Vendier, R. E. Piau, I. M. Dixon, **M. Boggio-Pasqua**, F. Alary, J.-L. Heully, A. Igau, A. Juris, *Chem. Commun.* 48, **2012**, 741–743.

16. Adiabatic versus nonadiabatic photoisomerization in photochromic ruthenium sulfoxide complexes: a mechanistic picture from density functional theory calculations

A. J. Göttle, I. M. Dixon, F. Alary, J.-L. Heully, **M. Boggio-Pasqua**, *J. Am. Chem. Soc.* 133, **2011**, 9172–9174.

17. Controlling the photoreactivity of the photoactive yellow protein chromophore by substituting at the *p*-coumaric acid group

M. Boggio-Pasqua, G. Groenhof, *J. Phys. Chem. B* 115, **2011**, 7021–7028.

18. Towards the limit of atropochiral stability: H-MIOP, an N-heterocyclic carbene precursor and cationic analogue of the H-MOP ligand

I. Abdellah, **M. Boggio-Pasqua**, Y. Canac, C. Lepetit, C. Duhayon, R. Chauvin, *Chem. Eur. J.* 17, **2011**, 5110–5115.

19. Theoretical investigation on the photophysical properties of model ruthenium complexes with diazabutadiene ligands $[Ru(bpy)_{3-x}(dab)_x]^{2+}$ (x=1–3)

T. Guillon, **M. Boggio-Pasqua**, F. Alary, J.-L. Heully, E. Lebon, P. Sutra, A. Igau, *Inorg. Chem.* 49, **2010**, 8862–8872.

20. Computer simulations of photobiological processes: the effect of the protein environment
G. Groenhof, **M. Boggio-Pasqua**, L. V. Schäfer, M. A. Robb, *Adv. Quantum Chem.* 59, **2010**, 181–212.

21. Fluorescence of the perylene radical cation and an inaccessible D_0/D_1 conical intersection: An MMVB, RASSCF and TD-DFT computational study
A. M. Tokmachev, **M. Boggio-Pasqua**, D. Mendive-Tapia, M. J. Bearpark, M. A. Robb, *J. Chem. Phys.* 132, **2010**, 044306.

22. Spin-orbit effects on the photophysical properties of $Ru(bpy)_3^{2+}$
J.-L. Heully, F. Alary, **M. Boggio-Pasqua**, *J. Chem. Phys.* 131, **2009**, 184308.

23. Hydrogen bonding controls excited-state decay of the photoactive yellow protein chromophore
M. Boggio-Pasqua, M. A. Robb, G. Groenhof, *J. Am. Chem. Soc.* 131, **2009**, 13580–13581.

24. A counterintuitive absence of an excited-state intramolecular charge transfer reaction with 2,4,6-tricyanoanilines. Experimental and computational results
K. A. Zachariasse, S. I. Druzhinin, V. A. Galievsky, S. Kovalenko, T. A. Senyushkina, P. Mayer, M. Noltemeyer, **M. Boggio-Pasqua**, M. A. Robb, *J. Phys. Chem. A* 113, **2009**, 2693–2710.

25. Ligand selection in Ru^{II} complexes for direct one-electron photooxidation of guanine: a combined computational and experimental study
M. Boggio-Pasqua, P. Vicendo, M. Oubal, F. Alary, J.-L. Heully, *Chem. Eur. J.* 15, **2009**, 2759–2762.

26. Photostability via sloped conical intersections: a computational study of the pyrene radical cation
A. M. Tokmachev, **M. Boggio-Pasqua**, M. J. Bearpark, M. A. Robb, *J. Phys. Chem. A* 112, **2008**, 10881–10886.

27. Theoretical characterization of the lowest triplet excited states of the tris-(1,4,5,8-tetraazaphenanthrene) ruthenium dication complex
F. Alary, **M. Boggio-Pasqua**, J.-L. Heully, C. Marsden, P. Vicendo, *Inorg. Chem.* 47, **2008**, 5259–5266.

28. Chromophore protonation state controls photoswitching of the fluoroprotein asFP595
L. V. Schäfer, G. Groenhof, **M. Boggio-Pasqua**, M. A. Robb, H. Grubmüller, *PLoS Comput. Biol.* 4, **2008**, e1000034.

29. Arginine52 controls the photoisomerization process in photoactive yellow protein
G. Groenhof, L. V. Schäfer, **M. Boggio-Pasqua**, H. Grubmüller, M. A. Robb, *J. Am. Chem. Soc.* 130, **2008**, 3250–3251.

30. Ultrafast deactivation channel for thymine dimerization
M. Boggio-Pasqua, G. Groenhof, L. V. Schäfer, H. Grubmüller, M. A. Robb, *J. Am. Chem. Soc.* 129, **2007**, 10996–10997.

31. Molecular mechanics-valence bond method for planar conjugated hydrocarbon cations
K. F. Hall, A. M. Tokmachev, M. J. Bearpark, **M. Boggio-Pasqua**, M. A. Robb, *J. Chem. Phys.* 127, **2007**, 134111.

32. CASSCF calculations for photoinduced processes in large molecules: choosing when to use the RASSCF, ONIOM and MMVB approximations
M. J. Bearpark, F. Ogliaro, T. Vreven, **M. Boggio-Pasqua**, M. J. Frisch, S. M. Larkin, M. Morrison, M. A. Robb, *J. Photochem. Photobiol. A* 190, **2007**, 207–227.

33. Ultrafast deactivation of an excited cytosine-guanine base pair in DNA

G. Groenhof, L. V. Schäfer, **M. Boggio-Pasqua**, M. Goette, H. Grubmüller, M. A. Robb, *J. Am. Chem. Soc.* 129, **2007**, 6812–6819.

34. Towards a mechanistic understanding of the photochromism of dimethyldihydropyrenes
M. Boggio-Pasqua, M. J. Bearpark, M. A. Robb, *J. Org. Chem.* 72, **2007**, 4497–4503.

35. Photoswitching of the fluorescent protein asFP595: mechanism, proton pathways, and absorption spectra
L. V. Schäfer, G. Groenhof, A. R. Klingen, G. M. Ullmann, **M. Boggio-Pasqua**, M. A. Robb, H. Grubmüller, *Angew. Chem. Int. Ed.* 46, **2007**, 530–536.

36. Photostability via sloped conical intersections: a computational study of the excited states of the naphthalene radical cation
K. F. Hall, **M. Boggio-Pasqua**, M. J. Bearpark, M. A. Robb, *J. Phys. Chem. A* 110, **2006**, 13591–13599.

37. Photochemical reactivity of 2-vinylbiphenyl and 2-vinyl-1,3-terphenyl: the balance between nonadiabatic and adiabatic photocyclization
M. Boggio-Pasqua, M. J. Bearpark, F. Ogliaro, M. A. Robb, *J. Am. Chem. Soc.* 128, **2006**, 10533–10540.

38. Excited states of conjugated hydrocarbons using the Molecular Mechanics – Valence Bond (MMVB) method: conical intersections and dynamics
M. J. Bearpark, **M. Boggio-Pasqua**, M. A. Robb, F. Ogliaro, *Theor. Chem. Acc.* 116, **2006**, 670–682.

39. Photostability via a sloped conical intersection: a CASSCF and RASSCF study of pyracylene
M. Boggio-Pasqua, M. J. Bearpark, M. A. Robb, *J. Phys. Chem. A* 109, **2005**, 8849–8856.

40. Intramolecular charge transfer in 4-aminobenzonitriles does not necessarily need the twist
I. Gómez, M. Reguero, **M. Boggio-Pasqua**, M. A. Robb, *J. Am. Chem. Soc.* 127, **2005**, 7119–7129.

41. A computational strategy for geometry optimization of ionic and covalent excited states, applied to butadiene and hexatriene
M. Boggio-Pasqua, M. J. Bearpark, M. Klene, M. A. Robb, *J. Chem. Phys.* 120, **2004**, 7849–7860.

42. Can diarylethene photochromism be explained by a reaction path alone? A CASSCF study with model MMVB dynamics
M. Boggio-Pasqua, M. Ravaglia, M. J. Bearpark, M. Garavelli, M. A. Robb, *J. Phys. Chem. A* 107, **2003**, 11139–11152.

43. Excited states of conjugated hydrocarbon radicals using the molecular mechanics – valence bond (MMVB) method
M. J. Bearpark, **M. Boggio-Pasqua**, *Theor. Chem. Acc.* 110, **2003**, 105–114.

44. Dihydroazulene/Vinylheptafulvene photochromism: A model for one-way photochemistry via a conical intersection
M. Boggio-Pasqua, M. J. Bearpark, P. A. Hunt, M. A. Robb, *J. Am. Chem. Soc.* 124, **2002**, 1456–1470.

45. Visible emission from the vibrationally hot C_2H radical following vacuum-ultraviolet photolysis of acetylene: Experiment and theory
S. Boyé, A. Campos, S. Douin, C. Fellows, D. Gauyacq, N. Shafizadeh, P. Halvick, **M. Boggio-Pasqua**, *J. Chem. Phys.* 116, **2002**, 8843–8855.

46. Trajectory surface hopping study of the C + CH reaction
P. Halvick, **M. Boggio-Pasqua**, L. Bonnet, A. I. Voronin, J.-C. Rayez, *Phys. Chem. Chem. Phys.* 4, **2002**, 2560–2567.

47. Coupled ab initio potential energy surfaces for the two lowest $^2A'$ electronic states of the C_2H molecule
M. Boggio-Pasqua, A. I. Voronin, P. Halvick, J.-C. Rayez, A. J. C. Varandas, *Mol. Phys.* 98, **2000**, 1925–1938.

48. Global analytical representations of the three lowest potential energy surfaces of C_2H, and rate constant calculations for the $C(^3P) + CH(^2P)$ reaction
M. Boggio-Pasqua, A. I. Voronin, P. Halvick, J.-C. Rayez, *Phys. Chem. Chem. Phys.* 2, **2000**, 1693–1700.

49. Analytical representations of high level ab initio potential energy curves of the C_2 molecule
M. Boggio-Pasqua, A. I. Voronin, P. Halvick, J.-C. Rayez, *J. Mol. Struct. (Theochem)* 531, **2000**, 159–167.

50. Ab initio study of the potential energy surfaces for the reaction $C + CH \rightarrow C_2 + H$
M. Boggio-Pasqua, P. Halvick, M.-T. Rayez, J.-C. Rayez, J.-M. Robbe, *J. Phys. Chem. A* 102, **1998**, 2009–2015.

51. Ab initio study of the structure, cooperativity and vibrational properties of the $H_2O:(HCl)_2$ hydrogen bonded complex
M. Kreissler, L. Lavialle, **M. Boggio-Pasqua**, Y. Hannachi, *J. Mol. Struct. (Theochem)* 542, **1998**, 55–66.

Invited conferences

1. Computational studies of photoactivable and photoswitchable systems, *International Collaborative Laboratory for Supraphotoactive Systems meeting,* 10 March 2015, Toulouse, France.
2. Theoretical mechanistic studies of photoinduced linkage isomerizations in ruthenium complexes, *Breaking and Making Bonds with Light (TSRC workshop)*, 30 June – 4 July 2014, Telluride (Colorado), USA.
3. On the role of extended intersection seams in ultrafast photochemistry, *Chemical Reactivity 2014: From accurate theories to simple models*, 21–23 January 2014, Bordeaux, France.
4. CASSCF and CASPT2 study of 2-hydroxypyridine, *EPSRC UK National Service for Computational Chemistry Software (NSCCS) workshop*, 28–29 September 2013, London, UK.
5. Photophysique de monocations d'hydrocarbures aromatiques polycycliques isolés: contribution théorique, *Spectroscopie et modélisation moléculaire d'assemblages complexes (symposium)*, 28 September 2012, Toulouse, France.
6. Theoretical mechanistic studies of photochromic systems: the central role of conical intersections, *Breaking and making bonds with light (TSRC workshop)*, 2–6 July 2012, Telluride (Colorado), USA.
7. On the role of extended intersection seams in ultrafast photochemistry, *International Meeting on Atomic and Molecular Physics and Chemistry (IMAMPC 2011)*, 5–8 July 2011, Rennes, France.
8. The role of extended conical intersection seams in photochromic systems, *VIIIth International Conference of Computational Methods in Sciences and Engineering (ICCMSE 2010)*, 3–8 October 2010, Kos, Greece.
9. How do conical intersections control photostability and photochemical reactivity?, *Radiation Damage in Biomolecular Systems (RADAM'04) workshop*, 24–27 June 2004, Lyon, France.

Conference proceedings

1. The role of extended conical intersection seams in photochromic systems
M. Boggio-Pasqua, M. J. Bearpark, M. A. Robb, *AIP Conf. Proc.* 1642, **2015**, 453–456.

2. Computer simulations of photochemistry in complex environments: Photo-isomerization and excitation energy transfer
G. Groenhof, D. Morozov, C. F. Burmeister, L. Vukovic, **M. Boggio-Pasqua**, *Abstracts of Papers of the American Chemical Society* 247, **2014**, PHYS 29.

3. Light-induced processes in biological systems: From first principles to biotechnology
G. Groenhof, L. V. Schaefer, **M. Boggio-Pasqua**, H. Grubmüller, M. A. Robb, *Abstracts of Papers of the American Chemical Society* 236, **2008**, COMP 334.

4. CASSCF calculations for excited states of large molecules: Choosing when to use the RASSCF, ONIOM and MMVB approximations
M. J. Bearpark, F. Ogliaro, T. Vreven, **M. Boggio-Pasqua**, M. J. Frisch, S. M. Larkin, M. A. Robb, *AIP Conf. Proc.* 963, **2007**, 583–585.

5. MMVB for conjugated hydrocarbon cations: Method development and application to photochemistry in interstellar clouds
K. F. Hall, M. J. Bearpark, A. M. Tokmachev, **M. Boggio-Pasqua**, M. A. Robb, *Abstracts of Papers of the American Chemical Society* 234, **2007**, PHYS 729.

6. Excited state CASSCF/forcefield dynamics computations on systems of biological interest
G. Groenhof, L. V. Schaefer, H. Grubmüller, **M. Boggio-Pasqua**, M. A. Robb, *Abstracts of Papers of the American Chemical Society* 234, **2007**, PHYS 282.

Other articles

1. Methods for controlling photochemical reactivity: applications to photochemical switches and photostability
M. Boggio-Pasqua, M. J. Bearpark, M. A. Robb, *The Spectrum* 21, **2008**, 28–31.

Communications in congress, symposium

Oral communications

1. Mechanistic pictures of linkage photoisomerizations in photochromic ruthenium complexes from DFT calculations, *Modeling Photoactive Molecules. (MPM 2015 conference)*, 21–24 April 2015, Nantes, France.
2. A mechanistic picture of the photoisomerization in photochromic ruthenium sulfoxide complexes, *Excited states and non-adiabatic processes in complex systems. Theoretical approaches. (WATOC 2011 Satellite meeting)*, 25–27 July 2011, Sant Feliu de Guíxols (Girona), Spain.
3. The role of hydrogen bonds in the ultrafast non-radiative decay of the photoactive yellow protein chromophore, *XXIIIrd IUPAC symposium on photochemistry*, 11–16 July 2010, Ferrara, Italy.
4. Ultrafast deactivation of an excited guanine-cytosine base pair in DNA, *Radiation Damage in Biomolecular Systems (RADAM'07) workshop*, 19–22 June 2007, Dublin, Ireland.
5. Role of the extended intersection seam in photoswitchable molecules, *From molecular switches to molecular motors BIOMACH workshop*, 20–23 September 2005, Ascona, Switzerland.

Posters

1. Rationalization and design of enhanced photoinduced cycloreversion in photochromic dihydropyrenes by theoretical calculations, *Modeling Photoactive Molecules. (MPM 2015 conference)*, 21–24 April 2015, Nantes, France.
2. Photoisomerization of photoactive yellow protein chromophores in water, *Modelling of biologically-inspired photoactive systems workshop*, 30 mars – 1 April 2011, Marseilles, France.
3. Photostability of polycyclic aromatic hydrocarbons in the interstellar medium, *PAHs and the Universe symposium*, 31 May – 4 June 2010, Toulouse, France.
4. Ligand selection in Ru(II) complexes for direct one-electron photooxidation of guanine, *XXIV International Conference on Photochemistry (ICP 2009)*, 19–24 July 2009, Toledo, Spain.

5. Use of acyclic alpha-diimine ligands to tune the photophysical properties of Ru(II) polypyridyl complexes, *XXIV International Conference on Photochemistry (ICP 2009)*, 19–24 July 2009, Toledo, Spain.
6. DFT and TD-DFT studies of the lowest excited states of polypyridyl ruthenium complexes, *XXIInd IUPAC symposium on photochemistry*, 28 July – 1er August 2008, Gothenburg, Sweden.
7. Etude de la photophysique des radicaux pyrène$^{\bullet+}$ et pérylène$^{\bullet+}$ par la méthode hybride MMVB, *XI^{ème} Rencontre des Chimistes Théoriciens Francophones (RCTF 2008)*, 30 June – 4 July 2008, Dinard, France.
8. Intramolecular charge transfer in 4-aminobenzonitriles: internal conversion without twist, *7th Congress of the World Association of Theoretically Oriented Chemists (WATOC 2005)*, 16–21 January 2005, Cape Town, South Africa.
9. Can diarylethene photochromism be explained by a reaction path alone? A CASSCF study with model MMVB dynamics, *Faraday Discussion 127*, 5–7 April 2004, Oxford, UK.

Seminars, workshops

1. Rôle des liaisons hydrogène sur la désactivation non-radiative ultra-rapide du chromophore de la protéine jaune photo-active, *invited seminar*, Ecole Normale Supérieure de Paris, 18 November 2011, Paris, France.
2. Rôle des liaisons hydrogène sur la désactivation non-radiative ultra-rapide du chromophore de la protéine jaune photo-active, *invited seminar*, Laboratoire de Chimie Physique, 15 April 2011, Orsay, France.
3. Le rôle des liaisons hydrogène dans la désactivation non-radiative du chromophore de la protéine jaune photo-active, *local symposium*, Journées Expérience – Théorie, 4 December 2009, Toulouse, France.
4. Photochimie ultra-rapide: modélisation moléculaire mécanistique, *invited seminar*, Laboratoire des IMRCP, 31 March 2009, Toulouse, France.
5. Photochimie ultra-rapide: modélisation moléculaire mécanistique, *invited seminar*, IRSAMC, 8 December 2008, Toulouse, France.
6. Theoretical study of the photophysics of isolated PAH radical cations, *Toulouse Interstellar Nanograin workshop*, 13–14 November 2008, Toulouse, France.
7. Le rôle des intersections coniques dans le contrôle de la photoréactivité et de la photostabilité, *invited seminar*, Laboratoire Francis Perrin (CEA Saclay), 29 May 2008, Gif sur Yvette, France.
8. Désactivation non-radiative ultra-rapide d'une paire de bases cytosine-guanine excitée dans l'ADN, *local symposium*, Journées de Dynamique du Sud-Ouest, 20–21 May 2008, Montpellier, France.
9. On the role of the extended intersection seam in ultrafast photochemistry, *invited seminar*, Max Planck Institute for Biophysical Chemistry, 21 May 2007, Göttingen, Germany.
10. Désactivation non-radiative ultra-rapide d'une paire de bases cytosine-guanine excitée dans l'ADN, *invited seminar*, Laboratoire de Chimie et Physique Quantiques, 22 March 2007, Toulouse, France.
11. The role of the extended intersection seam in photochemistry, *invited seminar*, Laboratoire de Chimie et Physique Quantiques, 11 January 2006, Toulouse, France.
12. The RASSCF method with correlation adapted orbitals: applications to excited-state photochemistry, *COST (European Cooperation in Science and Technology) meeting*, June 2005, Valencia, Spain.

13. The extended nature of the conical intersection seam: implications for mechanistic photochemistry, *invited seminar*, 21 February 2005, Imperial College London, London, UK.

14. Intramolecular charge transfer in 4-aminobenzonitrile, *Radiation Damage in Biomolecular Systems (RADAM) working group meeting*, 30 October 2004, Brussels, Belgium.

Book chapters

1. Excited state dynamics in biomolecules

G. Groenhof, L. V. Schäfer, **M. Boggio-Pasqua**, M. A. Robb, In *Handbook of Molecular Biophysics*, Ed. H. Bohr, Wiley-VCH, Weinheim, **2009**, pp. 93–134.

2. Conical intersections and photochemical mechanisms: characterizing the conical intersection hyperline using gradients, second derivatives, and dynamics

M. A. Robb, M. J. Bearpark, **M. Boggio-Pasqua**, P. A. Hunt, M. Paterson, M. Olivucci, L. Blancafort, G. Groenhof, In *Quantum Dynamics at Conical Intersections*, Eds. S. Althorpe and G. Worth, CCP6, Warrington, **2004**, pp.1–3.

Others

1. Suivez le guide !, written contribution in the magazine *2011, une année avec le CNRS en Midi-Pyrénées*.

2. Qu'est-ce-que la photobiologie ?, written contribution in the magazine *2009, une année avec le CNRS en Midi-Pyrénées*.

3. Extended MC-SCF Calculations on Conjugated Polycyclic Hydrocarbons, M. J. Bearpark, M. Boggio-Pasqua, *Scientific highlight in EPSRC UK National Service for Computational Chemistry Software (NSCCS) editorial*, issue 11, 23 July 2007, pp. 2–4.

4. Exhibitor for Gaussian Inc., *7th Congress of the World Association of Theoretically Oriented Chemists (WATOC 2005)*, 16–21 January 2005, Cape Town, South Africa.

5. Contribution in *Faraday Discussion 127: Non-adiabatic effects in chemical dynamics*, 5–7 April 2004, Oxford, UK.

Teaching and Overseeing

Teaching

- 4-hour lecture given to M2 Erasmus Mundus TCCM students (2014). *Computational Mechanistic Photochemistry.*
- 10-hour lecture given to PhD students of Ecole Doctorale des Sciences de la Matière in Toulouse (2014). *Computational photochemistry*.
- 2-hour lecture given to ENSIACET students in Toulouse (2014). *Towards understanding photochromic materials at the molecular level: how can theoretical chemistry be helpful?*
- Master lecture for Pôle Sud-Ouest du Réseau Français de Chimie Théorique (2008, 2010 and 2012). 6-hour lecture and practical work. *QM/MM calculations of excited states*.
- Numerical labs and tutorials in physical chemistry for 1st year students at Imperial College London (2004-2007).
- Exercise corrections and practical labs in physical chemistry for 1st and 2nd year students at Université de Bordeaux 1 (1996-2000).

Overseeing

- Tatiana Lemishko (TCCM Erasmus Mundus Master)

3-month assignment, February-April 2015.
Theoretical study of the fragmentation of guanine upon electron attachment.

- Juan Sanz Garcia (PhD)

3-year PhD thesis, October 2013–October 2016. Co-direction (50%) with J.-L. Heully.
Theoretical study of ruthenium nitrosyl complexes.

- Serra Arslancan (TCCM Erasmus Mundus Master)

4-month assignment, March-June 2014.
Theoretical study of the photochemistry of dimers of thiosubstituted pyridine bases.

- Mohamed Elshakre (mobility of an Egyptian researcher from Cairo)

1-month placement, December 2013.
Theoretical study of the photoisomerization of heterocyclic aromatic azides.

- Kathy Chen (TCCM Erasmus Mundus Master)

4-month assignment, January-April 2013.
Theoretical study of the deactivation pathways in 4-thiouracil and 2,4-dithiouracil.

- Juan Sanz Garcia (BSc research project)

4-month assignment, September 2012-January 2013.
Theoretical calculations of enantiomerization barriers in atropochiral biaryls.

- Olivier Vieuxmaire (post-doctoral researcher, ANR funding)

2-year assignment, October 2011-October 2013.
Theoretical study of the P→O linkage photoisomerization in a phosphinidene oxide ruthenium complex.

- Adrien Göttle (PhD)

3-year PhD thesis, October 2010–October 2013. Co-direction (50%) with F. Alary.
Theoretical study of the photophysical and photochemical properties of ruthenium complexes.

- Cloé Lanthony (Master)

5-month assignment, January-June 2010.
Theoretical study of ruthenium complexes functionalized with organophosphorus ligands for solar energy conversion in photovoltaic systems.

- Thomas Guillon (temporary lecturer)

10-month assignment, October 2008-July 2009.
Theoretical study of ruthenium complexes with diazabutadiene ligands.

- Mohamed Oubal (Master)

5-month assignment, January-June 2008.
Photoreactivity of ruthenium complexes with a DNA basis.

- Moira Prete (Master)

6-month Erasmus assignment at King's College London, September 2001-March 2002. Co-supervision with M. Robb.
A theoretical study of the Bergman reaction: A CASSCF approach for modeling the enediyne anticancer drugs.

- Anna Zagolin (Master 2ème année)

6-month Erasmus assignment at King's College London, October 2000-April 2001. Co-supervision with M. Robb.
Theoretical study of an iron complex.

Scientific and Administrative Duties

- In charge of the organization of the lab (LCPQ) and institute (IRSAMC) seminars.
- Member of the Scientific Board of CALMIP since 2010. Reviewer in the evaluation process of the projects for getting HPC computing resources on Hyperion (2010–2014) and Eos (2014–).

- Member of the Scientific Board of the “Labex” NEXT (2015–).
- Regular reviewer in journals of ACS, RSC, Springer, AIP and Elsevier. Occasional reviewer for Wiley, Taylor & Francis and Biophysical Society.
- Reviewer of ANR, ERC and FNRS projects.
- Member of the tribunal of the international PhD defense of Lara Martinez (Madrid, 4 November 2014).
- Member of the organization committee of RCET (Toulouse, 2015).
- Member of the organization committee of PEM2 symposium (Toulouse, 2015).
- Partner in ANR programs PhosphoRuIr (2010–2014) and Gasparim (2010–2013).

To my beloved wife, Marjorie